

Dendrimer Biopharmaceutics: Toward Active Dendrimer-Cannabinoid Drugs

A thesis submitted in accordance with the conditions
governing candidates for the degree of
Philosophiae Doctor in Cardiff University

By

Ghaith Aljayyousi

December 2011

Welsh School of Pharmacy

Cardiff University

Acknowledgements

I would firstly like to sincerely thank my supervisor Mark Gumbleton for all his encouragement and support during my PhD studies. Thanks to Mark, I have finally understood the true meaning of being a scientist. I would also like to thank my second supervisor Will Ford for his support, and to Neil McKeown for his invaluable advices and ideas that were vital for the achievement of this work.

Thanks to members of the Mark Gumbleton lab, especially to Mat, Chris, Marc and Lee. Special thanks to Jenna for the constant supply of food. And to Reem, with whom I spent countless hours writing (and not writing) this thesis.

Finally, words will never suffice to express my deepest love and gratitude to my dear family who unceasingly supported me at all times during my studies.

Summary

The ultimate aim of the work described in this thesis was to (1) utilise PAMAM dendrimers as a tool to achieve differential transport across the intestinal mucosa and the blood brain barrier, where these dendrimers can be used to achieve oral bioavailability but avoid BBB penetration and CNS access and (2) to create cannabinoid-dendrimer conjugates that are active in their own right and whose penetration to the brain is prevented but whose intestinal activity is afforded for the treatment of IBD.

Overall, the work described in this thesis has promoted a strategy whereby an active polymer (dendrimer)-drug conjugate could be formed that is active in its own right and where the polymer can serve to provide differential biological barrier transport which with regard to cannabinoid pharmacology obviates adverse CNS effects.

The work in this thesis describes the design and synthesis of novel and active cannabinoid structures that should have commercial interest. These novel compounds served to further elucidate SAR in amino alkyl indole cannabinoids. SAR findings have revealed a site on these cannabinoids that can be functionally altered without loss of pharmacological activity.

Additionally, studies in this thesis have led to the development of a novel radiolabelling strategy for anionic polymers that offers a number of distinct advantages over other approaches.

Ultimately, a novel stable Dendrimer-cannabinoid conjugate has been synthesised but to date has not shown biological activity in the models utilised in this work.

Table of Contents

Chapter 1: General Introduction.....	8
1.1 Dendrimers	9
1.1.1 Overview	9
1.1.2 Dendrimer Syntheses	11
1.1.3 General Characteristics and Properties	13
1.1.4 General Biomedical Applications.....	17
1.2 Cannabinoids.....	22
1.2.1 Therapeutic uses of Cannabinoids	25
1.2.2 Irritable bowel disease and the role of Cannabinoids	29
1.3 Aims and Objectives	37
Chapter 2: Dendrimer Transport across Biological Barriers	40
2.1 Introduction.....	41
2.1.1 The Intestinal Barrier	41
2.1.2 The Blood Brain Barrier.....	43
2.1.3 <i>in-vitro</i> Assessment of transport across the intestinal and blood brain barriers.	45
2.1.4 Aims and Objectives	47
2.2 Materials and Methods.....	48
2.2.1 Materials.....	48
2.2.2 Methods	49
2.3 Results and Discussion	57
2.3.1 Synthesis, Purification and Stability Testing of anionic PAMAM – OG and cationic PAMAM-FITC conjugates	57
2.3.2 Assessment CaCo-2 monolayers for Transport Studies.....	62
2.3.3 Transport of anionic PAMAM –OG conjugates across CaCo-2 monolayers	65
2.3.4 Transport of Cationic PAMAM-FITC conjugates across CaCo-2 monolayers.	74
2.3.5 Transport of anionic PAMAM dendrimers across MDCK I and MDCK II monolayers	81

2.3.6	Permeability Studies with Intrinsically Fluorescent Dendrimers in MDCK I and MDCK II cell lines.	88
2.3.7	The effect of Tumour Necrosis Factor - α (TNF- α) on MDCK-II and CACO-2 restrictiveness and permeability to anionic PAMAM-OG dendrimers.	91
2.3.8	<i>Isolated Perfused Rat gut (IPrG)</i>	95
2.4	<i>Summary</i>	101
Chapter 3: Synthesis and Pharmacological Evaluation of Novel Cannabinoid Derivatives		104
3.1	<i>Introduction</i>	105
3.1.1	<i>Cannabinoid Receptor Pharmacology</i>	105
3.1.2	<i>Endogenous Cannabinoids</i>	110
3.1.3	<i>Structure Activity Relationship (SAR) of Cannabinoids</i>	111
3.1.4	<i>Assessment of anti-inflammatory activity of Cannabinoid compounds</i>	118
3.1.5	<i>Aims, Objectives and Overall Strategy</i>	120
3.2	<i>Material and Methods</i>	122
3.2.1	<i>Materials</i>	122
3.2.2	<i>Methods</i>	123
3.3	<i>Results and Discussion</i>	126
3.3.1	<i>Choice of a model for WIN 55,212-2</i>	127
3.3.2	<i>Reductive Amination with WIN 55,212-2</i>	136
3.3.3	<i>Synthesis of a new cannabinoid model</i>	138
3.3.4	<i>Structural Similarities between JWH007 and WIN 55,212-2</i>	140
3.3.5	<i>Biological Evaluation of JWH007 and WIN 55,212-2</i>	141
3.3.6	<i>Synthesis of Novel Cannabimimetic indoles</i>	143
3.3.7	<i>Toxicity Studies</i>	160
<i>Appendix A : Chemical Syntheses</i>		165
Chapter 4: Dendrimer Conjugates		176
4.1	<i>Introduction</i>	177
4.1.1	<i>Dendrimers as Drug Carriers</i>	177
4.1.2	<i>Active Dendrimer-drug conjugates</i>	180
4.1.3	<i>Aims and Objectives</i>	181
4.2	<i>Materials and Methods</i>	182
4.2.1	<i>Materials</i>	182

4.2.2	<i>Methods</i>	182
4.3	<i>Results and Discussion</i>	187
4.3.1	<i>Radiolabeling of G3.5 PAMAM dendrimers</i>	187
4.3.2	<i>Cannabinoid-Dendrimer Conjugation</i>	196
Chapter 5: General Discussion and Conclusions		205
5.1	<i>General Discussion</i>	206
5.2	<i>Conclusions</i>	212
	<i>References</i>	214

List of Figures

Figure 1.1 A typical dendrimer	11
Figure 1.2 Dendrimer Syntheses. The Divergent and convergent approaches ..	13
Figure 1.3 The four different classes of Cannabinoid Agonists	25
Figure 1.4 Role of Cannabinoids in the treatment of inflammatory bowel disorders.....	34
Figure 2.1 Absorption in humans Vs. apparent P_{app} across CaCo-2 monolayers [.....	47
Figure 2.2 Experimental setting for the isolated perfused gut model.....	57
Figure 2.3 Synthesis and Purification of anionic PAMAM-OG conjugates.	59
Figure 2.4 Synthesis and Purification of cationic PAMAM – FITC conjugates	60
Figure 2.5 Stability of anionic PAMAM-OG and cationic PAMAM-FITC conjugates.....	62
Figure 2.6 Cumulative transport of [^3H] Propranolol , [^{14}C] Mannitol and F-Na across CACO-2 monolayers.	64
Figure 2.7 Standard Curve for F.Na.	67
Figure 2.8 Cumulative transport of ^{14}C Mannitol, Oregon Green Cadaverine, PAMAM 1.5-OG, PAMAM 3.5-OG and PAMAM 5.5-OG across CACO-2 monolayers over 120 minutes.....	67
Figure 2.9 Relationship between probes' molecular weight and P_{app} across CACO-2 monolayers.	69
Figure 2.10 Stability of anionic PAMAM-OG conjugates during transport studies across CACO-2 studies.....	71
Figure 2.11 The influence of OG and anionic PAMAM-OG conjugates on the cumulative transport of [^{14}C] Mannitol and [^3H] Propranolol	72
Figure 2.12 Stability of cationic PAMAM-FITC conjugates during transport studies across CACO-2 monolayers.	75
Figure 2.13 Cumulative transport of cationic PAMAM-FITC conjugates across CACO-2 monolayers.	77
Figure 2.14 Permeability coefficients of anionic and cationic PAMAM dendrimers corrected to molecular size.....	78
Figure 2.15 Effect of Cationic PAMAM dendrimers (G3 and G4) on the integrity of CACO-2 monolayers	79
Figure 2.16 The cumulative transport of F-Na across MDCK I and MDCK II monolayers.	83
Figure 2.17 Cumulative transport of PAMAM 1.5-OG. And PAMAM 3.5-OG across MDCK I and MDCK II cell lines.....	85
Figure 2.18 Hypothesised effect of molecular weight upon the permeability of a probe across the tight MDCK I and the less restrictive MDCK II.	88

Figure 2.19 Poly(amido-amine) Dendrimers bearing a fluorescent core,	91
Figure 2.20 Permeability Coefficients of a group of intrinsically fluorescent poly(amido-amine) (G0.5, G1.5 and G2.5) across MDCK I and MDCK II monolayers.	91
Figure 2.21 The effect of TNF- α on the cumulative transport of PAMAM G3.5-OG and and [14 C] Mannitol across MDCK II cells.....	94
Figure 2.22 Effect of TNF- α on CACO-2 TEER.....	96
Figure 2.23 A part of the mesenteric bed after 5 minute perfusion with buffer containing trypan blue (5 mg/mL)	99
Figure 2.24 Cumulative transport of [14 C] Mannitol, F-Na and [3 H] Propranolol across the isolated perfused rat gut.	100

Figure 3.1 Activation of signal transduction pathways via Cannabinoid receptors.	110
Figure 3.2 Chemical structure of anandamide, an endogenous cannabinoid..	112
Figure 3.3 General Structure of classic cannabinoids and THC	113
Figure 3.4 Structure of JWH-133: a classical CB2 selective cannabinoid	114
Figure 3.5 Structure of WIN 55,212-2.....	116
Figure 3.6 The general structure of a cannabimimetic aryl alkyl indole	116
Figure 3.7 Two amino alkyl indole cannabinoids	117
Figure 3.8 Structure of WIN 55,212-2 showing carbonyl group.....	128
Figure 3.9 Benzophenone, chosen as model to manipulate carbonyl group on cannabinoid drug.	129
Figure 3.10 Structures of WIN 55,212-2 and JWH007. Moieties contributing to cannabinoid pharmacological activity marked in circles.....	141
Figure 3.11 The effect of synthesised JWH007 and WIN 55212,2 (10 μ M) to suppress production of TNF- α in RAW 264.7.	143
Figure 3.12 The effect of GA001 and JWH007 in suppressing TNF- α in RAW 264.7.	147
Figure 3.13 The effect of GA002 and JWH007 in suppressing production of TNF- α in RAW 264.7.....	150
Figure 3.14 The effect of GA002 and JWH007 in suppressing LPS induced production of TNF- α in RAW 264.7.	153
Figure 3.15 The effect of GA005 and JWH007 in suppressing production of TNF- α in RAW 264.7.....	158
Figure 3.16 The effect of GA006 and JWH007 in suppressing production of TNF- α in RAW 264.7.....	161
Figure 3.17 Effect of 0.1% DMSO and 200ng/mL LPS upon the viability of RAW 264.7 macrophage cell line as assessed using the MTT+ assay.	163
Figure 3.18 Effect of the in-house synthesised cannabinoid JWH007 and the prototype amino-indole alkyl cannabinoid WIN 55,212-2 upon the viability of RAW 264.7 macrophage cell line as assessed using the MTT+ assay.	164

Figure 3.19 Effect of novel synthesised cannabinoids GA001, GA003 and GA006 upon the viability of RAW 264.7 macrophage cell line as assessed using the MTT+ assay.165

Figure 4.1 Overlayed GPC chromatograms of pure Dendrimer-Og conjugate and free [3H] acetic acid.190

Figure 4.2 GPC chromatogram of crude reaction mixture of PAMAM G3.5 and acetic anhydride and GPC chromatogram for pure radiolabelled dendrimer ..191

Figure 4.3 Stability of PAMAM-radiolabel conjugates195

Figure 4.4 TLC analysis of PAMAM G3.5 dendrimers and cannabinoid GA006..199

Figure 4.5: NMR spectra for PAMAM G3.5-GA006 conjugate and free GA006201

Figure 4.6 The effect of PAMAM G3.5, PAMAM G3.5-GA006 conjugate and JWH007 in suppressing production of TNF- α in RAW 264.7.204

Figure 5.1 an amino alkyl indole showing sites that were manipulated in SAR studies.212

List of Tables

Table 2.1 Comparison between the intestinal and the blood brain barriers.....	40
Table 2.2 Table summarising TEER, and permeability to [¹⁴ C] Mannitol and [³ H] Propranolol across CaCo-2 monolayers	59
Table 2.3 Molecular weights, stoke's diameters, and permeability coefficients of different anionic PAMAM-OG conjugates and small molecular weight compounds across CACO-2 monolayers.	64
Table 2.4 Effect of Oregon green and different anionic PAMAM-OG conjugates on CACO-2 monolayer integrity observed through changes in TEER and permeation of [¹⁴ C] Mannitol and [³ H] Propranolol	67
Table 2.5 Molecular weights, stoke's diameters, and permeability coefficients of two cationic PAMAM-FITC conjugates across CACO-2 monolayers.	71
Table 2.6 Permeability Coefficients of Sodium Fluorescein (A-Na), PAMAM G1.5-OG and PAMAM G3.5-OG as calculated across MDCK I and MDCK II cell lines. Results are Mean ± S.D. n number specified in the table.	80
Table 2.7 Effect of TNF-α on TEER, PAMAM G3.5 and ¹⁴ C Mannitol permeation (expressed as permeability coefficient x 10 ⁻⁶ cm.s ⁻¹) across MDCK II cells	88
Table 3.1 Strategies used to manipulate carbonyl group and introduce an amine in benzophenone	125
Table 4.1 Stability of radiolabeled PAMAM dendrimers..	190

Chapter 1

General Introduction

1.1 Dendrimers

1.1.1 Overview

Dendrimers are iteratively branched, mono-disperse polymers that emanate from a functional core [1, 2]. The word 'dendrimer' is derived from the Greek words '*dendron*' and '*meros*' meaning 'tree' and 'parts', respectively [3]. The first controlled dendrimer synthesis was achieved and reported by Vögtle's group in Bonn in 1978 [4]. It wasn't until 7 years later, however, that dendrimers started to raise interest in the medical field upon the publication of Tomalia's seminal work on the subject in 1985 [5].

Dendrimers generally possess three distinctive features: An encapsulated core, multiple branching units, and an outer shell that comprises multiple surface groups and is the major contributor to the dendrimer's physical chemical properties and reactivity [3, 6, 7]. The iterative branching of dendrimers that occurs at specific focal points can define the dendritic structure in terms of 'generations' where each layer that is formed at every subsequent branching step marks a new generation that increases in number from 0. 'the zeroth' generation is generally attributed to the generation number for the core itself [8]. *Figure 1.1* gives a better understanding of dendritic generational structure.

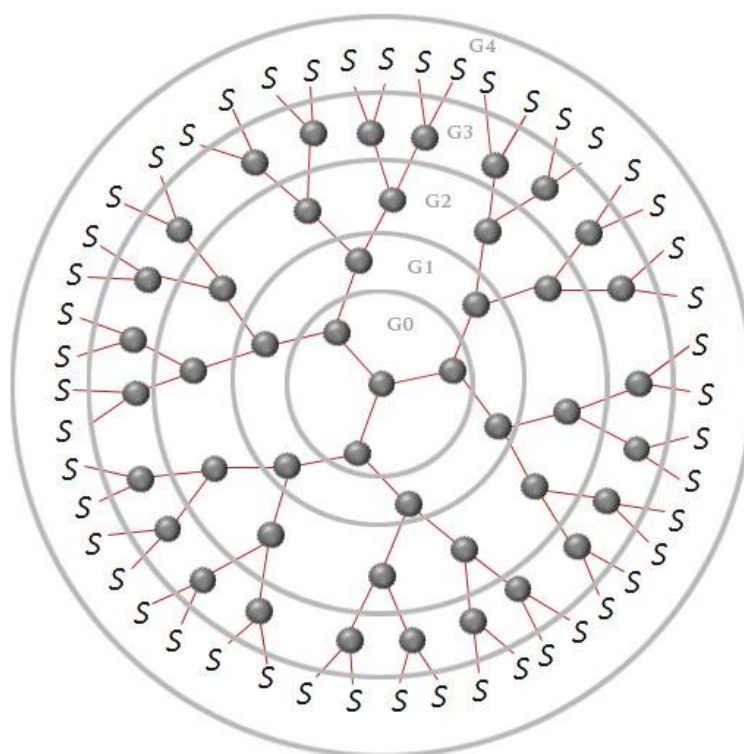


Figure 1.1 A typical dendrimer displaying a core from which multivalent branching occurs creating multiple layers commonly known as generations. The generation number increases from G0 at the core to G4 at the surface at every layer as shown. 'S' denotes surface groups.

Among the first fully synthesised and characterised dendrimers are Starburst[®] PAMAM dendrimers [5].

PAMAM dendrimers possess a nitrogen based core (ammonia or ethylenediamine) to which multiple amines are covalently attached by amide bonds forming iterative 'amidoamine' branches which grow radially from the core [5]. These dendrimers can be cationic, anionic or neutral when they possess positively charged amine groups, negatively charged carboxylic groups or neutral hydroxyl groups, respectively, on their surfaces [9].

1.1.2 Dendrimer Syntheses

Dendrimers are generally synthesised using the divergent or the convergent approach [10]. In the divergent approach, dendrimers are synthesised from a core where multiple protected monomers are attached at multiple steps. Each step forms a new generation where the protection groups are removed and more monomers are added to form another generation and so on. This method, although simple, has many draw-backs including the occurrence of undesirable side reactions causing synthetic errors and higher polydispersity, ultimately leading to lower final yields. The convergent method on the other hand, first developed by Frechét et al. [11], applies a counter intuitive approach where dendrimer synthesis starts from its outer shell: multiple dendrimer segments, often called dendrons or dendritic wedges, are synthesised independently and attached in the last step to form the final dendrimer. *Figure 1.2* shows the difference between the divergent and convergent approaches.

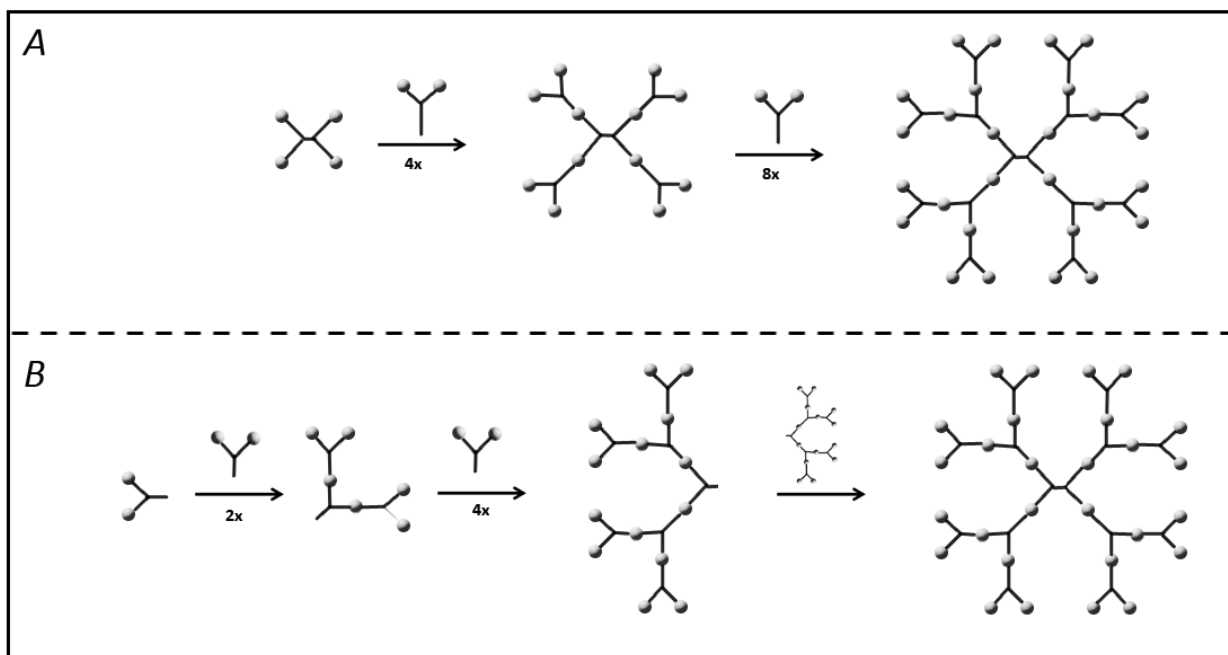


Figure 1.2 Dendrimer Syntheses. The Divergent (A) and the convergent (B) approaches

The convergent approach offers a more controlled technique in dendrimer synthesis. Simply in the convergent method, less reactive sites are exposed at each synthetic step. The presence of less reactive sites at every step in polymer synthesis decreases the chances of undesired side reactions and hence increases the efficiency of the synthesis leading to more mono-disperse products at lower costs. . The divergent approach, on the other hand, exposes the entirety of the dendrimer surface to reactions at each step of its synthesis.

1.1.3 General Characteristics and Properties

The branched structure that is observed in a typical dendrimer is far from uncommon in biological systems. In fact, it's one of the most recurring structures that are observed in life. Dendritic structures can be observed through a wide scale extending from the branching structure of trees and their roots, to the circulatory and neuronal structures in higher organisms. One of the hypotheses behind the universal evolution of these structures in life is that they provide an extended interface for interaction with the environment. It can be argued that this is the same reason behind the vitality of dendrimers as a new class of synthetic polymers in the biomedical field [12].

One of the major attributes that distinguish dendrimers from conventional synthetic polymers is their multivalency: a property that increases the available interaction sites on the dendrimer, hence enhancing its binding affinity in biological systems. Dendrimer's polyvalent properties facilitate the efficient conjugation of these polymers to various drugs. Dendrimers' multivalent surface groups make them generally highly water soluble. PAMAM dendrimers possessing charged amine or carboxylic groups on their surfaces, for instance, are highly water soluble, which facilitates their application in the biomedical field.

Dendrimer molecular diameters have been shown to range between 1.1nm (G1 dendrimers) and 12.4nm (G10 dendrimers)[9]. They hence possess a molecular

size range that is similar to that of endogenous proteins. Another attribute that distinguishes dendrimers is their tendency to form three dimensional globular spheres at higher generations (G4 and higher)[13]. Because of their similar molecular sizes and globular structures [12, 14], higher generation dendrimers have been proposed as protein mimics. Unlike proteins, however, dendrimers are more robust and less flexible as they are formed entirely from covalent bonding.

Although highly robust, dendrimer topology is highly affected by the polarity and the acidity of the solvent in which it is dissolved, adapting either a denser or a more extended conformation according to the conditions of the solvent. This is essentially due to the different repulsion and attraction forces that are formed between the interior and the exterior of the dendrimer in different solvents [15, 16].

Higher generation dendrimers, because of their globular and branching structures, contain many intra-molecular cavities. These cavities can serve as pockets where (hydrophobic) drugs can be noncovalently encapsulated for controlled drug delivery purposes [17].

Unlike conventional polymers, dendrimers have very precise structures with extremely narrow polydispersity indices. This comes as a result of the controlled stepwise fashion in which they are synthesised[5].

Because of their structure, dendrimers generally form tight spheres when in solution, in contrast to linear or conventionally branched polymers which extend when dissolved. This makes dendrimer solutions less viscous than solutions of linear polymers of similar molecular weights, a property that facilitates their use in the medical field [7].

Dendrimers display toxicity profiles that are a function of the chemical nature of their surface groups and the core. The relative effects of the surface groups and the core on the toxicity of the dendrimer depend on the size or generation of the said polymer. The surface groups are the major contributor to larger sized dendrimers' toxicity while the core can have a significant effect on the biocompatibility of smaller dendrimers. The reason behind this discrepancy is that the core in larger sized dendrimers is less accessible to the cells as it is protected by the dendrimer branching and terminal groups [18].

Cationic (PAMAM) dendrimers, like most cationic macromolecules, are expected to display some degrees of toxicity *in-vitro* and *in-vivo*. Cationic macromolecules are generally more toxic because of the vigorous interactions that occur between their strong positive charge and the negatively charged cellular membranes; this leads to membrane rupture and cell lysis[19]. Roberts et al.[20] have shown that cationic PAMAM dendrimers display a generation dependant toxicity *in-vitro* and *in-vivo* with higher generations (possessing a greater number positive charges) being more toxic than lower generation dendrimers. Anionic PAMAM dendrimers, on the other hand, display

significantly lower toxicity profiles both *in-vitro*[21, 22] and *in-vivo*[23]. It has also been shown that the modification or coverage of the cationic surfaces of some PAMAM dendrimers using PEG branches significantly decreases their toxicity [22, 24].

Dendrimers' chemistry and structure can offer a versatile platform for manipulating biological barrier permeability to these polymers and their conjugates. Given the large size of dendrimers (especially at higher generations), it is expected that dendrimer-drug conjugates will have characteristics that are more similar to the dendrimer itself than with the conjugated drug.

In addition to the high molecular size, the high water solubility of PAMAM dendrimers is expected to make them less likely to permeate across tight biological barriers such as the BBB. However, lower generations of these globular polymers (G2.5 and lower) can still theoretically permeate across the intestinal barrier utilising the paracellular pathway as it has been shown that molecules up to 3nm in diameter can still pass between the tight junctions of the intestinal epithelium in the rat [25]. It has also been suggested that larger dendrimers can cross the intestinal barrier through uptake by enterocytes in a transcytotic mechanism [26].

1.1.4 General Biomedical Applications

The distinguishing properties of dendrimers that were discussed in the previous section have encouraged scientists to exploit them in the biomedical field. Since they emerged in the early 1990s on the hands of Tomalia et al., Starburst[®] dendrimers¹ have been utilised in many aspects of the biomedical field.

Dendrimers have been extensively used in the field of anticancer chemotherapy and radiotherapy. Barth et al.[27] were among the pioneering groups that conjugated boronated monoclonal antibodies (MAb) to dendrimers to achieve better tumour targeting. Highly water soluble PAMAM G3.5-Cisplatin conjugates have been designed for the slow release of platinum in cancer therapy displaying superior anti-tumour activities *in-vitro* and *in-vivo* [23].

Cationic dendrimers can serve as good gene transfection agents because their cationic amine terminals can readily interact with the phosphate groups that constitute the plasma membrane [28] and hence cationic dendrimers have been widely used in gene transfection where they serve as non-viral gene vectors that transfer specific genes into the cell [29]. A few dendrimer based *in-vitro* transfection agents have been commercialised (PolyFect[®] and SuperFect[®]).

¹ The term 'Starburst dendrimers' was adopted by Tomalia et al. [5] to describe classical dendrimers with radial architectures that were first synthesised by the same group

Dendrimers were also applied in the field of imaging diagnostics where traditional contrast agents in Magnetic Resonance (MR) imaging like gadolinium ions are conjugated to dendrimers' surfaces. The attachment of gadolinium ions to robust structures with high molecular sizes such as dendrimers improves their specificity and sensitivity as contrast agents [30], dendrimers have been implemented in the specific MR imaging of organs such as kidney [31] and tumour blood vessels [32]. Dendrimers have been utilised in the field of *in-vitro* diagnostics as well: fixed dendrimer-immunoglobulin conjugates were used for the rapid detection of cardiac-muscle damage related proteins in blood samples in a method developed by *Dade International Inc.* [28].

Dendrimer structures afford them the potential use for the solubilisation of hydrophobic drugs. Several groups have exploited the dendritic structure that usually possesses hydrophobic cores with hydrophilic surfaces (e.g. cationic and anionic PAMAM dendrimers) creating a form of unimolecular micelles that can encapsulate hydrophobic drugs and enhance their aqueous solubility [33, 34].

Dendrimers have also been used as therapeutic agents by their own virtue and have shown intrinsic therapeutic activities against many diseases. Dendrimers have shown microbicidal activity against sexually transmitted viruses such as HIV [35] and HSV [36]. Indeed, a dendrimer based product, *VivaGelTM* from *StarPharma*, which is a vaginal gel that can be used to protect women from HIV

and HSV based STDs, has already shown promising results in clinical trials [37, 38]. Dendrimers have also shown activity against prion related diseases and Alzheimer's [39, 40] ; it has been proposed that dendrimers can alter the nucleation and elongation rates of prions and hence have the potential to modulate the aggregation processes of these proteins [40]. Additionally, quaternary ammonium functionalised dendrimers have shown potent antimicrobial and biocidal effects that are superior to effects exhibited by conventional polymers of similar structure and size [41]. Dendrimers have also been shown to display intrinsic activities against cancer [42] and inflammation [43].

Dendrimers in Different Delivery Routes

Dendrimers have been proposed as carriers in the delivery of various drugs through almost every major drug delivery route from intravenous to ocular delivery.

Dendrimers have been proposed as drug carriers in many parental routes such as intravenous [23, 44] and intramuscular routes[45]. One of the major obstacles that stand in the path of developing parental dosage forms is the low aqueous solubility of hydrophobic drugs [46, 47]. Dendrimers, as discussed earlier, can aid in the solubilisation of hydrophobic drugs to overcome this obstacle.[46] Additionally, the most common route for the administration of

anti-cancer drugs is usually the parental one and the fact that dendrimers can be administered intravenously while causing only weak or no immunogenic responses[20] facilitates the future *in-vivo* application of the many dendrimer-anti cancer formulations that have been developed so far. In the field of chemotherapeutics also, intra-tumoural [48] and intra-peritoneal [49] preparations of dendrimer-anticancer agents have been applied at an *in-vivo* level.

Bai et al.[50] reported that their *in-vivo* results in the rat lung showed that cationic dendrimers can enhance the pulmonary delivery of enoxaparin, a low molecular weight form of heparin. Morris et al. [51] studied the transport of various anionic PAMAM dendrimers across the intact rat lung and showed a size dependant trend in their permeation across the lung epithelium.

Transdermal delivery (TDD) is also one of the routes where dendrimers were proposed as carriers. TDD offers a controlled delivery of the drug to the systematic circulation and maintains stable effective concentrations without peaks and troughs in the blood [52]. The skin, however, represents a thick barrier that can hinder the absorption of various drugs. (Cationic) PAMAM dendrimers with their hydrophobic interiors and hydrophilic exteriors can act as transdermal enhancers that enhance the solubility of hydrophobic drugs and disrupt the epidermal barrier facilitating more drug absorption across the skin [53].

Oral drug delivery remains as one of the most prevalent routes that are exploited in the drug industry as it offers the most convenient method for the administration of multiple dosage forms. It remains a serious challenge, however, to get many drugs to permeate across the intestinal epithelium to the systematic circulation and achieve acceptable oral bioavailability levels due to various reasons like poor aqueous solubility, stability in the gastrointestinal environment and efflux transporters[54]. The oral route is one of the most explored routes in dendrimer drug delivery. Various *in-vitro* transport studies across cells that simulate the intestinal lumen, such as the CaCo-2 and the MDCK-II cell lines, have shown that various PAMAM dendrimers can permeate to extents that correlate with orally bioavailable compounds [24, 55, 56]. Dendrimers, as previously discussed can offer an avenue for the evasion of efflux transporters and can hence enhance oral bioavailability of small molecular weight drugs that are substrates of P-gp. Wiwattanapatapee et al.[26] have shown that both anionic and cationic dendrimers can permeate across the rat gut sac at different rates. Florence et al. [57] have studied the uptake and translocation of poly-lysine dendrimers and shown that they can permeate across the rat intestine *in-vivo*.

The ocular region is one of the delivery routes that present many challenges in drug formulation: while the ideal ocular formulation is one that achieves long residence times and acceptable bioavailability at the intended site of action in the eye, most drugs fail to cross the barriers presented by the eye (such as the

cornea and conjunctiva) [58]. These issues have instigated the search for different carriers of drugs that target the eye tissue, and various (polymeric) preparations were used to address the issues in ocular delivery[59]. Dendrimers have been suggested as ophthalmic carriers in this context. Vandamme et al. [58] have shown that the concomitant presence of various cationic and anionic PAMAM dendrimers of various sizes with pilocarpine and tropicamide can increase the residence time of these drugs in the albino rabbit's eye cornea. Shaunak et al. [60] developed novel glucosamine-PAMAM (G3.5) conjugates that displayed anti-angiogenic and anti-immunogenic activities when applied on the albino rabbit's eye.

1.2 Cannabinoids

Marijuana, Hashish or Cannabis are terms that describe the psychomimetically active resin of the *Cannabis Sativa* flowers [61]. It is one of the most widely used recreational drugs [62]. The biological activities exerted by Marijuana stem from its most (psycho)active chemical constituent Δ^9 -Tetrahydrocannabinol (THC), which has been first isolated and characterised by Gaoni et al. in 1964. [61]. The exploitation of cannabis as a therapeutic, however, is far from recent. In fact, the use of cannabis for medicinal purposes dates back to the third millennium BC as evident from ancient Chinese texts

that described the use of the psychoactive herb in treating stomach pain and cramps [63].

Cannabinoid compounds can be generally classified into four major groups based on their chemical structure: (1) classical cannabinoids, whose prototype is Δ^9 – THC, and are generally naturally derived. (2) Non-classical (bicyclic) cannabinoids, such as CP 55,940. (3) Fatty acid amides or esters (eicosanoids), which are generally produced endogenously in the body such as the endogenous cannabinoid anandamide, or (4) aminoalkyl indoles, whose prototype is known as WIN 55,212-2.

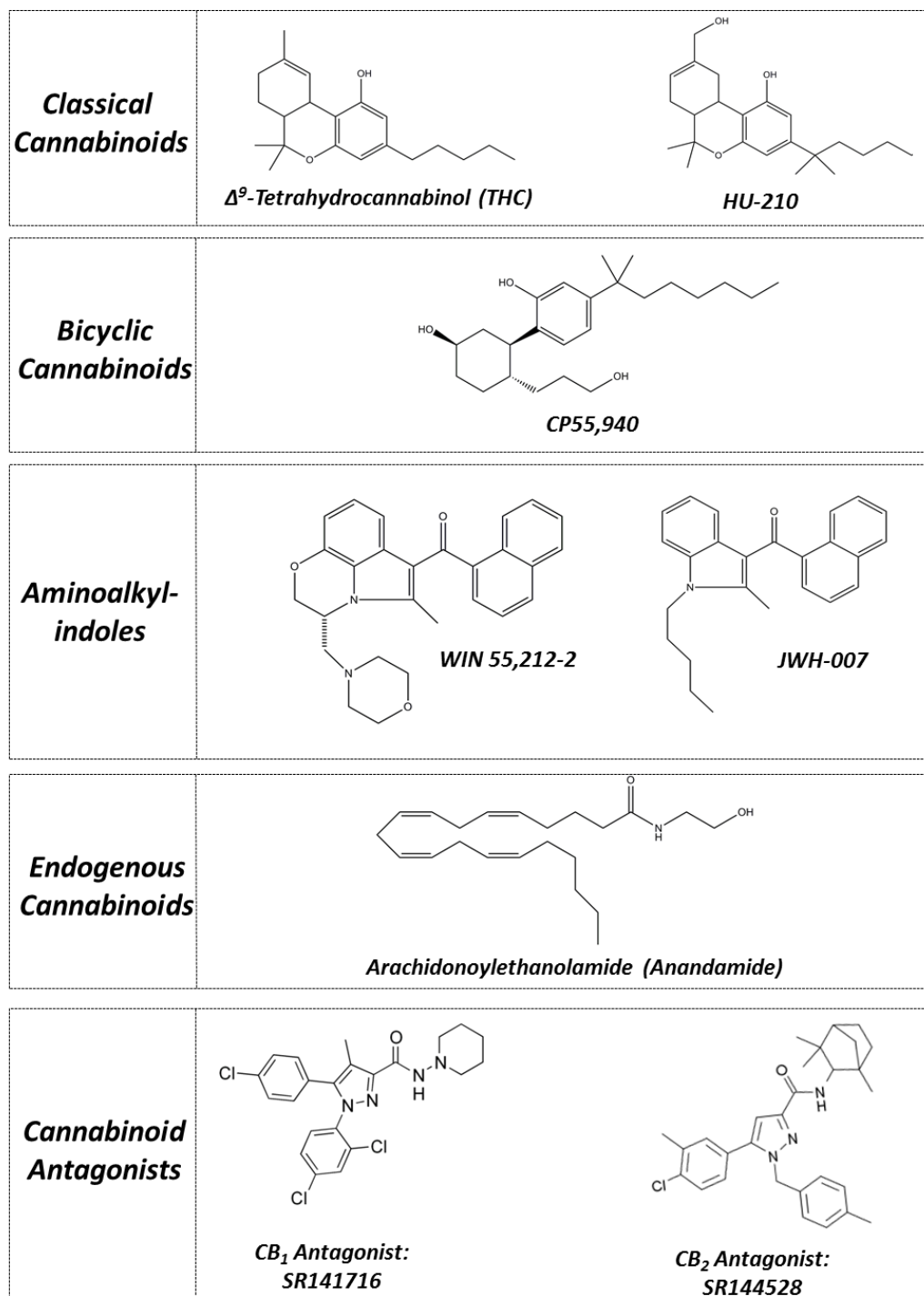


Figure 1.3 The four different classes of Cannabinoid Agonists: 1- Classical cannabinoids such as the natural compound THC, and its synthetic derivative HU-210, 2- Bicyclic (Non-classical) cannabinoids such as CP55,940, 3- aminoalkylindoles such as WIN 55,212-2 and JWH-007, and 4- Endogenous cannabinoids such as anandamide. Last panel shows two cannabinoid antagonists The CB₁ selective SR141716 and the CB₂ selective SR144528.

Cannabinoid agonists exert their effects through interacting with specific G-protein coupled receptors which are expressed in many body tissues. Those are primarily the cannabinoid receptors CB₁ and CB₂. The CB₁ receptor is most abundant in the central nervous system [64] and its activation mediates the psychoactive effects of cannabinoid agonists [65]. The CB₁ receptor however is also expressed in other body tissues such as in the gastro-intestinal tract [66] and can mediate therapeutic effects that will be later discussed in this chapter. The CB₂ receptor on the other has a very low expression in the CNS and does not mediate any psychoactive effects upon activation [67], it has been shown however that CB₂ is not completely absent from the CNS and that it is expressed at the mRNA and protein level in the rodent spinal cord [68]. CB₂ is mainly expressed in immune organs and white blood cells such as macrophages, neutrophils and basophils [69]. Its activation mediates anti-inflammatory and analgesic effects that will be discussed later in this chapter.

1.2.1 Therapeutic uses of Cannabinoids

1.2.1.1 Pain

Several groups have shown that cannabinoids can exert antihyperalgesic effects either through central CNS or peripheral mechanisms. The first evidence showing an involvement of cannabinoid receptors in antinociception was introduced by Calignano et al. [70] who demonstrated that the endogenous cannabinoid palmitoylethanolamide (PEA) can produce pain relief

effects in rats using the formalin test; this effect was blocked using a selective CB₂ antagonist, SR144528, indicating that the antinociceptive effect is predominantly mediated via the CB₂ receptor. These findings were further supported by the development of CB₂ selective agonists that lack CNS activity such as HU308 and AM1241 but which both resulted in pain relief while exerting no centrally mediated effects. Hanus et al. [67] showed the exclusivity of CB₂ receptors in mediating antinociception responses through demonstrating that the selective CB₁ antagonist SR141716A does not block the analgesic effects of different cannabinoid agonists in contrast to the CB₂ selective antagonist, SR144528.

The mechanism through which CB₂ activation result in anti-hyperalgesic mechanism is not completely understood, but it is hypothesised that this is mediated through neuronal mechanisms through activation of CB₂ receptors present at nerve termini and the spinal cord [68] and non-neuronal mechanisms mediated via CB₂ receptors present at

1.2.1.2 Cardiovascular effects

Cannabinoids exert benefits in cardiovascular disorders through many pathways. Bouchard et al. [71] investigated the cardio-protective effects of the endogenous mixed cannabinoid agonist, palmitoylethanolamide (PEA) in isolated perfused rat hearts exposed to ischemic reperfusion. The group showed that this agonist decreased myocardial damage upon pre-conditioning

ischemic reperfusion. This effect was blocked upon the use of the CB₂ selective antagonist SR144528 which indicates that CB₂ receptors play a major cardio-protective role upon ischemic reperfusion. The cardio-protective effect exerted by stimulating CB₂ receptors in the heart upon ischemic reperfusion have also been demonstrated *in-vivo* where pre-conditioning the heart with the mixed cannabinoid agonist WIN 55,212-2 decreased infarct size after re-perfusion, an effect that was blocked by the selective CB₂ antagonist AM251 [72].

Cannabinoid drugs have also been shown to have an anti-arrhythmic effect. The endogenous cannabinoid agonist, anandamide, was reported to decrease the occurrence of ischemic-induced ventricular fibrillation in rodents [73]. This anti-arrhythmic effect seems to be exclusively mediated through the CB₂ pathway as it was only selective CB₂ antagonists that blocked this effect and not CB₁ antagonists [74].

The cannabinoid system seems to have a role in heart failure as well. It was shown that animals experiencing experimentally induced heart failure with the selective CB₂ cannabinoid antagonist SR141716A increases blood pressure and has a negative effect upon the survival rate of the treated animals [75]. Wagner et al. have additionally shown that the mixed cannabinoid agonist HU-211 improves cardiac function in animals with induced chronic myocardial infarction as evident from an increase in diastolic and systolic cardiac pressure in the ventricles and atria [76].

1.2.1.3 Cancer

The first reported evidence behind the anti-neoplastic effects that can be exerted by a cannabinoid dates back to 1975 when Munson et al. showed that THC can inhibit the growth of Lewis lung cancer through blocking DNA synthesis in malignant cells [77, 78]. Various reports followed showing that cannabinoids can inhibit the growth of a number of cancer cell lines such as L1210 and K-562 leukemia cell lines also through blocking DNA synthesis [79, 80].

Further studies showed that cannabinoids can inhibit the tumour growth and induce apoptosis in a number of common cancers such as gliomas, lymphomas, breast, prostate, skin, and pancreatic cancers [81]. The mechanism by which these cannabinoids inhibit tumour growth has not been completely elucidated yet, although it has been shown that cannabinoids exert these effects through mechanisms that are receptor mediated where CB₁/CB₂ activation by cannabinoid agonists leads to the down regulation of protein kinase B (Akt), phosphoinositide 3-kinase (PI3K), and extracellular signal-regulated kinase (ERK) signalling pathways which all play a role in tumour growth [82]. Anti-tumour activities were also displayed by cannabinoid agonists through non-receptor mediated mechanisms [83].

1.2.1.4 Appetite

The endocannabinoid system and appetite to food seem to be strongly correlated in humans. Activation of Cannabinoid receptors using cannabinoid agonists seems to stimulate appetite. Few studies reported that administration of low oral doses of THC (2.5mg) can induce food appetite in people who suffer cancer or AIDS related anorexia [84, 85]. Mattes et al. additionally conducted a comprehensive study which investigated the appetite inducing effects of oral, rectal and pulmonary delivery of THC, which all resulted in an increase in appetite to varying extents.

Reversely, inhibiting cannabinoid receptors using cannabinoid antagonists suppresses appetite [86]. In fact, Rimonabant, selective CB₁ antagonists has been commercialised as a weight loss drug until its license was withdrawn by the FDA due to its psychiatric side effects which include depression and suicidality [87].

1.2.2 Irritable bowel disease and the role of Cannabinoids

Inflammatory bowel disease (IBD) is a term that covers two distinct chronic inflammatory bowel conditions: Crohn's disease (CD) and ulcerative colitis (UC) [88]. Whilst Crohn's can affect any part of the gastrointestinal tract i.e. from the mouth to the anus, ulcerative colitis is restricted to the colon. Additionally, a key difference between the two disorders is that CD affects the entirety of the bowel wall (transmural) while UC is restricted to the epithelial barrier of the gut (non-transmural) [89].

IBD disorders generally cause an increase in intestinal motility and faecal transit, leading to poorer digestion and consequently pain and diarrhoea which make medical treatment essential. In fact, up to 50% of those suffering from IBD would ultimately require surgical intervention at some point during their illness [90]. IBD is classically treated with anti-inflammatory salicylates (such as Mesalazine, olsalazine and sulfasalazine) [91-93] and steroids (such as hydrocortisone, budesonide and cortisone) [94-97]. Immunosuppressants such as azathioprine, tacrolimus and methotrexate are also used [98-101]. Despite this wide range of therapeutics that is used in the treatment of IBD, patients constantly develop resistance to these drugs. This justifies the continued efforts to find alternative therapies for these gastrointestinal disorders.

Massa et al. [102] have been among the first to suggest that the cannabinoid system can play a significant role in protecting the gut from chronic inflammations. In fact cannabinoids can help patients suffering IBD through interacting with two distinct cannabinoid receptors that are present in the gut and in plasma; CB₁ and CB₂.

Griffin et al. [66] showed that CB₁ receptors, unlike CB₂, are expressed at the mRNA level in the guinea pig myenteric plexus, while both CB₁ and CB₂ receptors were detected in the whole gut, possibly due to contamination with macrophages which highly express the CB₂ receptor. CB₁ receptors have been additionally shown to be expressed at the mRNA level in the human stomach and colon [103]. Furthermore, CB₁ receptors have shown immunoreactivity in

the mesenteric plexus of the ileum and colon of the pig gut in immunohistochemistry studies [104].

CB₂ receptors on the other are more associated with the body's immune system which plays a vital role in IBD. CB₂ receptors have been shown to be highly expressed in monocytes, macrophages and B and T immune cells at the mRNA level through RT-PCR analyses [105, 106]. Using flow cytometry, Graham et al. [69] recently reported the protein expression of CB₂ receptors in natural killer (NK) cells, B-lymphocytes, monocytes and neutrophils.

Cannabinoid agonists can exert their virtues in the therapy of IBD and gastrointestinal disorders in general through a multitude of pathways.

The cannabinoid agonist WIN 55,212-2 has been shown to significantly reduce stress induced gastric ulcers in rodents which were specifically blocked by CB₁ antagonists and not CB₂ antagonists indicating that the anti-ulcerative effect is exclusive to the CB₁ pathway [107]. This effect could be associated with the demonstrated ability of WIN 55,212-2 to inhibit the pentagastrin induced acid secretion in the rat gut [108].

Additionally, Cannabinoid receptor agonists (such as WIN 55,212-2, Δ^9 -tetrahydrocannabinol (THC) and cannabidiol) have been shown to modulate gastric motility and emptying only through CB₁ receptors [109, 110] as evident from the exclusive ability of CB₁ selective antagonists to block this effect.

CB₁ receptors seem to play an important role in the inhibition of intestinal motility and are up-regulated in inflammatory bowel disease [111]. Cannabinoid agonists have been shown to inhibit electrically induced contractions in the guinea pig myenteric plexus in a manner similar to that mediated by α_2 -adrenoceptors and μ -opioid receptors. Using α_2 -adrenoceptor and μ -opioid antagonists however does not block the activity of cannabinoid agonists, unlike the selective CB₁ cannabinoid antagonist SR141716A which blocked the effect of WIN 55,212-2 in inhibiting electrically induced contractions of intestinal segments. This proves that the intestinal motility inhibitory effects exerted by cannabinoid agonists are purely and directly mediated through the cannabinoid system.

CB₂ receptors also play a vital role in the treatment of IBD. CB₂ activation by mixed cannabinoid agonists such as WIN 55,212-2 has been shown to attenuate the LPS induced acceleration of gastrointestinal transit in rats [112]. CB₂ activation also leads to suppressing the levels of cyclooxygenases and inducible nitric-oxide synthase, which indicates that nitric oxide and prostaglandins play a role in mediating the CB₂ mediated effect upon intestinal motility and transit. Cannabinoids have also been reported to exert an anti-inflammatory effect in mice that were chemically induced with colitis [102].

It can also be argued that CB₂ receptors play a role in pain management in IBD. As previously mentioned, CB₂ receptors mediate antinociception effects when

activated by agonists [67, 70] which can offer the additional benefit of pain relief in patients suffering from IBD.

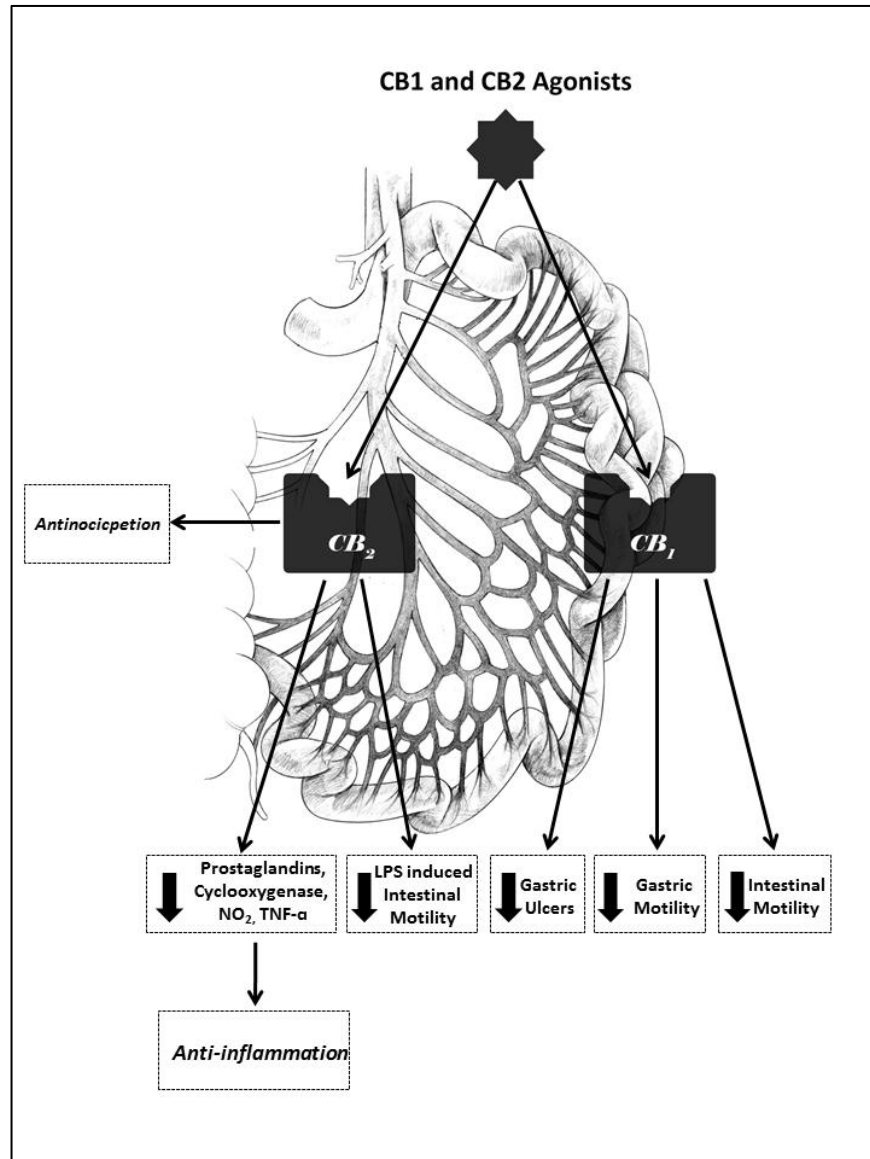


Figure 1.4 Role of Cannabinoids in the treatment of inflammatory bowel disorders. CB_1 receptors, present in intestinal tissue, mediates intestinal and gastric motility and suppresses the formation of gastric ulcers. CB_2 receptors which are present in a number of white blood cells such as macrophages, neutrophils and monocytes suppresses inflammation by inhibiting the release of pro-inflammatory mediators such as prostaglandins, cyclooxygenase, Nitric oxide (NO_2) and $TNF-\alpha$ also mediates anti-hyperalgesic effects

CNS Adverse effects of Cannabinoids

Despite the previously discussed virtues of cannabinoids in the biomedical field, the CNS adverse effects that are produced by these compounds remain a major obstacle that limits the application of cannabinoids in the treatment of many illnesses.

The first accounts of the documented CNS effects produced by cannabinoids come from various anecdotal reports that recorded observed psychotic effects in people who smoked cannabis [113-117]. The reported effects varied, but among the common psychotic effects reported were paranoia, persecutory and grandiose delusions, hallucinations, depersonalisation and memory impairment.

In a more controlled study, the LaGuardia Committee reported in 1944 that 12.5% of subjects who were exposed to 30-50mg oral or 8-30mg inhaled cannabis suffered from different CNS adverse effects [118]. Similarly Ames studied the effect of orally ingested THC at doses of 50-70mg with 12 subjects. They reported classical psychotic effects such as paranoia, thought and action dissociation, hallucinations and memory impairment [119]. In a more comprehensive study, D'Souza et al. investigated the dose dependant CNS effects of intravenously injected THC and showed a clear association between THC dose and CNS effects such as memory impairment in verbal recall, attention and memory [120].

The resemblance between the mental symptoms produced by cannabinoid consumption and schizophrenia is strong and was recently reviewed by Sewell et al. [121]. Positive symptoms manifested in schizophrenia such as suspiciousness, paranoia, grandiose delusions and fragmented thinking have been also reported in subjects treated with varying doses of THC [119, 120, 122]. Negative symptoms observed in schizophrenia such as emotional withdrawal and psychomotor retardation have been similarly reported in healthy volunteers getting I.V. doses of THC [120]. Cognitive deficits such as difficulties in learning and impairment of short-term memory and failure in decision making, that are produced upon consuming cannabis are very common in patients suffering from schizophrenia. Retardation in verbal memory seems to be the most expressed cognitive deficit produced upon cannabis consumption [123] and observed in schizophrenia patients [124].

Biomarkers in the nervous system were used to study the effect of cannabinoids on brain function. These biomarkers are measured as a function of electroencephalography (EEG) responses to various stimuli. These include 'auditory sensory gating' which is a measure for salient (auditory) stimuli. Auditory sensory gating can be disrupted as a result of acute exposure to cannabinoid agonists in animals [125, 126] and chronic exposure in humans [127, 128]. Another biomarker, P300, which is associated with memory updating and attention, has been shown to be altered upon acute exposure to cannabinoids [129].

Although it can be argued that cannabis, despite its obvious transient alteration of mental function, is relatively a safer drug to be consumed than alcohol [130], the chronic exposure of the CNS to this compound has been shown to be highly associated with the development of psychotic disorders such as schizophrenia in later life [131]. The extent of cannabinoid harmfulness in the short and long term might be disputed, but there is a consensus in the scientific community that the CNS dangers produced by cannabinoids cannot be overlooked if these compounds were to be used in the treatment of chronic diseases such as IBD. It is hence vital to find an avenue where cannabinoids can be therapeutically used in the periphery while averting access to the CNS which might lead to the previously discussed adverse effects.

A few groups attempted to therapeutically exploit the cannabinoid receptors in the periphery while maintaining minimal access to the brain. Cluny et al. [132] reported a mixed cannabinoid agonist, SAB-378, which was successful in suppressing intestinal motility in mice through the CB₁ receptor and had minimal effect upon psychomotor function in mice. The drug however, failed in decreasing the degree of colitis when experimentally induced in mice. Additionally, Mitchell et al. [133] reported a THC derivative (ajulemic acid) that exerted anti-hyperalgesic activity in mice but did not disrupt psychomotor function in mice.

1.3 Aims and Objectives

The work described in this thesis aims at identifying possible pathways through which a cannabinoid drug can be stably conjugated to a polymer while maintaining its pharmacological activity. It is hypothesised that stably conjugating a cannabinoid compound to an anionic PAMAM dendrimer can maintain oral bioavailability of the said cannabinoid while retarding its access across the blood brain barrier.

If such a conjugate is pharmacologically active and can still activate cannabinoid receptors, this would achieve the therapeutic aim of cannabinoid agonists in the treatment of many diseases such IBD when administered orally. Additionally, the hydrophilic and molecularly large nature of the polymer is expected to retard the access of the conjugate across the tight blood brain barrier which would lead to avoiding the many adverse CNS effects that are exerted by cannabinoid agonists. The major two objectives of this thesis are hence:

- 1- Identifying a chemical pathway through which a cannabinoid agonist can be modified and conjugated to a polymer without any loss in its pharmacological activity.
- 2- Proving that PAMAM dendrimers, which are to be conjugated to the cannabinoid agonist, are capable of permeating across the intestinal mucosa and not the blood brain barrier.

Chapter 2 looks into the biopharmaceutics of PAMAM dendrimers and the permeability of different *in-vitro* cell models to these dendrimers. This chapter aims at showing that anionic PAMAM dendrimers permeate readily across *in-vitro* intestinal models such as the CaCo-2 cell model. Additionally the transport of these dendrimers across tighter cell monolayers that have been used as *in-vitro* models for the blood brain barrier is also investigated. This chapter looks additionally into the effect of pro-inflammatory mediators upon the permeability of different cell barrier models to PAMAM dendrimers.

Chapter 3 in this thesis aims at a better understanding of the structure activity relationship (SAR), and identifying sites on specific cannabinoid agonists that can be chemically modified without any loss of pharmacological activity in preparation for conjugating it to a PAMAM polymer. Specific functional groups can then be introduced through this site which facilitates the interaction between the cannabinoid agonist and the PAMAM polymer to create a stable conjugate which is the ultimate aim of this chapter. To achieve these objectives, a series of different novel cannabinoid agonists were synthesised in house with different modifications. The pharmacological activity of these compounds was tested using a macrophage cell model to assess the anti-inflammatory activity of these novel cannabinoids.

Chapter 4 describes two different PAMAM conjugations and aims at:

- 1- Synthesis of PAMAM-radiolabel conjugates using an amide linkage and testing stability of these conjugates in biological conditions. These radiolabelled dendrimer were synthesised to probe the stability of the amide linkage in biological conditions to assess its ability for the stable coupling of a cannabinoid to a dendrimer. Additionally, the radiolabelled PAMAM dendrimers can be used as a tool to probe their biopdistribution in future *in-vivo* studies.
- 2- Synthesis of a PAMAM-cannabinoid conjugate using a similar amide linkage and assessment of the pharmacological activity of the conjugate.

Chapter 2

***Dendrimer Transport across Biological
Barriers***

2.1 Introduction

2.1.1 The Intestinal Barrier

The intestinal barrier represents the largest interface between a higher organism's systemic circulation and its environment. While it plays a significant role in protecting the body from the permeation of many xenobiotics and micro-organisms, it also offers a large surface area and a long transit time where useful nutrients and drugs can permeate to the blood.

The interface between the intestinal lumen and the blood includes many components that influence intestinal permeability [134].

The unstirred water layer is estimated to be between 200 μ m and 800 μ m in depth [135], this outermost component of the intestinal barrier can limit the absorption of many hydrophobic compounds. The mucous layer can protect the intestinal epithelia from bacterial adhesion, physical friction and chemical interaction with the contents of the intestinal lumen but it can limit the permeation of many compounds. The epithelial layer represents the most important barrier between the intestinal lumen and the systemic circulation where tight junctions can restrict the permeation of potentially harmful substances such as endotoxins, and consequently many drugs and therapeutic molecules.

The connective tissue plays a very limited role in the intestinal permeability to most compounds. Ghandehari et al.[136] showed that the connective tissue doesn't play a role in the passage of macromolecules.

The intestinal restrictiveness is usually assessed by investigating the permeation of different paracellular markers (sugars like sucrose and mannitol and high molecular weight markers such as PEG polymers) and transepithelial markers (hydrophobic molecules such as propranolol) across the intestine. Intestinal restrictiveness can be also assessed and quantified in terms of transepithelial electrical resistance (TEER) which is a measure of the restrictiveness to ion transport across the epithelial barrier and is measured as a function of the area of the barrier in $\Omega \cdot \text{cm}^2$.

Mannitol permeability coefficients across the rat intestine have been reported to range between $1.5 \times 10^{-6} \text{ cm} \cdot \text{s}^{-1}$ in the colon to $5.5 \times 10^{-6} \text{ cm} \cdot \text{s}^{-1}$ in the jejunum while propranolol permeability coefficients ranged between $20 \times 10^{-6} \text{ cm} \cdot \text{s}^{-1}$ and $120 \times 10^{-6} \text{ cm} \cdot \text{s}^{-1}$ in the rat jejunum and colon, respectively [137]. These results come in correspondence with reported TEER values in the rat intestine: 20-60 $\Omega \cdot \text{cm}^2$ in the jejunum, and up to 180 $\Omega \cdot \text{cm}^2$ in the colon. [137, 138]

2.1.2 The Blood Brain Barrier

The central nervous system (CNS) is protected from harmful compounds by the blood brain barrier (BBB), a barrier that is far more restrictive than the intestine. Whilst the physical barrier of the BBB is primarily formed by the tight apposition of endothelial cells lining the microvasculature, the restrictiveness of the barrier is further governed through the interplay between astrocytes, pericytes and the brain endothelial microenvironment in general [139].

- *Astrocytes* envelop the majority of the microvascular endothelial surface in the brain (>99%)[140] and play an important role in the restrictiveness of the BBB. This is evidenced by increases in TEER and decreases in mannitol permeability across brain microvascular endothelial cells when cultured in the presence of astrocytes [141, 142]. It is thought that astrocytes enhance BBB restrictiveness through up regulation of tight junctional proteins and efflux transporters such as P-gp [143].
- *Pericytes* are smooth muscle cells located on the microvascular surface of the BBB. Pericytes contribute to vessel formation and blood flow regulation in the brain [144]. Recently, it has been suggested that pericytes can enhance the restrictiveness of the BBB to a wide variety of compounds through expressing a number of digesting enzymes that can

limit the entry of their substrates [145, 146]. Additionally, pericytes play a role in the phagocytosis of other molecules [147].

Unlike the intestinal barrier, which is permeable to a wide variety of compounds, most xenobiotic molecules have limited or no access to the CNS due to the blood brain barrier's high restrictiveness. BBB TEER values, for instance, were reported to be between 1500 and 2000 $\Omega \cdot \text{cm}^2$ [148, 149] where the permeability coefficient of [^{14}C] Mannitol across the blood brain barrier of the rat has been shown to be as low as $0.085 \times 10^{-6} \text{ cm} \cdot \text{s}^{-1}$ [150]

Table 2.1 summarises the essential differences between the previously discussed intestinal and blood-brain barriers studied *in-vivo*.

Table 2.1 Comparison between the intestinal and the blood brain barriers

Barrier Property	Intestinal Barrier	Blood Brain Barrier
Major cellular component	Epithelial layer [134]	Capillary endothelial layer [139]
Components contributing to restrictiveness	Unstirred water layer Mucous gel Capillary endothelium [134]	Astrocytes Pericytes [139]
<i>in-vivo</i> TEER ($\Omega.cm^2$)	20 – 60 (Small Intestine) 100 - 180 (Colon) [137, 138]	1500 – 2000 [148, 149]
Permeability to [^{14}C] Mannitol $\times(10^{-6} cm.s^{-1})$	5.5 (Small Intestine) 1.5 (Colon) [137]	0.085 [150]
Expression of Efflux Transporters	Moderate	Very High

2.1.3 *in-vitro* Assessment of transport across the intestinal and blood brain barriers.

One of the most efficient methods that can provide some judgement on the rate and extent of absorption of new molecular entities across different biological barriers is the assessment of their transport across *in-vitro* cell monolayers that in some way mimic the biological barrier of interest. The transport of a molecule across a cell barrier is typically expressed in the terms

of a 'permeability coefficient (P_{app})' which expresses the relative rate of a drug's transport across a cell line normalised to the applied mass of molecule.

CaCo-2 cells are human derived epithelial adenocarcinoma cells. CaCo-2 cell monolayers are utilised as an *in-vitro* model for intestinal absorption. Transport data from CaCo-2 cell models has been very well correlated with the intestinal barrier permeability to many small molecular weight drugs [151, 152] as shown in *Figure 2.1*.

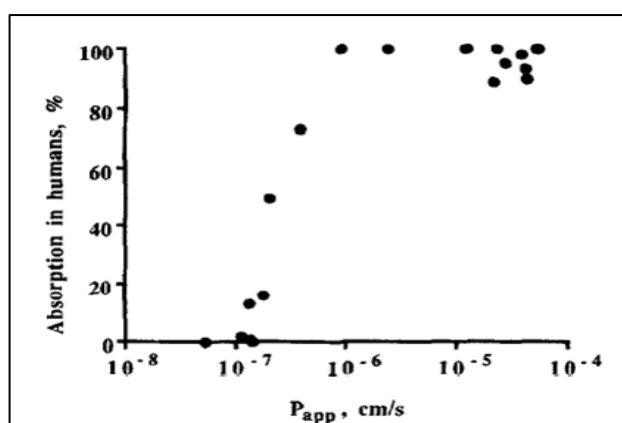


Figure 2.1 % Absorption in humans Vs. apparent P_{app} across CaCo-2 monolayers [151]

This model has been hence used as an *in-vitro* tool to predict the intestinal absorption of various drugs [153].

Another tool used for the *in-vitro* screening of intestinal permeability is the Canine Madin-Darby Canine Kidney (MDCK II). Like CACO-2 cells, MDCK cells can develop into epithelial cells and form tight junctions [154]. Chao et al. [155] was among the first to discuss the use of the MDCK cell line as an *in-vitro*

barrier for assessing intestinal transport . P_{app} data in the MDCK II model has been shown to strongly correlate with human absorption data and not surprisingly with P_{app} data in CACO-2 cells [156].

The blood brain barrier is far more restrictive than the intestinal barrier as previously discussed. Therefore, an *in-vitro* system that models the blood brain barrier has to be a very restrictive one. The previously discussed MDCK cell line comprises two different clones. The MDCK II, has been extensively used to predict intestinal permeability. The MDCK I clone however is significantly more restrictive and can achieve transepithelial electrical resistance (TEER) values of more than $2000\Omega\cdot\text{cm}^2$. Although the MDCK I is not a perfect model for the BBB as it doesn't simulate metabolism and efflux mechanisms expressed *in-vivo*, its high resistance and the ease with which the cells can be grown has led many to use it as a permeability screen for BBB penetration of various drugs [157].

2.1.4 Aims and Objectives

The ultimate aim of the work in thesis as described earlier is to create dendrimer-cannabinoid conjugates that achieve oral bioavailability and pharmacological effect in the treatment of IBD in the periphery while limiting CNS access and hence central side effects of the cannabinoids. The work described in this chapter aims to investigate the transport of different anionic and cationic dendrimers across different *in-vitro* barrier models. These studies were conducted to predict the transport extents of dendrimers with various

sizes across different biological barriers such as the intestinal mucosa and the blood brain barrier. This was attempted to test the hypothesis that dendrimers can serve as vehicles for drugs with CNS side effects such as cannabinoids to achieve selective transport across the intestinal barrier and not the BBB. Additionally, it was attempted to predict the influence of pro-inflammatory mediators such as TNF- α which are over expressed in illnesses such as IBD upon the permeability of the intestinal barrier to different dendrimers, as it was hypothesised that inflamed intestinal tissue would be more permeable to dendrimers than non-inflamed tissue which would achieve better targeting in the therapy of IBD.

2.2 Materials and Methods

2.2.1 Materials

PAMAM dendrimers (G1.5, G3.5, G3, G4 and G5.5), sodium fluorescein (F-Na), sodium fluorescein isothiocyanate (FITC) and N-hydroxysulfosuccinimide (sulfo-NHS) were from Sigma-Aldrich (Poole, UK). Oregon Green 488-cadaverine was from Invitrogen (Paisley, UK) 1-Ethyl-3(3-dimethylaminopropyl) carbodiimide hydrochloride (EDC) was from Pierce (Cramlington, UK). Radiolabeled compounds [^{14}C] Mannitol and [^3H] Propranolol American Radiolabeled Chemicals (St. Louis, USA). All other chemicals were from Fisher Scientific (Loughborough, UK).

2.2.2 Methods

Synthesis and purification of Oregon Green- anionic PAMAM conjugates

Dendrimers are fluorescently labelled to allow analysis and quantification in cell transport studies. Anionic PAMAM dendrimers were fluorescently labelled with Oregon Green cadaverin 488 (OG). Anionic PAMAM dendrimers (supplied as 10% wt. /v solutions in methanol) were transferred to a round bottom flask and dried at 40°C *in vacuo*. The PAMAM residue was then redistilled in phosphate buffer saline (PBS), pH 7.4 to create a final concentration of 10mg PAMAM/mL. After 5 minutes of stirring, 30 fold excess of EDC and 10 fold excess of sulfo-NHS were added to the flask. The solution was then allowed to stir for 30 minutes. Three molar equivalents of pre-prepared 5mg/mL OG-cadaverine solution in DMSO were added to the mixture and the reaction mixture was allowed to react overnight in the dark and samples were taken periodically for thin layer chromatography (TLC) analysis using methanol as a mobile phase. Crude reaction mixtures were dried at 40°C *in vacuo* and reconstituted in 1mL of distilled water. PAMAMs G3.5, G5.5 were then purified from unreacted fluorophore, buffer salts and catalysts by gel filtration chromatography using disposable PD-10 columns (GE healthcare, UK) for three consecutive times. G1.5 PAMAM reconstituted solutions were transferred to disposable dialysis chambers (MWCO 1,000, Float-A-Lyzer, Spectrum Europe

BV) and thoroughly dialysed overnight against large volumes of distilled water and further purified using gel filtration chromatography (Sephadex G10).

Synthesis and purification of fluorescein isothiocyanate (FITC) - cationic PAMAM conjugates

Cationic PAMAM dendrimers (G3 and G4) were fluorescently labelled with fluorescein isothiocyanate (FITC). Cationic PAMAM dendrimers (supplied as 10% wt. /v solutions in methanol) were transferred to a round bottom flask and dried at 40°C *in vacuo*. The PAMAM residue was then re-distilled in phosphate buffer saline (PBS), pH 7.4 to create a final concentration of 10mg PAMAM/mL. After 5 minutes of stirring, 1.5 molar equivalents of pre-prepared FITC solution in acetone were added to the mixture and the reaction mixture was allowed to react overnight in the dark and samples were taken periodically for thin layer chromatography (TLC) analysis using methanol as a mobile phase. Crude reaction mixtures were dried at 40°C *in vacuo* and reconstituted in 1mL of distilled water. PAMAMs G3 and G4 were then purified from unreacted fluorophore and buffer salts by gel filtration chromatography using disposable PD-10 columns (GE healthcare, UK) for three consecutive times.

Cell cultures

CaCo-2, MDCK I and MDCK II cells were obtained from the European Tissue Culture Collection ECACC (London, UK) and cultured using Dulbecco's Modified Eagle medium (DMEM) supplemented with 10% (v/v) heat inactivated FBS and 2% penicillin G/Streptomycin (100U/mL). Cell cultures were maintained at 37°C in 5% CO₂/ 95% atmospheric air and relative humidity. While cells were grown in T-25 and T-75 culture flasks, they were routinely cultured to 70-80% confluence. CaCo-2 cells were seeded at densities of 250,000 cells/cm² while MDCK I and MDCK II cells were seeded at densities of 45,000 cells/cm² on Transwell® clear culture inserts (24 well, 6.5mm diameter, 0.4µm pore size, Corning, UK). CaCo-2 cells were cultured on inserts for 21-28 days post confluence and MDCK I and MDCK II cells were cultured for 3-4 days in preparation for cell transport studies.

Transport Studies

Transport studies were conducted upon CaCo-2, MDCK I and MDCK II cell monolayers that displayed TEER values of at least 300 Ω.cm², 3000 Ω.cm² and 120 Ω.cm², respectively. TEER values were measured using an EVOM volt-ohm meter (World Precision instruments, Sarasota, USA) connected to an Endohm chamber.

Culture media was aspirated and the apical media was carefully washed twice with warm PBS. The inserts were transferred to fresh 24 well plates. Pure DMEM F-12 (without phenol red) media was applied to the washed apical and

basal compartments of the inserts and the cells were left to equilibrate for 30 minutes at 37°C. 200µL doses of the probe (PAMAM dendrimers, Sodium Fluorescein, Oregon Green, [¹⁴C] mannitol or [³H] Propranolol) were carefully added to the apical chamber. Inserts were then placed on an orbital shaker rotating at 50RPM at 37°C. Cumulative transport of probes was assessed by quantifying the probe in 200 µL samples that were taken at pre-determined time points over 2 hours. All aspirated samples were directly replaced with the same volume of blank DMEM-F12.

PAMAM-OG and PAMAM-FITC conjugate stability in transport studies

Stability of fluorescent PAMAM conjugates (including OG and FITC) was tested in all transport studies by analysing samples before and after the transport studies conducted across cells at 37°C in relative humidity using gel filtration chromatography. PD-10 pre-packed columns (comprising Sephadex G25 gel) were used to analyse all dendrimers except PAMAM G1.5 whose smaller molecular size has necessitated the use of a gel with a smaller pore size, Sephadex G-10. All the used gels were validated using known high molecular size and small molecular size markers.

Analysis of fluorescent and radiolabeled probes

Fluorescent Samples were analysed using micro plate fluorescence reader (FLUOstar Optima, BMG) using excitation and emission wavelengths of λ_{ex} 485nm and λ_{em} 520nm, respectively for PAMAM-OG, PAMAM-FITC and F-Na.

Fluorescent readings were quantified using calibration curves constructed in cell transport media (i.e. DMEM F-12). Background fluorescence values were subtracted from the calibration curve and the total mass of the probe absorbed was quantified by correcting to the total volume of the receiver chamber and loss during sampling.

Analysis of radiolabeled probe accumulation in the receiver chamber was determined using liquid scintillation counter (LSC) (Wallac 1409, PerkinElmer Life Sciences, Boston, MA, USA).

Biocompatibility Testing

The effect of PAMAM dendrimers on the integrity of the monolayers in transport studies was assessed by measuring TEER before and after transport experiments and by the assessment of the permeation of the paracellular marker, [^{14}C] mannitol and the transcellular marker [^3H] Propranolol across the monolayers in the presence or absence of co-incubated PAMAM dendrimers.

Isolated Perfused Rat Gut (IPrG)

Male Sprague Dawley Rats (weight 250-350g) were euthanized using terminal anaesthesia delivered as an intraperitoneal injection of 200mg/kg pentobarbital (Euthatal[®]) followed by cervical dislocation. The rat was placed on a heating plate to maintain a warm temperature during the procedure. The abdomen was excised and the intestines were exposed and gently moved to the left-hand side of the animal to expose the mesenteric artery. The mesenteric artery was pierced using a G25 needle and a PE-10 tubing (attached

to a perfusate reservoir) through a peristaltic pump is inserted to the mesenteric artery through the formed piercing and tied using a surgical stitch. The portal vein is then located at proximity of the liver and incised using surgical scissors. A PE-50 tubing is inserted to the vein and secured by tying it using surgical stitches.

The perfusate was an isotonic, buffered (pH 7.4) solution of Glucose (2.0g/L) , KCl (0.35g/L), MgSO₄.7H₂O (0.29g/L) , NaHCO₃ (2.10g/L) , CaCl₂.2H₂O (0.37g/L) , NaCl (6.92g/L) , KH₂PO₄ (0.16g /L), Bovine Serum Albumin (BSA) (40.0g/L) in distilled water.

The perfusate (warmed at 37°C, continuously bubbled with 95% CO₂/5% O₂ and continuously stirred using a magnetic stirrer) is pumped through the mesenteric artery at 8mL/min and the blood was cleared out from the mesenteric bed and drained out of the portal vein for two minutes before redirecting the out flow from the portal vein to the feeding perfusate reservoir to create a closed re-circulating system.

The intestines are then clamped using two clamps, one positioned at 4 cms down from the stomach and one 8 cms down from the stomach. The clamped section is rested on gauze wetted with warm saline and is continuously wetted with warm saline to maintain its humidity. A 2mL probe solution dissolved in PBS, pH 7.4 is intraluminally injected between the two clamps, and the needle is then secured in the injection site to avoid fluid leakage out of the lumen.

Figure 2.2 displays the setting of the experiment.

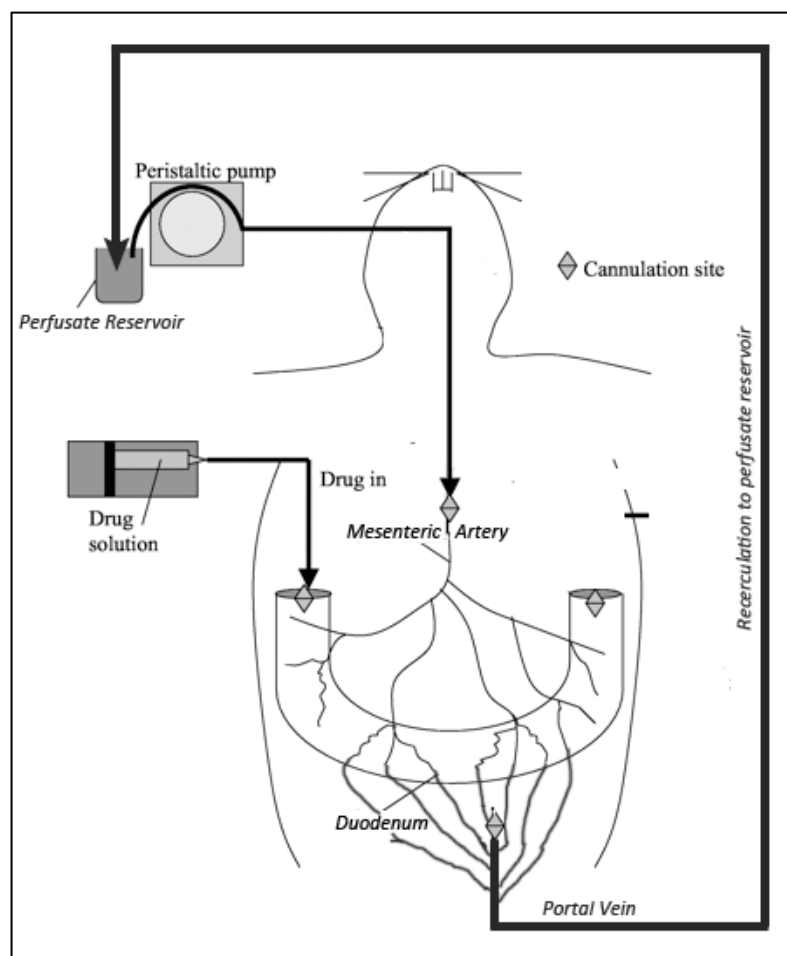


Figure 2.2 Experimental setting for the isolated perfused gut model. Adapted from [158]

2.3 Results and Discussion

2.3.1 *Synthesis, Purification and Stability Testing of anionic PAMAM – OG and cationic PAMAM-FITC conjugates*

The lack of a chromophore that absorbs UV light at wavelengths in PAMAM dendrimers makes it very difficult to quantify these polymers at low concentrations. Hence, it was necessary to fluorescently label both anionic and cationic PAMAM dendrimers to facilitate their quantitation in cell transport experiments. Oregon Green Cadaverine (OG) was the fluorescent label of choice for labelling anionic PAMAM dendrimers as it contains a free amine that can react with the carboxylic groups at the surface of these negatively charged polymers. *Figure 2.3* illustrates the synthesis and purification of a PAMAM G3.5-OG conjugate. All other anionic PAMAMs were conjugated to OG cadaverine using the same methods.

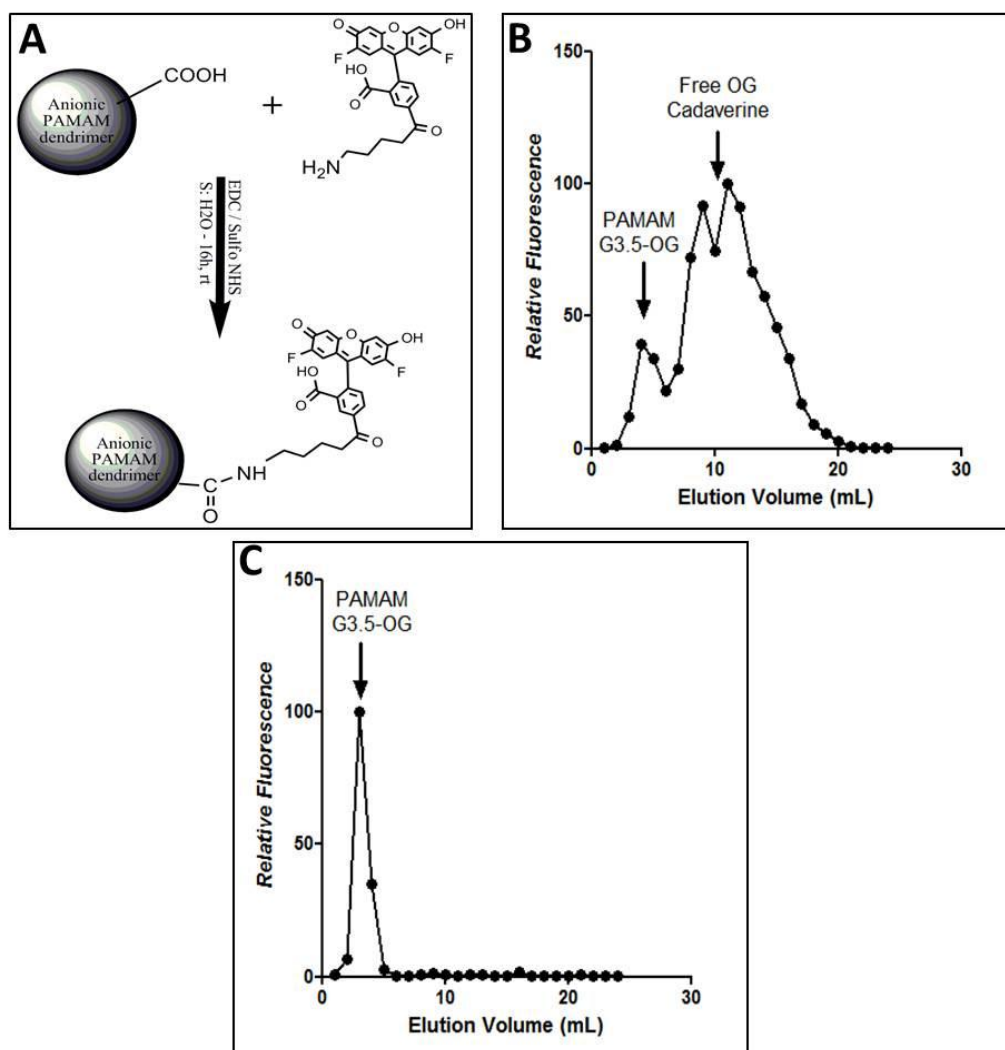


Figure 2.3 (A) Schematic showing the synthesis of conjugating an anionic PAMAM dendrimer to OG cadaverine. (B) GPC chromatogram (using PD-10 columns) of a crude PAMAM G3.5-OG synthesis mixture after a 16 hour reaction. (C) GPC chromatogram (using PD-10 columns) of the PAMAM G3.5-OG conjugate after its purification from the crude mixture using GPC.

After purification, the number of OG molecules attached to each dendrimer was quantified by UV analysis. Although 3 molar equivalents of Oregon Green were used in each reaction, the average number of Oregon Green molecules attached to each dendrimer ranged between 1 and 1.4.

Cationic PAMAM dendrimers were labelled using fluorescein isothiocyanate (FITC) which readily reacts with the free amines present on the cationic PAMAMs' surfaces. *Figure 2.4* illustrates the synthesis and purification of a PAMAM G3-FITC conjugate. All other cationic PAMAMs were conjugated to FITC using the same methods.

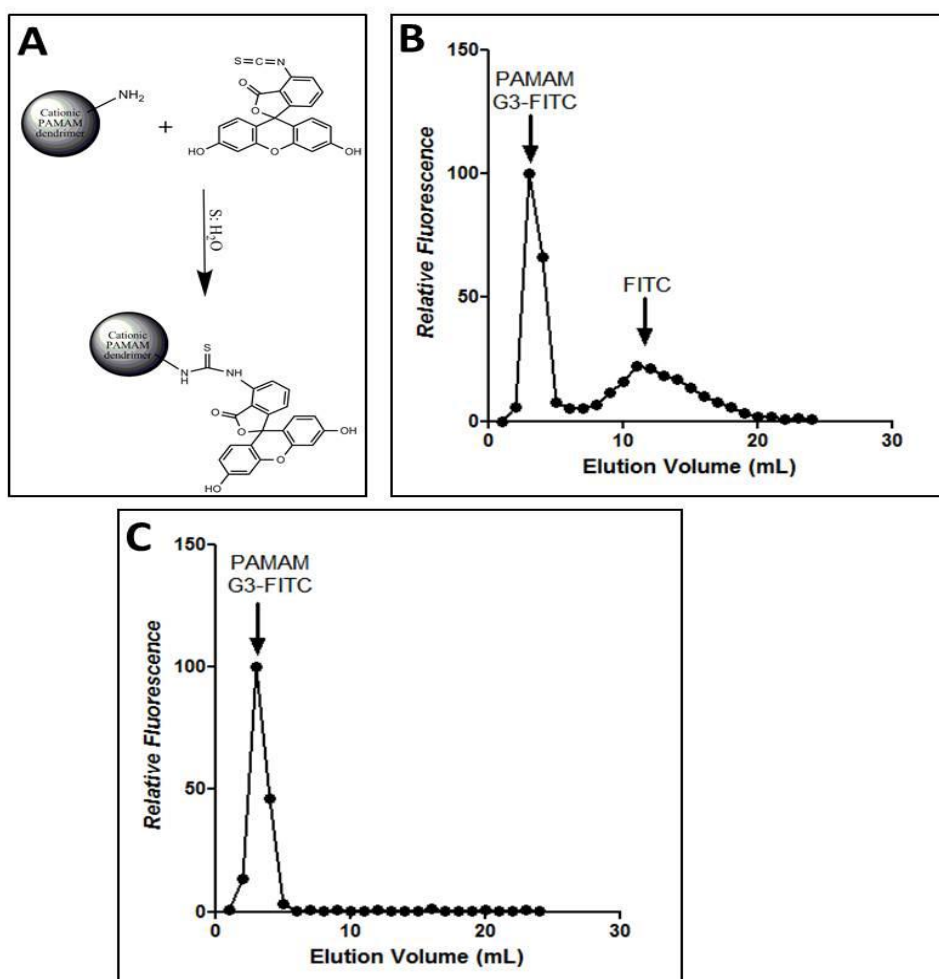


Figure 2.4 (A) Schematic showing the procedure of conjugating a cationic PAMAM dendrimer to FITC. (B) GPC chromatogram (using PD-10 columns) of a crude PAMAM G3-FITC synthesis mixture after a 4 hour reaction. (C) GPC chromatogram (using PD-10 columns) of the PAMAM G3-FITC conjugate after its purification from the crude mixture using GPC.

Figure 2.4 (B) shows the GPC chromatogram of the crude reaction mixture of PAMAM G3 dendrimer and FITC after a 4 hour reaction period. It displays high cationic PAMAM - FITC reaction efficiency in comparison to OG - anionic PAMAM reactions. This can be noticed from the GPC chromatogram which shows that the area corresponding to the free fluorescent label (eluting at 10-20mL) is significantly smaller than that corresponding to the fluorescently labelled dendrimer (In contrast to the GPC chromatogram of crude anionic PAMAM-OG reaction (*Figure 2.3*) which displays that a significantly larger fraction of free OG is left unreacted after a 24 hour reaction period although OG and anionic PAMAM dendrimers were used in the same stoichiometric ratio that was used in FITC-cationic PAMAM reactions.) This has necessitated the use of a lower stoichiometric ratio of FITC-cationic PAMAM dendrimer than that used in OG anionic PAMAM reactions to achieve similar fluorescent dye:dendrimer ratios for both anionic and cationic dendrimers. Hence, only a 1.5 molar ratio of FITC : cationic PAMAM dendrimer was used in labelling cationic dendrimers while a molar ratio 3:1 of OG : anionic PAMAM was used in labeling anionic PAMAM dendrimers. Using the molar ratios described above in labelling cationic and anionic dendrimers, UV analyses have shown that the pure FITC: dendrimer ratio in a fluorescently labelled cationic dendrimer was between 1.2 and 1.4 which is similar to that achieved in anionic PAMAM – OG reactions).

To test the stability of anionic PAMAM-OG and cationic PAMAM-FITC conjugates in cell culture conditions, the purity of these PAMAM dendrimers was assessed before and after 24 hour incubations in cell culture media including 10% FBS at 37°C and relative humidity using GPC chromatography.

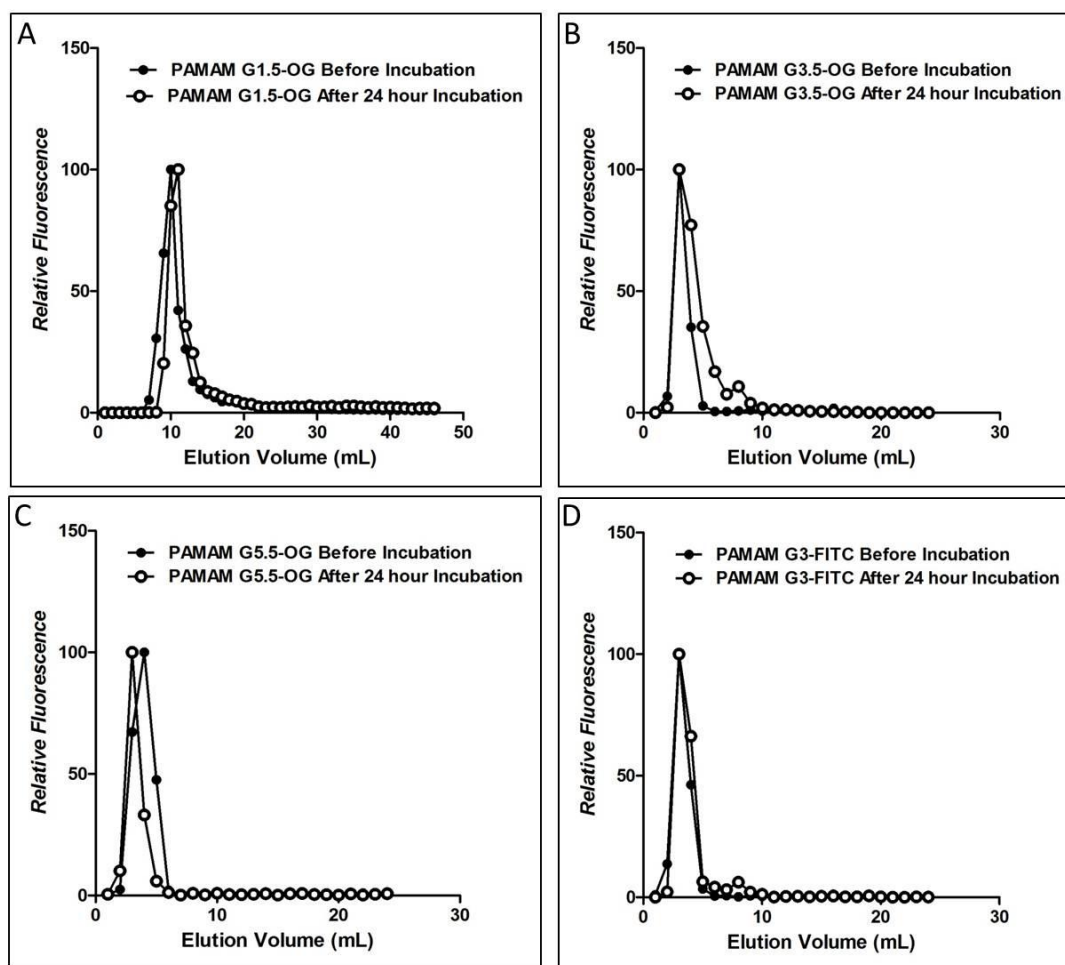


Figure 2.5 Stability of anionic PAMAM-OG and cationic PAMAM-FITC conjugates over 24 hours in physiological conditions as evidenced from gel permeation chromatography. (A) GPC (Sephadex-G10) chromatograms of PAMAM G1.5-OG. (B) GPC (PD-10) chromatograms of PAMAM G3.5-OG (C) GPC (PD-10) chromatograms of PAMAM G5.5-OG. (D) GPC (PD-10) chromatograms of PAMAM G3-FITC

Chromatograms shown in *Figure 2.5*, show that free fluorescent label signals corresponding to free OG or FITC do not appear at the expected elution volume (10-20mL in sephadex G-25 and 25-35mL in Sephadex G-10) before or after the incubations described earlier. This shows that all tested dendrimer-fluorescent label conjugates showed high stability in physiological conditions over 24 hours with minimal to no dissociation between the dendrimer and the fluorescent label.

The stability of fluorescently labelled dendrimers is vital for transport studies to ensure that transport data only reflects the transport of the dendrimers and not the free fluorophore which is much smaller than the dendrimers and is expected to pass through at much higher rates and can lead skewing the results.

2.3.2 Assessment CaCo-2 monolayers for Transport Studies

Assessment of the CaCo-2 monolayer integrity is crucial to ensure that any generated results reflect on permeation across intact monolayers.

Assessment of the integrity of the monolayers was carried out through measurement of TEER and assessment of CaCo-2 permeability to paracellular marker [¹⁴C] Mannitol and trans-cellular probe [³H] Propranolol.

Cell monolayers with TEER values that are less than 300 $\Omega \cdot \text{cm}^2$ were not used for any of the permeability studies. *Figure 2.6* and *Table 2.2* summarise the CaCo-2 monolayers' TEER and permeability to [³H] Propranolol and [¹⁴C] Mannitol.

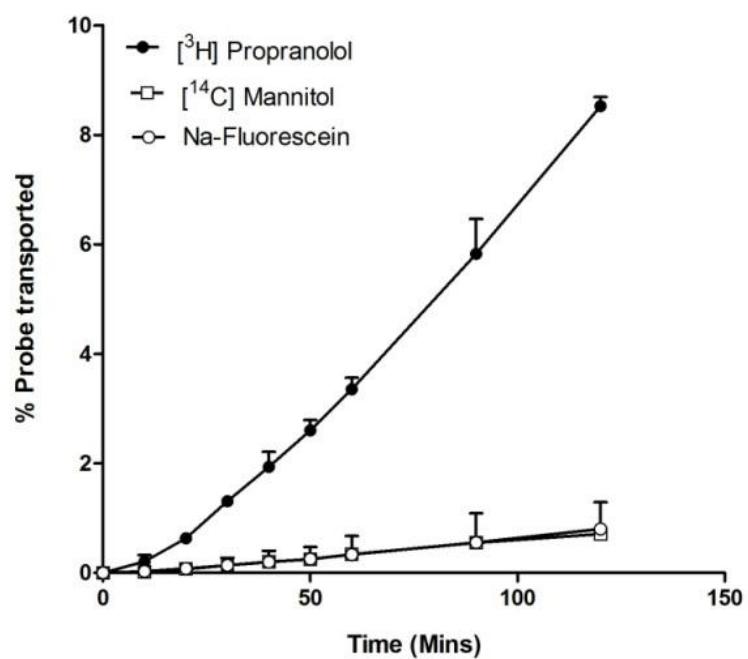


Figure 2.6 Cumulative transport of transcellular probe [^3H] Propranolol and paracellular markers [^{14}C] Mannitol and Na-Fluorescein across CACO-2 monolayers. Results are Mean \pm S.D., $n=4$

Table 2.2 Table summarising TEER, and permeability to [¹⁴C] Mannitol and [³H] Propranolol across a sample of CACO-2 monolayers used for transport experiments, n=4

Property of CACO-2 monolayer	Value
TEER ($\Omega \cdot \text{cm}^2$)	447 ± 17
[³ H] Propranolol Permeability Coeff. ($\times 10^{-6} \text{ cm} \cdot \text{s}^{-1}$)	7.24 ± 0.37
[¹⁴ C] Mannitol Permeability Coeff. ($\times 10^{-6} \text{ cm} \cdot \text{s}^{-1}$)	0.68 ± 0.044
Na- Fluorescein Permeability Coeff. ($\times 10^{-6} \text{ cm} \cdot \text{s}^{-1}$)	0.36 ± 0.036

These results show the integrity of the CaCo-2 monolayers (as judged by TEER measurements and P_{app} of [¹⁴C] Mannitol and [³H] Propranolol across the monolayers). Permeability data shows a high paracellular restrictiveness across CaCo-2 monolayers used in the transport studies as they displayed 10 fold lower permeability to hydrophilic paracellular markers [¹⁴C] Mannitol and Na-Fluorescein than to the lipophilic transcellular probe [³H] Propranolol.

Measured TEER values were significantly higher for these monolayers and were above the minimum accepted used in the literature of $250 \Omega \cdot \text{cm}^2$ [151].

2.3.3 Transport of anionic PAMAM –OG conjugates across CaCo-2 monolayers

The transport of a range of anionic PAMAM dendrimers (G1.5, G3.5, G5.5) was assessed across CACO-2 monolayers.

The donor concentration of PAMAM dendrimers used on the apical surfaces of cells was 0.5mM. A→B Permeability coefficients were then calculated using the following equation:

$$P_{app} = \frac{dQ/dt}{A \cdot C_0} \dots\dots\dots \text{Equation 2.1}$$

Where (dQ/dt) is the rate of cumulative transport, (A) is the area of the monolayer, and (C₀) is the donor concentration of the probe on the apical surface.

Fluorescence Standard curves for sodium fluorescein, Oregon green and all fluorescently labelled PAMAM dendrimers showed linearity over the experimental range. A standard curve for F-Na is shown in *Figure 2.7* for demonstration purposes.

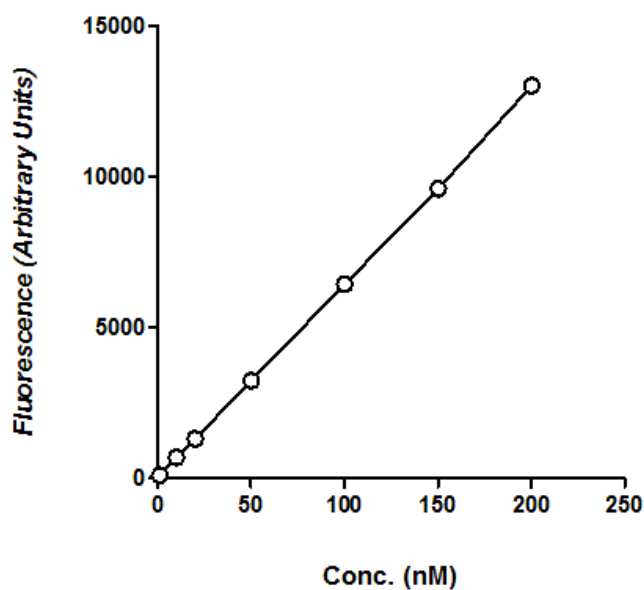


Figure 2.7 Standard Curve for F.Na over a concentration range of 0-200nM. Linear regression was performed using Graphpad Prism 5.0, $R^2 = 0.9999$.

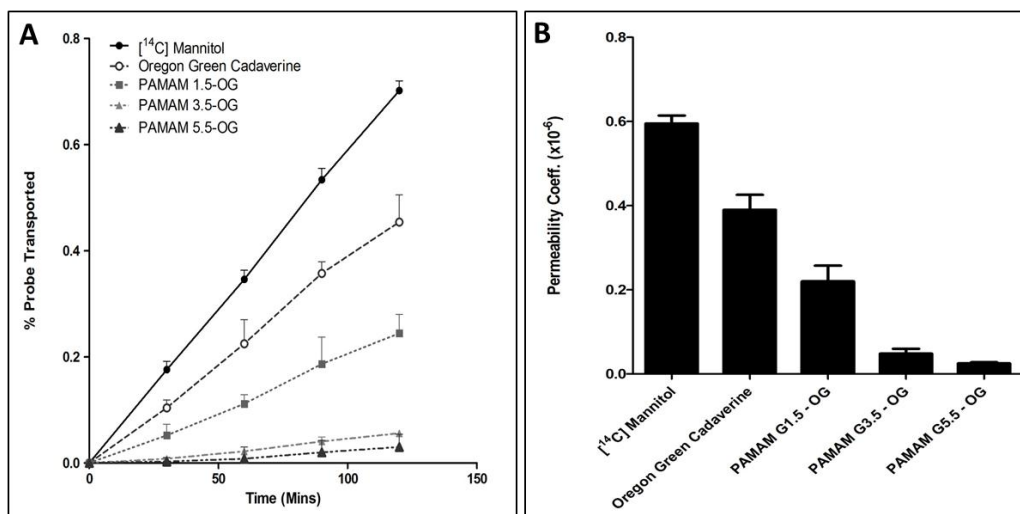


Figure 2.8 (A) The linear transport of ¹⁴C Mannitol, Oregon Green Cadaverine, PAMAM 1.5-OG, PAMAM 3.5-OG and PAMAM 5.5-OG across CACO-2 monolayers over 120 minutes. (B) Calculated P_{app} values of the previous probes displayed as a bar chart. Results are Mean \pm S.D., $n=4$.

Figure 2.8 (A) shows the percentage transported across CaCo-2 monolayers for each probe over 120 minutes. The P_{app} values were calculated for these probes according to the cumulative data of the probes' transport across CaCo-2 and are presented in *Figure 2.8* (B).

The transport data of anionic PAMAM dendrimers data therefore shows a size dependant trend, with permeability coefficients being highest for smaller PAMAM dendrimers and lowest for larger ones. This is displayed in *Figure 2.9* which shows an inverse relationship between the P_{app} values of the different probes across CaCo-2 monolayers and the reciprocal cube root of their molecular weight. This trend infers that the paracellular pathway is predominant in governing the transport of anionic PAMAM dendrimers across CaCo-2 monolayers. The results show that PAMAM dendrimers' permeation is hindered by the restrictiveness of the tight junctions as the increment in the dendrimer's size leads to a decrease in its overall transport.

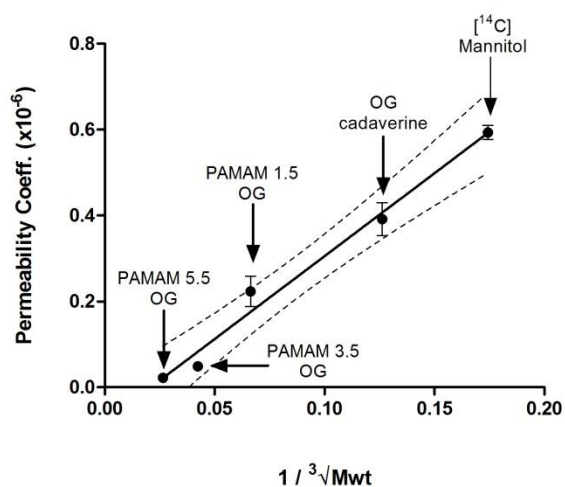


Figure 2.9 Relationship between probes' molecular weight (expressed as $1 / \sqrt[3]{Mwt}$ molecular weight (Mwt)) and their permeability coefficients across CACO-2 monolayers. Results are Mean \pm S.D., n=4. best fit line generated using linear regression (Graphpad Prism), $R^2 = 0.9840$.

Table 2.3 summarises the permeability coefficients of the tested anionic PAMAM-OG conjugates and smaller molecular weight compounds (Oregon Green Cadaverine and [14 C] Mannitol) across CaCo-2 cell monolayers.

Table 2.3 Molecular weights, molecular diameters, and permeability coefficients of different anionic PAMAM-OG conjugates and small molecular weight compounds across CACO-2 monolayers. Data shown for permeability coefficients and TEER values are Mean \pm S.D. (n=4)

Probe	Molecular Weight	Molecular Diameter (Å)	CACO-2 TEER ($\Omega \cdot \text{cm}^2$)	P_{app} ($\times 10^{-6} \text{ cm} \cdot \text{s}^{-1}$)
[¹⁴ C] Mannitol	189	6.5 [159]	529 \pm 22	0.59 \pm 0.017
OG Cadaverine	497	11	515 \pm 15	0.39 \pm 0.037
PAMAM 1.5-OG	3425	29 [9]	539 \pm 39	0.22 \pm 0.035
PAMAM 3.5-OG	13200	45 [9]	531 \pm 29	0.048 \pm 0.012
PAMAM 5.5-OG	54000	67 [9]	543 \pm 14	0.022 \pm 0.0069

To validate that fluorescence measurements in transport studies correspond only with fluorescently labelled PAMAM dendrimers and not the free Oregon green label that dissociated during the experiment, Gel permeation chromatography was performed for all PAMAM-OG conjugates before and after the transport experiments to assess if any dissociation of the free fluorescent label has occurred during the experiment.

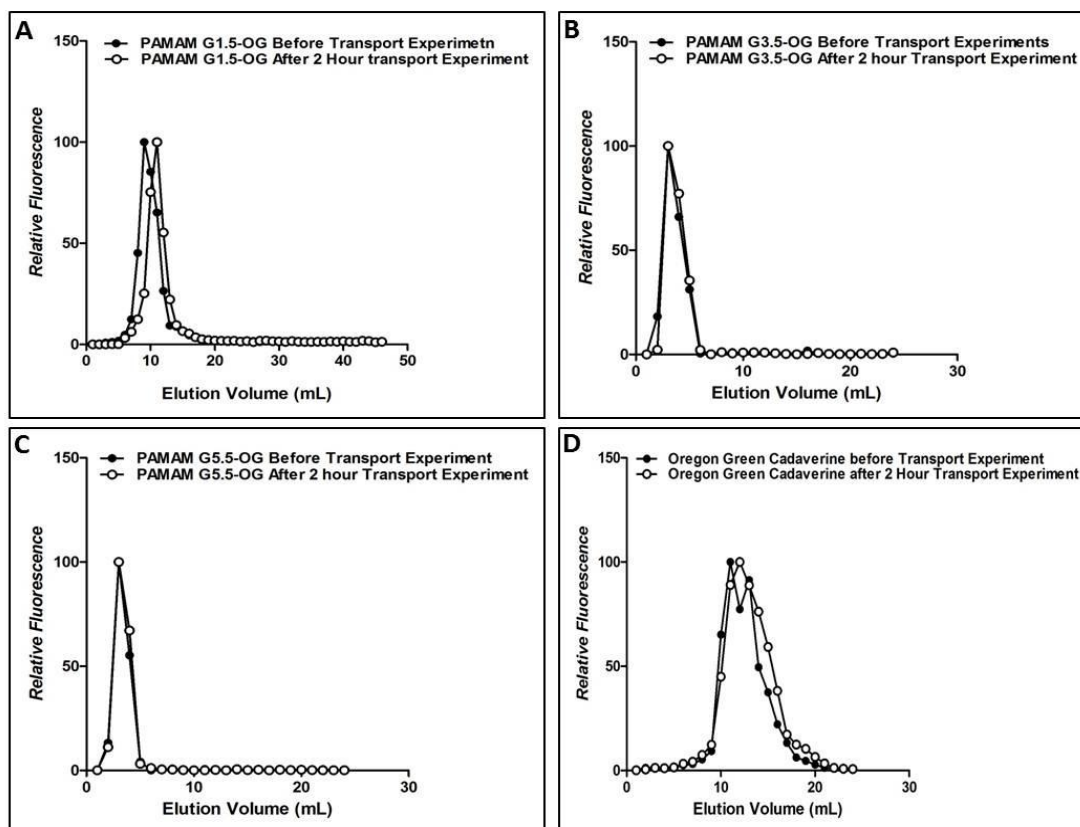


Figure 2.10 Stability of anionic PAMAM-OG conjugates during transport studies across CACO-2 studies. **(A)** GPC chromatograms (Sephadex G10) of PAMAM G1.5-OG before and after transport experiments. **(B)** GPC chromatograms (PD-10) of PAMAM G3.5-OG before and after CACO-2 transport experiment. **(C)** GPC chromatograms (PD-10) of PAMAM G5.5-OG before and after transport experiments. **(D)** GPC chromatograms (PD-10) of free Oregon Green Cadaverine before and after transport experiments.

Figure 2.10 shows that the anionic PAMAM-OG conjugates remain stable during the course of the 2 hour experiment as it clearly exhibits that no peaks associated with free OG peaks appear in the Sephadex G-10 chromatograms (where free OG elutes at 25-35 mL) or in the Sephadex G-25 chromatograms (where free OG elutes at 10-20mL).

2.3.3.1 Effect of anionic PAMAM dendrimers on monolayer integrity

The effect of anionic PAMAM-OG conjugates on the cell monolayer integrity was studied by investigating the influence of co-incubated dendrimers on TEER and permeation of an independent paracellular marker, ^{14}C Mannitol and a transcellular marker, ^3H Propranolol.

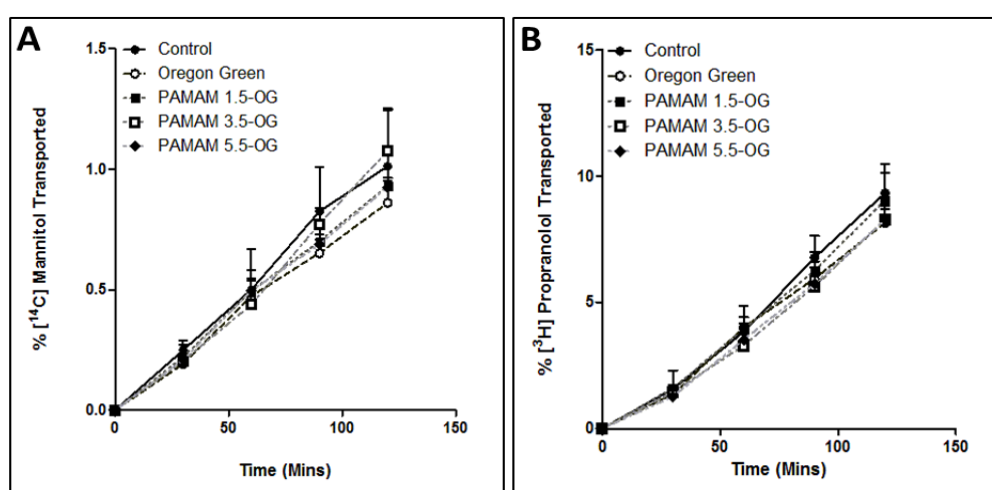


Figure 2.11 The influence of OG and anionic PAMAM-OG conjugates on the cumulative transport of ^{14}C Mannitol (A), ^3H propranolol (B), as compared to control (no co-incubated compounds). Results are Mean \pm S.D., $n=4$

Figure 2.11 shows the cumulative transport of ^{14}C Mannitol and ^3H Propranolol across CaCo-2 cells in the presence and absence of different anionic PAMAM dendrimers. This clearly shows that co-incubation of PAMAM dendrimers does not influence the transport of ^{14}C Mannitol or ^3H Propranolol (maintaining a 10 fold difference in the transport of both probes) across CaCo-2 cells when co-incubated with these marker over 120 minutes. All

Transport profiles in the presence and absence of co-incubated anionic PAMAM dendrimers show linearity over 120 minutes and are similar in the presence and absence of the labelled dendrimer indicating the stability of the monolayer over the duration of the transport experiment in the presence of these dendrimers.

Table 2.4 Effect of Oregon green and different anionic PAMAM-OG conjugates on CACO-2 monolayer integrity observed through changes in TEER and permeation of [¹⁴C] Mannitol and [³H] Propranolol. Results are Mean ± S.D., n=4.

Treatment	Control	Oregon Green	PAMAM 1.5-OG	PAMAM 3.5-OG	PAMAM 5.5-OG
TEER Before Experiment	529 ± 22	515 ± 15	539 ± 39	531 ± 29	543 ± 14
TEER After Experiment (% Change)	535 ± 13 (+1.2%)	511 ± 4 (-0.9%)	551 ± 36 (+2%)	537 ± 26 (+1.1%)	545 ± 8 (+0.4%)
[¹⁴ C]Mannitol Perm. Coeff (x 10 ⁻⁶ cm.s ⁻¹)	0.84 ± 0.14	0.75 ± 0.09	0.78 ± 0.16	0.92 ± 0.13	0.81 ± 0.02
[³ H]Propranolol Perm. Coeff. (x 10 ⁻⁶ cm.s ⁻¹)	7.94 ± 1.04	7.17 ± 0.47	7.73 ± 0.99	7.08 ± 0.59	7.18 ± 0.56

Table 2.4 shows that like [¹⁴C] Mannitol and [³H] propranolol transport across CACO-2 cells in the presence and absence of co-incubated anionic PAMAM dendrimers, TEER values haven't changed over the duration of the 2 hour transport experiment.

These results clearly indicate that the labelled PAMAM dendrimers did not influence the integrity of the monolayers, and the generated data for their transport across CACO-2 monolayers has not been skewed by negative effects inferred by these dendrimers upon the CACO-2 monolayers.

Ensuring that the tested probes do not alter the integrity of the cell barrier is vital to ensure that calculated rates of transport of these probes reflect only their inherent permeation and are not skewed due to altering the restrictiveness of the monolayers which can lead to the generation of misleading data that exaggerates the permeation rates and extents of certain compounds.

Although only a limited number of groups studied the transport of anionic PAMAM dendrimers across CaCo-2 cells, the literature nevertheless displays an extreme discrepancy over the P_{app} of these dendrimers across CaCo-2 monolayers: Kitchens et al. [160] reported P_{app} s that were greater than $5 \times 10^{-6} \text{ cm.s}^{-1}$ (PAMAM G3.5) and $2 \times 10^{-6} \text{ cm.s}^{-1}$ (PAMAM G2.5) while Jevprasesphant et al.[161] reported significantly lower values for P_{app} of $0.02 \times 10^{-6} \text{ cm.s}^{-1}$ and $0.15 \times 10^{-6} \text{ cm.s}^{-1}$, respectively; issues of different cell toxicity can be excluded as a basis.

Other studies looked into the transport of PAMAM dendrimers across CaCo-2 monolayers in the context of bypassing the P-gp efflux transporter and showed that conjugating P-gp substrates to PAMAM dendrimers increases their absorptive transport and uptake by CaCo-2 cells [162-164]

2.3.4 Transport of Cationic PAMAM-FITC conjugates across CaCo-2 monolayers.

Two cationic PAMAM dendrimers were chosen for transport studies across CaCo-2 monolayers, PAMAM G3 and PAMAM G4. Both dendrimers were conjugated with FITC as a fluorescent label.

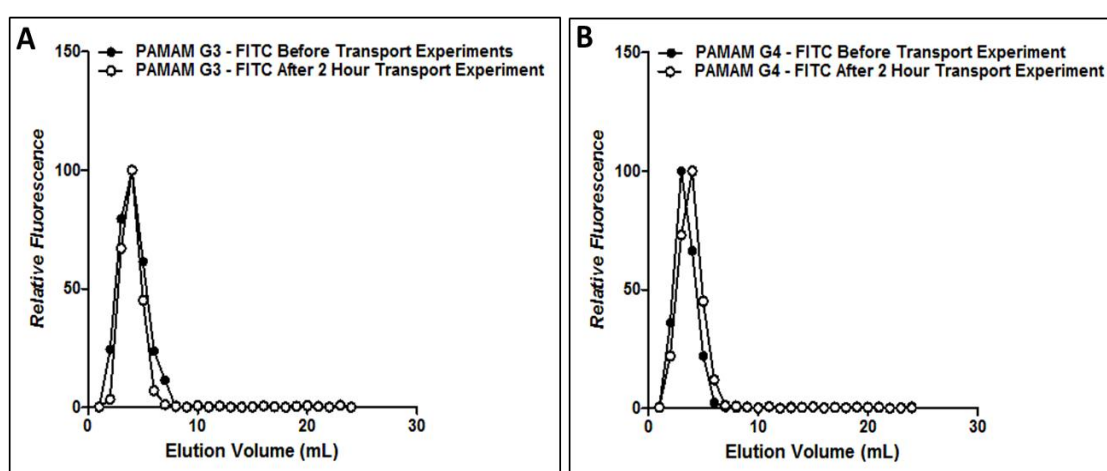


Figure 2.12 Stability of cationic PAMAM-FITC conjugates during transport studies across CaCo-2 monolayers. (A) GPC chromatograms (PD-10) of PAMAM G3-FITC before and after transport experiments. (B) GPC chromatograms (PD-10) of PAMAM G4-FITC before and after CaCo-2 transport experiment.

Figure 2.12 shows the GPC chromatograms of PAMAM G3 and PAMAM G4 FITC conjugates before and after transport experiments. While free FITC would only elute between 10-20mL as explained earlier, these chromatograms clearly show that the dendrimer-FITC conjugates were completely stable during the 2 hours when CaCo-2 transport experiments had been conducted as no elution of free FITC appears after the two hour experiments.

Results presented for permeation of cationic PAMAM-FITC conjugates in these studies hence, only represent the transport of the intact PAMAM-FITC conjugate with no contamination from the free unconjugated fluorescent label as no dissociation of the label occurs during the entirety of the experiment.

Figure 2.13 shows the cumulative transport of FITC labelled cationic PAMAMs G3 and G4 across CACO-2 cells. Both PAMAM dendrimers show fairly linear trends although transport seems to slightly accelerate after 90 minutes.

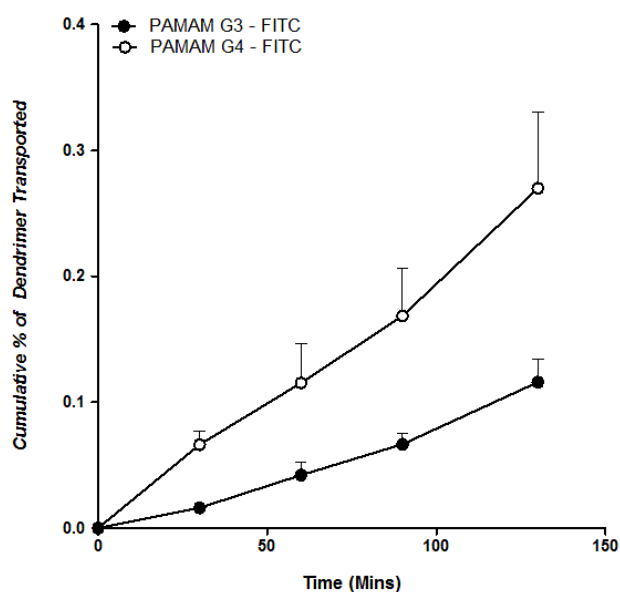


Figure 2.13 Cumulative transport of cationic PAMAM-FITC conjugates G3 and G4 across CACO-2 monolayers. Data shown is mean \pm S.D., $n=4$.

Table 2.5 Molecular weights, stoke's diameters, and permeability coefficients of two cationic PAMAM-FITC conjugates across CACO-2 monolayers. Data shown for permeability coefficients and TEER values are Mean \pm S.D. (n=4)

Dendrimer	Molecular Weight (Da)	Molecular Diameter (Å)	CACO-2 TEER (Ω.cm²)	Permeability Coefficient ($\times 10^{-6}$ cm.s⁻¹)
PAMAM G3 – FITC	6,909	36	533 \pm 12	0.096 \pm 0.0012
PAMAM G4 - FITC	14,215	45	544 \pm 18	0.22 \pm 0.05

Results in *Table 2.5* and *Figure 2.13* show that the permeation of cationic PAMAMs G3 and G4 is directly proportional to their molecular size where CaCo-2 monolayers exhibited greater permeability to the larger dendrimer (PAMAM G4 – FITC) than to the smaller G3 cationic PAMAMs. This contrasts to CaCo-2 permeability to anionic PAMAM dendrimers where smaller dendrimers displayed higher permeation than PAMAMs with greater size.

In comparing permeability data in anionic and cationic dendrimers, it is noted that while anionic dendrimers and PAMAM G3 dendrimers show similar permeability according to their molecular sizes (*Figure 2.14*), PAMAM G4 shows a significantly greater permeability given its molecular size across the monolayers when compared to other PAMAMs.

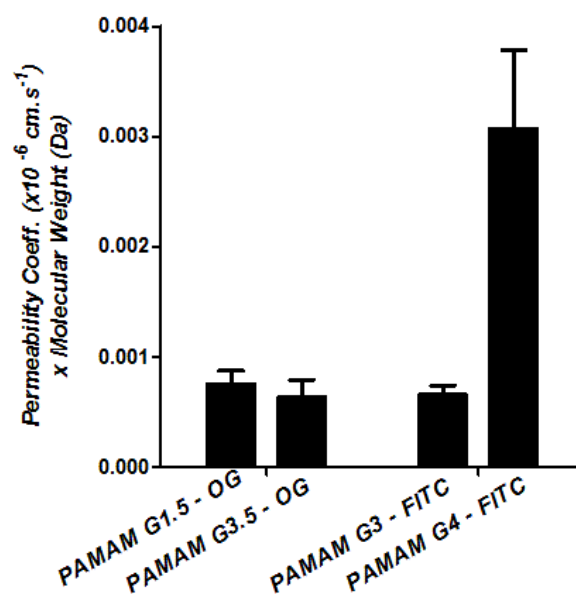


Figure 2.14 Permeability coefficients of anionic and cationic PAMAM dendrimers corrected to molecular size. Data is expressed as permeability coefficient ($\times 10^{-6} \text{ cm.s}^{-1}$) x molecular weight (Da). Results are Mean \pm S.D. , $n=4$.

The high permeation of PAMAM G4 dendrimers across CaCo-2 may be attributed to its deleterious effects upon the cell monolayers because of the high positive charge density on its outershell which can vigorously interact with the negatively charged plasma membrane resulting in cell lysis [19] .

Effect of Cationic PAMAM dendrimers on monolayer integrity

The effect of cationic PAMAM dendrimers upon the integrity of CaCo-2 monolayers was tested by assessment of the polymers' effects upon TEER of CaCo-2 monolayers and permeability to [¹⁴C] Mannitol in their presence and absence as shown in *Figure 2.15*.

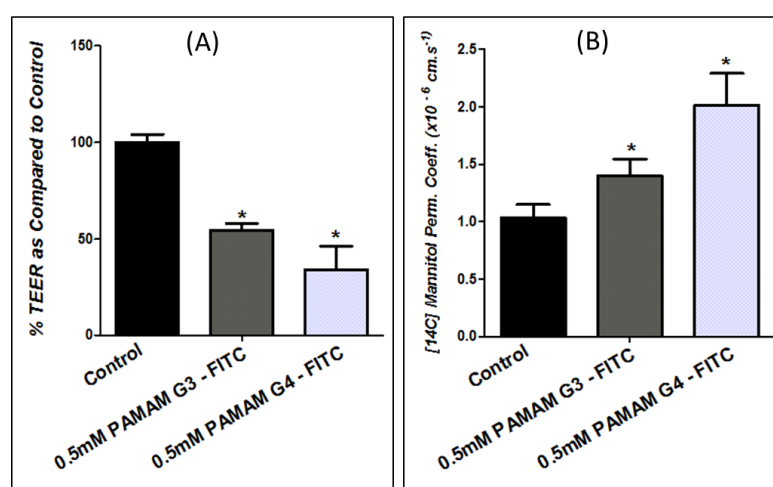


Figure 2.15 Effect of Cationic PAMAM dendrimers (G3 and G4) on the integrity of CaCo-2 monolayers as evident from effect on TEER (A) and the permeability coefficient of the independent paracellular marker [¹⁴C] Mannitol. Results are Mean \pm S.D., n=4. * indicates P<0.05, One Way Anova, Dunnet's post-test.

Figure 2.15 shows the effect of cationic PAMAM dendrimers upon the integrity of CaCo-2 monolayers through displaying their effect upon TEER and the monolayers' permeability to [¹⁴C] mannitol when co-incubated with this paracellular marker. Results show that both cationic PAMAMs G3 and G4 compromise CaCo-2 monolayer integrity as evidenced from the decrease in

TEER and the increase in the permeability coefficients of the independent paracellular marker [¹⁴C] Mannitol.

Interestingly, CaCo-2 permeability to PAMAM G3-FITC was similar to anionic PAMAM dendrimers given the molecular size. PAMAM G3-FITC however, unlike anionic PAMAM dendrimers has compromised the monolayer integrity and increased permeability to an independent paracellular marker. This indicates that the observed permeability coefficient for this dendrimer is higher than it should be which suggests that the cationic PAMAM dendrimer may have a lower intrinsic permeability than other anionic PAMAM dendrimers given its molecular size. This can be attributed to the binding that cationic molecules display in general to the negatively charged lipid membranes [165] which decreases their overall permeation. Indeed, this comes in agreement with Witwanapatapee's results which suggest that anionic PAMAM dendrimers cross the intestinal barrier at quicker rates than cationic ones which display more tissue association [26].

The detrimental effect of PAMAM G4 upon CaCo-2 monolayers however, was more pronounced in both decreasing TEER values and increasing [¹⁴C] Mannitol permeation which could explain its high permeation across CACO-2 monolayers given its molecular weight.

It is hence very important to handle data of cationic PAMAM dendrimers with care as it can be very misleading if the appropriate controls are not conducted and taken into consideration.

El-Sayed et al. [55] studied the permeability of CaCo-2 cells to fluorescently labelled cationic PAMAM dendrimers that range from G0 – G4. Their results have shown that the permeability coefficient of the tested cationic PAMAM dendrimers increases with the increase in the concentration and incubation time of these polymers. The same group also reported that the transport of the independent paracellular marker, [¹⁴C]-Mannitol, increases in the presence of cationic PAMAM dendrimers. Other studies have shown that while cationic PAMAM dendrimers show higher apparent rates of transport across CaCo-2 cells when compared to anionic PAMAM dendrimers of similar molecular sizes, the cationic species display concentration dependant toxicities to this cell line [161].

Some groups suggested that an endocytic mechanism is involved in the transport of PAMAM dendrimers across CaCo-2 cells, evidenced by the observed decreased transport of these dendrimers at 4°C and in the co-presence of endocytic inhibitors such as colchicine [162]

Because of their delirious and toxic effects on cell monolayers however, it was decided to avoid the use of cationic PAMAM dendrimers in future studies as it is difficult to investigate their biopharmaceutical behaviour when they exert these effects on biological systems.

2.3.5 Transport of anionic PAMAM dendrimers across MDCK I and MDCK II monolayers

MDCK I and MDCK II cells are both derived from cocker spaniel dog kidney [166]. MDCK I cells have been reported to exhibit TEER values that are far higher ($>3000\Omega\cdot\text{cm}^2$) than MDCK II strains ($\sim 200\Omega\cdot\text{cm}^2$). While MDCK I cells display properties of the kidney distal tubule epithelium, MDCK II cell line displays properties that are associated with the proximal tubule epithelium [167]. MDCK I cells, which possess higher TEER are derived from earlier passages of cells isolated from the canine's kidney while MDCK II cells dominate in earlier passages. The reason behind the discrepancy in the restrictiveness between the two cell lines lies behind the fact that the tight junctional protein Claudin-2 is expressed in MDCK II cells but not in MDCK I [168].

MDCK I cells represent a very restrictive barrier with TEER values that are reminiscent to values observed across the blood brain barrier, while MDCK II cell monolayers represent a less restrictive barrier with TEER values similar to those reported for the epithelial barrier of the gut. The two strains show a high degree of similarity in most biological aspects but exhibit a significant difference in paracellular restrictiveness. This makes the two strains a suitable *in-vitro* platform to help in the comparisons between intestinal absorption and blood brain barrier penetration of a certain compound.

In fact, the MDCK-II cell line has been extensively used as an *in-vitro* model to predict the intestinal absorption of drugs intended for oral use [169].

In these studies, Sodium fluorescein (F-Na), a fluorescent paracellular marker, was used as a control to provide a quantitative indicator of paracellular restrictiveness in the two strains of MDCK cells.

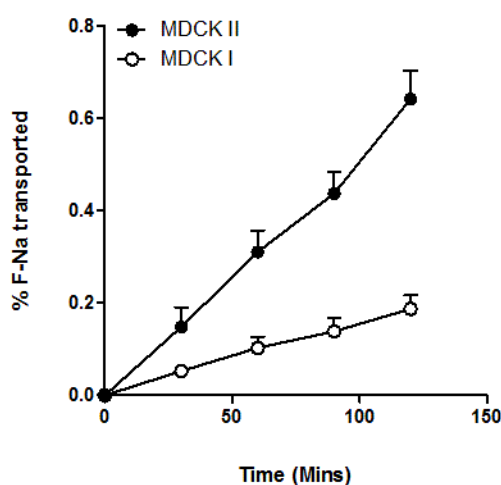


Figure 2.16 The cumulative transport of F-Na, a paracellular marker, across MDCK I and MDCK II monolayers. Results are Mean \pm S.D., $n=4$.

Figure 2.16 shows the transport of the paracellular marker F-Na across MDCK I and MDCK II monolayers. It is clear from results displayed in this figure that F-Na displays a significantly higher permeation rate and extent across the less restrictive MDCK II than across the tight MDCK I. This provides quantitative

evidence about the discrepancy in the restrictiveness between the two cell lines.

Given this quantitative evidence using a small molecular weight marker like F-Na, the transport of PAMAMs G1.5 and G3.5 was then examined across the two MDCK strains to investigate the differential effect of barrier restrictiveness on the permeability to these polymers.

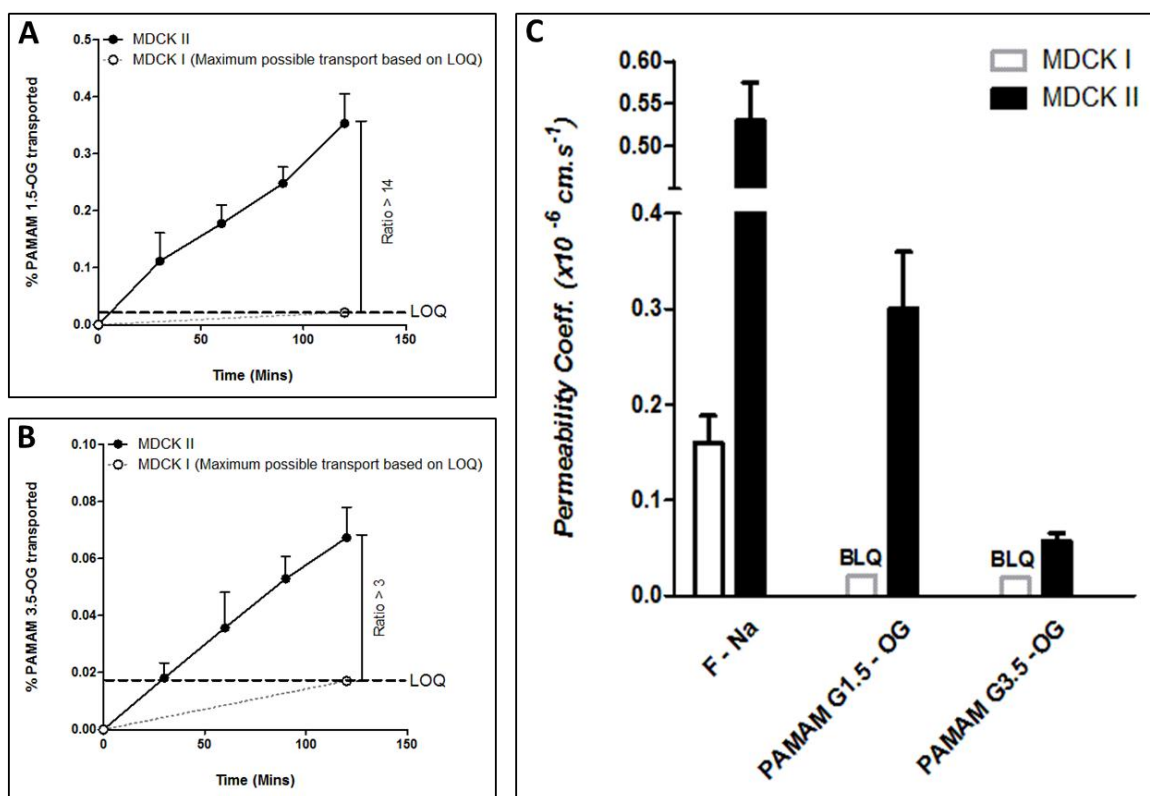


Figure 2.17 (A) Cumulative transport of PAMAM 1.5-OG. (B) Cumulative transport of PAMAM 3.5-OG, all across MDCK I and MDCK II cell lines. (C) Permeability coefficients PAMAM dendrimer and F-Na across MDCK I and MDCK II cell lines.

Table 2.6 Permeability Coefficients of Sodium Fluorescein (F-Na), PAMAM G1.5-OG and PAMAM G3.5-OG as calculated across MDCK I and MDCK II cell lines. Results are Mean \pm S.D. n number specified in the table.

Monolayer/ Property	MDCK I	MDCK II	MDCKII/ MDCKI ratio
TEER $\Omega.cm^2$	2959 \pm 72 (n=12)	223 \pm 4 (n=12)	0.075
F-Na (P_{app}) $\times 10^{-6} cm.s^{-1}$	0.16 \pm 0.028 (n=4)	0.53 \pm 0.05 (n=4)	3.3
PAMAM G1.5-OG (P_{app}) $\times 10^{-6} cm.s^{-1}$	\leq 0.021 Based on LOQ	0.30 \pm 0.06 (n=4)	> 14 Based on LOQ
PAMAM G3.5-OG (Perm. Coeff.) $\times 10^{-6} cm.s^{-1}$	\leq 0.02 Based on LOQ	0.057 \pm 0.01 (n=4)	> 3 Based on LOQ

Data shown in Figure 2.17 and Table 2.6 summarise the permeation results of PAMAMs G1.5 and G3.5 (and F-Na for direct comparison) across MDCK I and MDCK II cell lines. Not surprisingly, all these compounds showed a lesser extent of transport across the more restrictive MDCK I cell line when compared to the less restrictive MDCK II strain. Further, across the MDCK II cells, the permeability showed a progressive decrease as the molecular weight of the probe increases. Such that P_{app} for PAMAM G3.5 is some x10 fold lower than that for F-Na, and some x5 fold lower than that for PAMAM G1.5. Across MDCK I, the transport for both PAMAMs was so low as to be below the limit of quantitation (LOQ) for the entirety of the 2 hour experiment. This comes despite the use of the very highly fluorescent dye, Oregon Green, to label the

anionic dendrimers. Radiolabeling of the dendrimers was attempted as explained later in chapter 4, but the achieved specific radioactivity for these dendrimers would result in limits of quantitation similar to those with the fluorescently labelled dendrimers.

Because no PAMAM dendrimer could be quantified over the entirety of the experiment, P_{app} values for these PAMAM dendrimers were based upon the theoretical maximum according to the LOQ. In reality, it is the LOQ that sets the limit on the ratios and profoundly so for PAMAM G3.5 as it has a significantly lower rate of transport across MDCK II when compared to PAMAM G1.5. This means that the ratios of MDCK II : MDCK I transport of >14 : 1 for PAMAM G1.5 and >3:1 for G3.5 represent the minimum theoretical possible ratios in the transport of these dendrimers which could indeed be significantly higher than that.

The maximum amount of PAMAM - OG that could have been transported was calculated according to the fluorescent limit of quantitation (LOQ). LOQ was calculated as follows:

$$LOQ = BR + (10 \bullet STDEV \text{ of } BR) \dots\dots\dots \text{Equation 3.2}$$

BR symbolises the background fluorescent reading from cell culture media.

The reason behind this discrepancy in the differential transport of F-Na and PAMAM 1.5-OG across MDCK I monolayers and the less restrictive MDCK II monolayers can be attributed to the larger size of the G1.5 polymer.

It seems from results described earlier, that the increase in the molecular size of a certain probe has a greater impact upon decreasing the transport of this probe across a highly restrictive monolayer than across a less restrictive one as visualised in *Figure 2.18*.

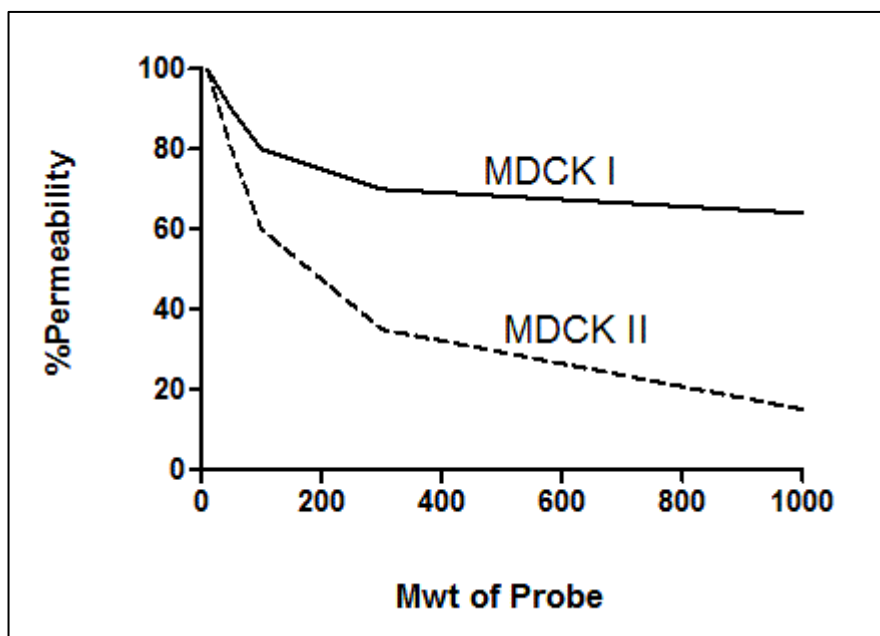


Figure 2.18 Hypothesised effect of molecular weight upon the permeability of a probe across the tight MDCK I and the less restrictive MDCK II. Graph shows that increment in molecular weight leads to higher difference in permeability between the two strains. Values are arbitrary.

This high degree of differential transport between restrictive and leaky barriers that is particularly exhibited by high molecular weight compounds has been described before in the context of targeted delivery to tumorous tissues that exploits the leakiness of tumour vasculature in contrast to the restrictiveness of vasculature that feeds healthy tissues in what is known as the enhanced permeation retention (EPR) effect [170].

Another group has investigated the permeation of cationic (but not anionic dendrimers) PAMAM dendrimers across MDCK II cells (but not MDCK I). Tajarobi et al.[56] inspected the transport of different cationic PAMAM dendrimers (G0-G4) and showed that they all permeate across the MDCK II monolayers at different rates that didn't correlate with the sizes of these dendrimers. These results, as described earlier, can be misleading as cationic dendrimers affect the integrity of cell monolayers and don't hence reflect the true intrinsic permeability of these dendrimers.

2.3.6 Permeability Studies with Intrinsically Fluorescent Dendrimers in MDCK I and MDCK II cell lines.

All permeation studies discussed so far were with dendrimers that have been labelled in house using a fluorescent dye such as Oregon Green or FITC. This is because dendrimers themselves are extremely difficult to be quantified as they do not contain any chromophores such as benzene rings where luminescent spectroscopy can be applied to quantify these polymers. The large size and high charge density makes their analysis difficult by mass spectrometry methods.

Even with OG labelling, detection issues were experienced. Although this might have been avoided by increasing the labelling stoichiometry, this would have

altered the physicochemical properties of the dendrimers and their overall transport across biological barriers, especially for smaller dendrimers.

To achieve dendrimers that can be more easily detected, a collaboration with polymer chemists was established, and novel dendrimers were developed comprising a fluorescent core, where it was hypothesised that with the fluorescent label being an integral part of the dendrimer at the core from which the dendrimer emanates, a better quantum yield of fluorescence can be achieved.

Dendrimers with fluorescent cores are shown in *Figure 2.19*. Synthesis of the dendrimer starts from the fluorescent dye and higher generations are achieved by attaching successive Dendrons onto to the fluorescent core rather than attaching a fluorescent dye at the surface.

Initial studies with these dendrimer however have shown that their fluorescence quantum yields are significantly lower than dendrimers labelled with Oregon green. Additionally, fluorescence of these dendrimers seems to decrease with the increase in generation making it more difficult to analyse larger dendrimers comprising the fluorescent dye as a core.

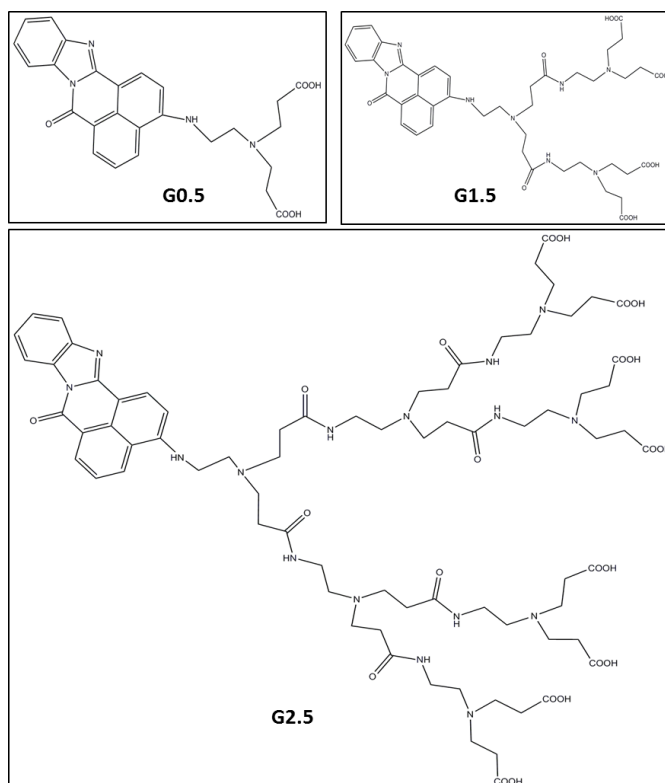


Figure 2.19 Poly(amido-amine) Dendrimers bearing a fluorescent core, (7H-benz[de]benzimidazo[2,1-a]isoquinoline-7-one), from where amido-amine dendrons emanate.

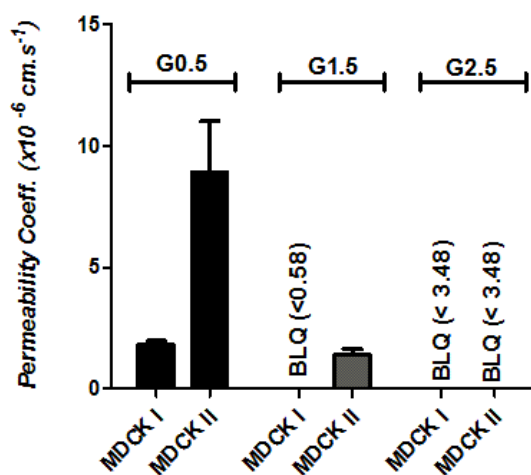


Figure 2.20 Permeability Coefficients of a group of intrinsically fluorescent poly(amido-amine) (G0.5, G1.5 and G2.5) across MDCK I and MDCK II monolayers. The permeability coefficients of G1.5 across MDCK I and G2.5 across MDCK I and MDCK II monolayers were calculated according to their limits of fluorescent quantification as no dendrimer was detected at the final 120 minute time point. Results are Mean \pm S.D., $n=4$.

It has also been ensured that these novel anionic dendrimers do not compromise the integrity of the monolayer integrity of either MDCK I or MDCK II. TEER values before and after incubation with these dendrimers have been measured and have been shown to be unaltered as previously shown with other dendrimers.

2.3.7 The effect of Tumour Necrosis Factor - α (TNF- α) on MDCK-II and CACO-2 restrictiveness and permeability to anionic PAMAM-OG dendrimers.

Cytokines are cell-signalling proteins that are produced by a number of immune cells and play a vital role in inflammation. These include a wide variety of Interleukins, inteferons, and tumour necrosis factors.

Many groups have shown that a few cytokines such as interferon- γ , interleukin- 1β , interleukin-12 and tumour necrosis factor- α (TNF- α) while playing a vital role as pro-inflammatory mediators, cause disruption of the intestinal barrier, modulation of its tight junctional properties and consequently increasing its overall paracellular permeability [171-173].

Because the aim of the transport studies in this chapter is to exploit PAMAM dendrimers as a delivery tool for cannabinoid drugs to be used in the treatment of IBD which is correlated with high blood levels of cytokines such

as TNF- α [174], it was important to study the effect of these mediators upon the overall transport of dendrimers and their conjugates. Clearly, inflammatory mediators which are predicted to alter the permeability and pharmacokinetic properties of the local barrier at which they are released as described earlier, can serve our strategy in using dendrimer-cannabinoid conjugates in the treatment of inflammatory bowel disease where the conjugate can be better directed to the inflamed and more permeable regions of the intestinal tissue than the healthy restrictive regions.

The effect of TNF- α on PAMAM dendrimer permeation across CaCo-2 and MDCK II cells was investigated.

Reported serum concentrations of TNF- α in patients suffering from Ulcerative Colitis and Crohn's disease ranged between 5 and 15 $\mu\text{g}/\text{mL}$ [174]. To investigate the effect of pro-inflammatory cytokines on the restrictiveness of *in-vitro* cell monolayers, TNF- α was used with the cell lines MDCK-II and CaCo-2. An intermediate concentration of 10 $\mu\text{g}/\text{mL}$ and a lower concentration of 1 $\mu\text{g}/\text{mL}$ were used for the experiments where cells were pre-incubated with the pro-inflammatory cytokine for a period of 20 hours before conducting the studies.

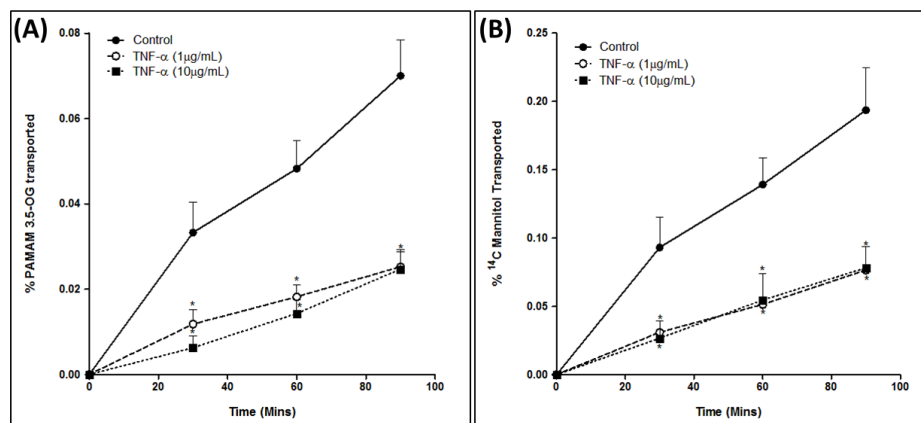


Figure 2.21 The effect of 20 hour pre-incubation with TNF- α at $1\mu\text{g/mL}$ and $10\mu\text{g/mL}$ on the cumulative transport of (A) PAMAM G3.5-OG and (B) ^{14}C Mannitol (expressed as % of donor mass) across MDCK II cells over 90 minutes. Results are Mean \pm S.D. * indicates $P < 0.05$ when compared to control. Two Way Anova Analysis, Bunferroni's post-test.

Table 2.7 Effect of TNF- α when applied at concentrations of $1\mu\text{g/mL}$ and $10\mu\text{g/mL}$ over 20 hours on TEER, PAMAM G3.5 and ^{14}C Mannitol permeation (expressed as permeability coefficient $\times 10^{-6} \text{ cm.s}^{-1}$) across MDCK II cells grown on semi-permeable inserts.

Treatment in MDCK II	Control	TNF - α ($1\mu\text{g/mL}$)	TNF - α ($10\mu\text{g/mL}$)
TEER ($\Omega.\text{cm}^2$)	127 ± 7	259 ± 9	259 ± 23
PAMAM G3.5-OG P.app ($\times 10^{-6} \text{ cm.s}^{-1}$)	0.057 ± 0.007	0.021 ± 0.0029	0.022 ± 0.004
[^{14}C] Mannitol P.app ($\times 10^{-6} \text{ cm.s}^{-1}$)	0.83 ± 0.1	0.44 ± 0.04	0.41 ± 0.05

Figure 2.21 shows the cumulative transport of PAMAM G3.5-OG and [^{14}C] Mannitol across MDCK II cells in the presence and absence of TNF- α . It is clear from the cumulative transport trend that TNF- α decreases the permeability of MDCK II cell monolayers to both the polymer and the paracellular marker. Results detailed in *Table 2.7* show that TNF- α *increased* the restrictiveness of the MDCK II monolayers as evident from the doubling in TEER values as compared to control treatments (No TNF- α) and a significant decrease in the permeability of the monolayers to the paracellular marker [^{14}C] Mannitol.

The increase in the restrictiveness of these cells has also resulted in about 50% decrease in PAMAM G3.5-OG permeation across MDCK II monolayers when compared to control treatments where no TNF- α was applied. The reason behind this result is not known, although a similar effect of TNF- α has been previously reported with MDCK II cells where incubation of MDCK II cells with TNF- α resulted in an increase in TEER of the monolayers [175]. Another group however, has showed that the incubation of MDCK cells with TNF- α at similar concentration significantly increase [^3H] Mannitol flux across MDCK monolayers [176].

The effect of TNF- α on CaCo-2 monolayers, however, was different. As shown in *Figure 2.22*, the incubation of fully differentiated CACO-2 monolayers with TNF- α at concentrations of 1 $\mu\text{g}/\text{mL}$ and 10 $\mu\text{g}/\text{mL}$ did not alter the restrictiveness of these monolayers as clearly evidenced from TEER measurements.

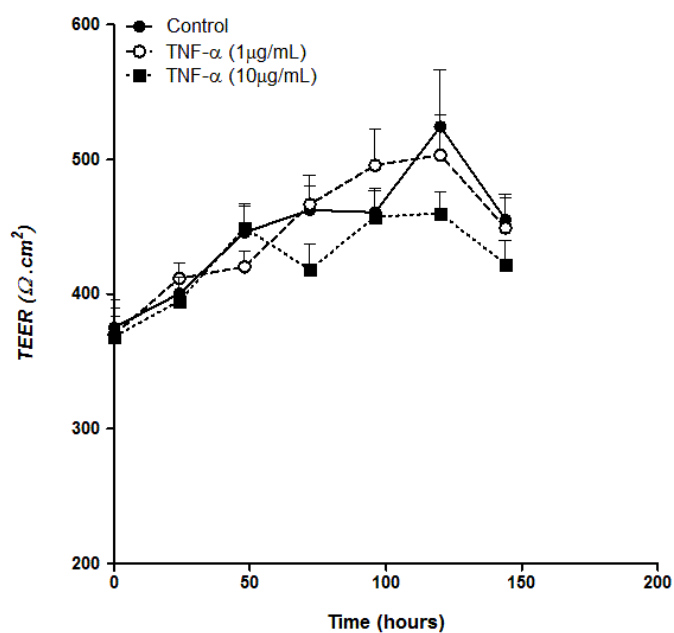


Figure 2.22 Effect of TNF- α at concentrations of 1 μ g/mL and 10 μ g/mL on CACO-2 TEER (expressed as Ω .cm²). Data are Mean \pm S.D., n=4. Two way anova analysis, Bunferroni's post-test show no significant difference between TEER values at any time point for all treatments.

2.3.8 Isolated Perfused Rat gut (IPrG)

A few groups have studied the transport of dendrimers across intact tissues. Florence et al. [57] studied the *in-vivo* translocation and uptake of a radiolabeled G4 poly-lysine dendrimer (MW 6,400) from the rat intestine. They reported that these dendrimers permeate across the rat intestine, albeit only to low extents, with maximum concentrations in blood at 6 hours not exceeding 3% of the administered dose. Wiwattanapatapee et al. [26], investigated the transfer and uptake of radiolabeled anionic and cationic PAMAM dendrimers in the everted rat gut sac. Their results showed a discrepancy in the transport between anionic and cationic PAMAM dendrimers

where the former displayed serosal transfer rates across the gut sacs that were higher than natural macromolecules of comparable sizes, while cationic PAMAM dendrimers displayed higher tissue association and lower transfer rates. Morris et al. [51] studied the transport of a range of fluorescently labelled anionic PAMAM dendrimers (G1.5 – G5.5) across the intact rat lung. Their results showed that all these PAMAM dendrimers permeate across the rat lung in a size dependant trend with smaller dendrimers displaying highest rates of transport.

After the success in assessing the permeability of different *in-vitro* barriers to different PAMAM dendrimers, the aim was to assess transport across an *ex-vivo* isolated perfused gut model. An *ex-vivo* model should more accurately predict the *in-vivo* permeability of the gut barrier to PAMAM dendrimers. An *ex-vivo* model can give a better prediction about the permeation of different PAMAM dendrimers across the gut as the model represents the gut barrier with its full architecture including unstirred water layer, mucus barrier, endothelium and connective tissue (unlike *in-vitro* intestinal models that generally only incorporate the epithelial barrier). Additionally, in comparison to the whole body pharmacokinetic oral dosing, an *ex-vivo* model can simplify the quantitation of dendrimer permeation across the gut as it isolates the circulation from the liver where metabolism can occur and from the whole

body in general. i.e. it is a direct measure of permeation from gut lumen to mesenteric blood vessels .

As explained in the methods section, in the isolated perfused gut model a perfusate circulates from the mesenteric artery across the mesenteric capillary bed and out to the portal vein, where the perfusate is re-circulated again. To visualise that the perfusate is circulating across this path, trypan blue was mixed with the circulating perfusate. Visual observation of the distribution of the perfusate confirmed recirculation across the mesenteric bed as expected. A part of the dyed mesenteric bed is shown in *Figure 2.23*. Full videos of the process were also captured during the setup.



Figure 2.23 A part of the mesenteric bed after 5 minute perfusion with buffer containing trypan blue (5 mg/mL)

To assess the integrity of the isolated perfused gut model, the permeation of two different paracellular markers, Na-Fluorescein and [^{14}C] Mannitol, and a transcellular marker, [^3H] Propranolol, were studied. These molecules were added to the perfusate circulating across the mesenteric bed and transport was investigated over 60 minutes. It is expected that the lipophilic transcellular marker [^3H] Propranolol would display a significantly higher permeation rate and extent across the gut barrier than the hydrophilic paracellular markers [^{14}C] Mannitol and Na-Fluorescein.

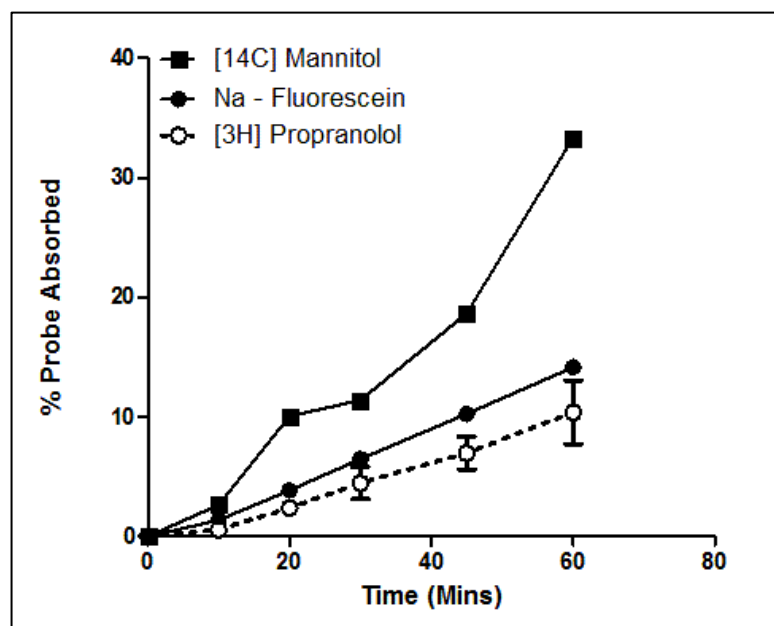


Figure 2.24 Cumulative transport of [^{14}C] Mannitol, F-Na and [^3H] Propranolol over 60 minutes across the isolated perfused rat gut.

Figure 2.23 shows the cumulative transport of the two paracellular markers, F-Na and [^{14}C] Mannitol and the transcellular marker [^3H] Propranolol across the isolated perfused gut to the circulating perfusate over 1 hour. These results show that the gut barrier was apparently more permeable to the paracellular probe than the transcellular probe. Although propranolol is reported to be a substrate for P-glycoprotein the more likely explanation of the data is that the integrity of the barrier was compromised. Indeed the formation of intraluminal oedema was evident within 10 minutes of most experiments as a result of apparent leakage of the circulating perfusate into the intestinal lumen. This issue is probably a result of the absence of an efficient oxygen carrier in the perfusate, the perfusate used was a Krebs buffer supplemented with 4%

Bovine serum Albumin. Successful application of the isolated perfused gut previously reported utilise whole rat blood as the perfusate of choice instead of krebs buffer [158, 177, 178]. The erythrocytes present in the blood can aid as an oxygen carrier which keeps the barrier in a viable state and consequently intact against any fluid leakage.

The substantially higher cost of using whole rat blood to conduct these experiments together with the development time that would be demanded meant that IPG studies were suspended as a tool for predicting the intestinal absorption of PAMAM dendrimers.

2.4 Summary

Studies conducted in this chapter have resulted in the following findings:

- OG labelling of anionic PAMAM dendrimers and FITC labelling of Cationic PAMAM dendrimers serves as a valuable tool to fluorescently analyse and quantify these dendrimers. The labels are biocompatible and completely stable in experimental conditions.
- Anionic PAMAM dendrimers are biocompatible at a generation range G1.5-G5.5 and their permeation across biological barriers is highly dependent on their molecular size with larger anionic dendrimers displaying less permeation across *in-vitro* cell monolayers than their smaller counterparts.
- Cationic PAMAM dendrimers on the other hand are not as biocompatible to *in-vitro* cell monolayers as their anionic counterparts. Cationic PAMAM dendrimers display toxicity and compromise the integrity of monolayers that increases with the increment of their molecular weight. Transport data generated from cationic PAMAM dendrimers have to be hence analysed carefully as results can be misleading.

- Anionic PAMAM dendrimers display more pronounced differential transport across highly restrictive and less restrictive barriers than small molecular weight markers such as F-Na. This was displayed through the high difference in the transport of PAMAM dendrimers across the tight MDCK I barrier and the less restrictive MDCK II; a difference that was more pronounced than that displayed by the small molecular weight marker F-Na. This supports the hypothesis that PAMAM dendrimers are a suitable candidate to achieve oral bioavailability across the relatively less restrictive intestinal mucosa while avoiding access to the CNS across the highly restrictive blood brain barrier.
- *In-vitro* barriers are a poor model to use for predicting the influence of pro-inflammatory mediators upon the permeability of biological barriers. TNF- α did not display an effect upon CaCo-2 monolayers while it surprisingly increased the restrictiveness of MDCK II monolayers. Another model might be more suitable to test the effect of TNF- α upon paracellular restrictiveness.
- The isolated perfused Gut was designed as a simple model to study the total permeability of the intestinal mucosa to dendrimers and other probes in isolation issues such as distribution and metabolism because

the circulation is isolated within the mesenteric system. This system has failed, probably due to issues of poor oxygen delivery to the epithelium. Whole blood is probably needed to be used to perfuse the system rather than the conventional Krebs based perfusate that has been used in these studies. The use of whole blood however is very expensive and would render the use of such a system impractical.

Chapter 3

***Synthesis and Pharmacological Evaluation
of Novel Cannabinoid Derivatives***

3.1 Introduction

3.1.1 Cannabinoid Receptor Pharmacology

The mechanism through which cannabinoids exert their effects (particularly psychoactive effects) was unclear until the mid-1960s. Before then the misconception that predominated the field of cannabinoid pharmacology was that these hydrophobic compounds exert their effects through nonspecific disruption of lipid membranes due to their highly lipophilic nature [179, 180]. It was later revealed however, that Δ^9 -tetrahydrocannabinol (THC), a natural cannabinoid agonist, produces its effects through a receptor mediated mechanism. This was demonstrated by showing that THC exerts specific pharmacological effects (such as the negative regulation of cAMP) in neuroblastoma cells, but not in other types of cells such as sperm cells [181].

Devane et al. [64] were among the first groups to study the presence of cannabinoid receptors in the CNS in 1988. The presence of such receptors in the brain was shown through demonstrating a saturable specific binding process of a radiolabeled full cannabinoid agonist, [^3H] CP 55490, with rat brain membrane preparations. The same ligand has also been used to demonstrate the presence of cannabinoid receptors in rat brain homogenates and whole rat brain sections [182, 183]. The binding of [^3H] CP 55490 to receptors in rat brain tissue has been also shown to be competitively inhibited by other cannabimimetic compounds. Furthermore, the extent of specific binding of [^3H]

CP 55490 to receptors in the rat brain tissue correlated with the cannabinoid agonist's psychoactive effects *in-vivo*, and its ability to inhibit the release of adenylate cyclase *in-vitro* [65].

Later on, two cannabinoid receptors were fully identified and characterised, CB₁ and CB₂, both of which are G-coupled protein receptors [62]. A third G-coupled protein cannabinoid receptor, GPR55, has been suggested to play a role in the interaction with cannabinoid compounds [184]. CB₁ and CB₂ receptors were first identified through molecular cloning in 1990 and 1993, respectively [185, 186]. Upon cloning, both of these receptors showed 44% identity (68% similarity in transmembrane domains) in their amino acid sequences [187].

In-vitro experiments with neuroblastoma cells and kidney COS cells (transfected with CB receptors) showed that both cannabinoid receptors CB₁ and CB₂ are predominantly coupled to G protein subtypes G_i and G_o [188, 189]. This has been shown through demonstrating that their activation upon the use of agonists (quantified by the accumulation cAMP), could be inhibited by pertussis toxin, guanosine-5'-O-(2-thiodiphosphate) and N-ethyl-maleimide [189], [190], [191], [192].

CB₁ receptors have been shown to be predominantly present in the brain. Although highly expressed in the brain, CB₁ receptors are not homogenously present in the CNS region. It has been shown that CB₁ receptors are most highly expressed in the cerebral cortex and hippocampus which are responsible

for motor function and movement, i.e. functions that are affected by cannabinoid drugs [193]. Other groups showed later that the presence of CB₁ receptors is not exclusive to the brain but is also expressed at various extents in different parts of the periphery including intestines, urinary bladder, heart, lung, bone marrow, adrenal glands, testicles, immune cells and the intestines [66, 105, 194-196].

CB₂ receptors on the other hand have a very low expression in the brain in comparison to CB₁ receptors. CB₂ is present at a high density in immune related tissues such as the tonsils, macrophages, mast cells and monocytes [105]. CB₂ receptors are additionally present in bone and cirrhotic cells of the liver (in cases of liver cirrhosis) [197].

It was demonstrated that interaction between cannabinoid agonists and the G-coupled CB₁ receptors can lead to inhibition of calcium currents. Cannabinoid agonists (of CB₁ receptors) such as WIN 55,212-2 have been shown to be highly potent in inhibiting calcium currents. The mixed cannabinoid agonist, WIN 55,212-2 exhibited activity at low concentrations of 1nM and also showed high stereoselectivity in its action; (The [-] enantiomer of WIN 55,212-2 showing no inhibition of currents up to concentrations of 1μM) [190]. This clearly indicates a specific ligand receptor interaction mediated effect. Additionally, other cannabinoids such as CP 55,940, Δ⁹- tetrahydrocannabinol (THC) and the endogenous anandamide demonstrated calcium channel inhibitory activity in various *in-vitro* cell models [191], [189], [192]. Although cannabinoid agonists

play an important role in the regulation of adenylate cyclase (AC), the inhibition of calcium currents exerted by these compounds is not mediated through AC (as evidenced by the fact that this calcium current inhibitory effect could not be reversed through the use of AMP analogues such as dibutyryl-cyclic AMP). The inhibition of calcium currents is mediated instead through N-type channels [190]. CB₁ receptors can additionally mediate the enhancement of inwardly rectifying potassium channels; Mackie et al [198] showed that WIN 55212,2 exhibits a stereoselective enhancement of these potassium channels in *Xenopus laevis* oocytes and murine tumour AtT-20 cells only when they're transfected with CB₁ receptors, confirming that these effects are CB₁ mediated.

CB₂ receptors, on the other hand, do not couple to calcium channels or inwardly rectifying potassium channels and hence don't exert any effects on these ion channels. Felder et al. [188] showed that intracellular calcium levels are inhibited by the non-selective cannabinoid agonist WIN 55,212-2 only when these cells are transfected with CB₁ receptors but not when they're transfected with CB₂ receptors. Similarly, Felder's group showed, using WIN 55,212-2 as an agonist, that only CB₁ receptors and not CB₂ receptors are involved in activation of inwardly rectifying potassium channels in the same cell line [188].

Figure 2.1 outlines the major pharmacological pathways of CB₁ and CB₂ receptors.

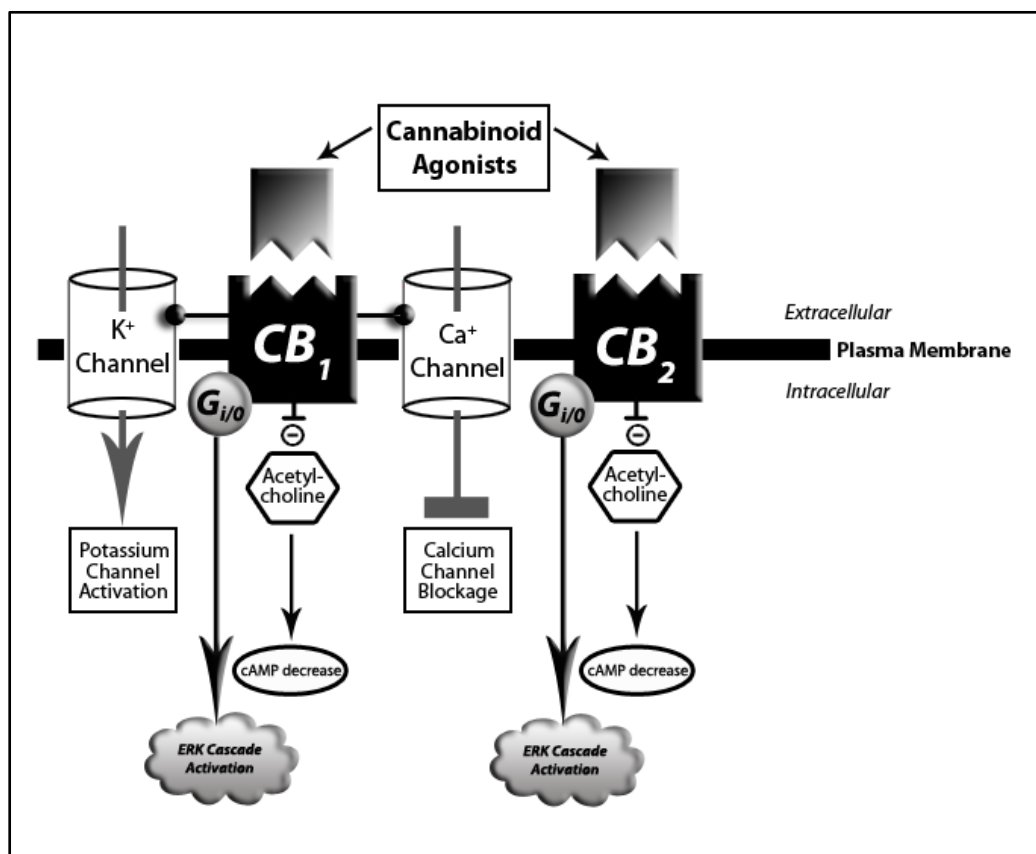


Figure 3.1 Activation of signal transduction pathways via Cannabinoid receptors. Cannabinoid agonists can activate the $G_{i/o}$ protein coupled CB_1 and CB_2 receptors. This results in the inhibition of adenylyl cyclase and the activation of the extracellular signal-regulated kinase (ERK) cascade. Additionally, CB_1 receptors can induce the inwardly rectifying potassium (K^+) channels and the inhibition of calcium channels as previously described.

Inhibition of calcium currents and activation of potassium conductance (which are both exclusively mediated through CB_1 receptors) are both related to the neuronal effects exerted through cannabinoid mixed agonists. This, in addition to the fact that CB_2 receptors are dramatically less expressed in the CNS than CB_1 receptors strongly suggest that neuronal effects of different cannabinoid agonists are mediated exclusively through CB_1 and not CB_2 receptors. This was further supported with the synthesis of a number of selective CB_2 agonists, such as HU-308 and AM1241 which didn't show any CNS side effects when

administered in mice in a tetrad of behavioural tests, unlike classical mixed cannabinoid agonists such as Δ^9 -tetrahydrocannabinol (THC) [199].

3.1.2 Endogenous Cannabinoids

After the identification of cannabinoid receptors, it was revealed that the brain produces its own endogenous cannabinoids which are capable of acting as agonists at CB₁ receptors. The most popular of these endocannabinoids, and the first to be discovered, is arachidonoyl ethanolamide, more commonly known as Anandamide, shown in *Figure 3.2*. This endogenous cannabinoid discovered by Devane et al. in 1992, has demonstrated high affinity to CB₁ receptors and produced THC-like effects when interacting with these receptors in the brain. However, later studies showed that Anandamide, albeit being a very weak CB₂ agonist, has a high affinity to CB₂ receptors and can hence act as a CB₂ antagonist.

Anandamide is released from neurons and is regulated by a number of mechanisms. A carrier mediated Anandamide transport mechanism contributes to the removal of the endogenous cannabinoid from its sites of action. Additionally, Anandamide is metabolised intracellularly via enzymatic hydrolysis (using the enzyme Anandamide amidohydrolase) [200].

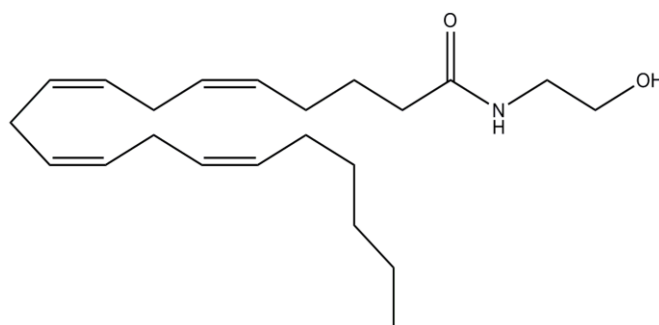


Figure 3.2 Chemical structure of anandamide, an endogenous cannabinoid

Subsequently, several other endocannabinoids have been discovered; these include 2-arachidonoylglycerol (2-AG) whose concentration is significantly higher than anandamide and is a more potent agonist at both CB₁ and CB₂ receptors when compared to anandamide.

3.1.3 Structure Activity Relationship (SAR) of Cannabinoids

The first systematic study investigating the relationship between cannabinoid chemical structure and pharmacological activity dates back to 1942 and involved a dog ataxia test as the biological model to assess the pharmacological end point of different cannabinoid drugs [201].

SAR studies of cannabinoid drugs were initially based on the natural cannabinoid THC (shown in *Figure 3.3, B*) which is the prototype for a classical cannabinoid (*Figure 3.3, A*). SAR investigations on THC utilised a number of

different biological models where the psychoactive and locomotor effects of the cannabinoid agonist are assessed. These models included the dog ataxia test, the mouse ring immobility test, monkey behavioural tests, and behavioural studies in humans [202]. SAR studies reveal the following key properties in the structure of THC as upon clinically testing a variety of cannabinoid compounds in human behavioural tests [203]:

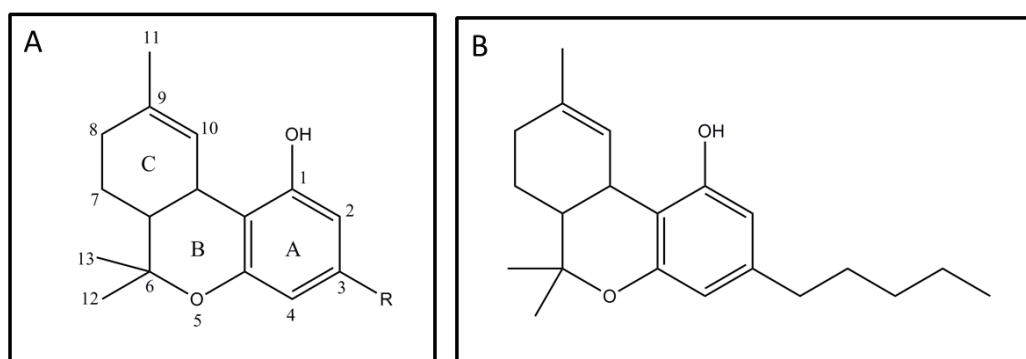


Figure 3.3 General Structure of a classic cannabinoid (A) and Δ^9 -Tetrahydrocannabinol (THC) (B)

- 1- The benzopyran ring system (A and B rings as shown in *Figure 3.3, A*) is essential for pharmacological activity, although benzopyran doesn't confer activity by its own virtue.
- 2- The attachment of an aliphatic cycle (i.e. ring C) to the benzopyran ring is essential, for activity. However, this aliphatic cycle can be spatially separated from the B ring through a methyl spacer as in BRL-4664 (Nonabine). Additionally, replacing the alicyclic ring with a heterocyclic one doesn't seem to alter activity.

- 3- The methyl group at position 9 is redundant for pharmacological activity and can be replaced with a number of substituents such as hydroxyl, hydroxymethyl, or a ketone group without any loss in activity.
- 4- Although the phenolic alcohol at position 1 is of vital importance in the cannabinoid's activity, it can be substituted with an ester group without any loss in activity. Elimination of this group usually leads to complete abolishment of activity or, as in the case of JWH-133 which is a classical cannabinoid that lacks this phenolic alcohol (*Figure 3.4*), elimination of this group can lead to CB₂ selectivity.

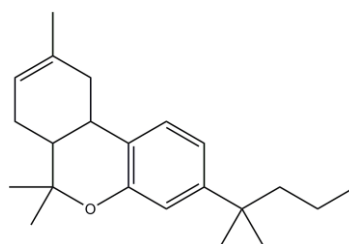


Figure 3.4 Structure of JWH-133: a classical CB₂ selective cannabinoid

- 5- A carbon chain at position 3 (R) is pivotal for activity, but can vary in length and structure. Decreasing the chain length to less than 3 carbons, however, diminishes pharmacological activity. The structure of the chain nevertheless can have an effect on the differential effect of the cannabinoids on CB₁ and CB₂ receptors. The alkyl chain can be attached directly to the benzene ring or through an ethereal linkage without loss or alteration in activity.

- 6- The stereochemistry of the classical cannabinoid is of key importance. It has been shown that most stereoisomers of classical cannabinoids are inactive. It has been shown that some of the inactive stereo-isomers of a number of cannabinoids can still bind the cannabinoid receptors without mediating any pharmacological activity and can hence be used as competitive antagonists at the cannabinoid receptors [204].

Since its discovery and characterisation more than 40 years ago, immense chemical research has been taking place to improve the potency and selectivity of THC through creating a number of its derivatives and analogues which are generally much more diverse than the natural product. Among these, are 3-arylcyclohexanols such as CP-55 940, and aryl alkyl indoles (AAIs) such as the prototype cannabinoid WIN 55212,2 which has been extensively used as a cannabinoid drug in many areas of research. The structure of WIN 55,212-2 is shown in *Figure 2.5*. Although it might appear that it doesn't share any commonalities with the natural product THC at a first glance, it has been postulated that the two structures share three major overlapping regions [205]:

- 1- The naphthyl ring in WIN 55,212-2 and the cyclohexene in THC
- 2- The carbonyl region in WIN 55,212-2 and the phenolic alcohol in THC
- 3- The morpholine unit in WIN 55,212-2 and the alkyl chain at position 3 in THC.

WIN 55,212-2 has been shown to have a 30-fold higher affinity to the CB₁ receptor and >100 fold higher affinity to the CB₂ receptor as compared to the natural compound THC [205].

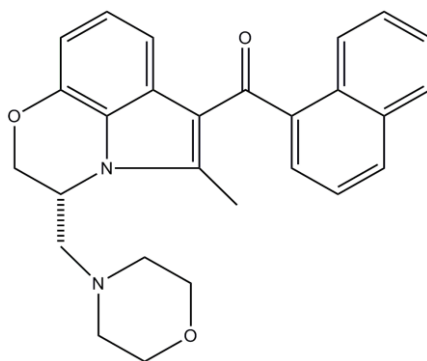


Figure 3.5 Structure of WIN 55,212-2

Aung et al. working the lab of JW Huffman [206] attempted to further elucidate the SAR of WIN 55212,2 through the synthesis of a number of cannabimimetic indoles in which the morpholine units of WIN 55,212-2 are replaced with alkyl hydrophobic chains of different lengths, as shown in *Figure 3.6*.

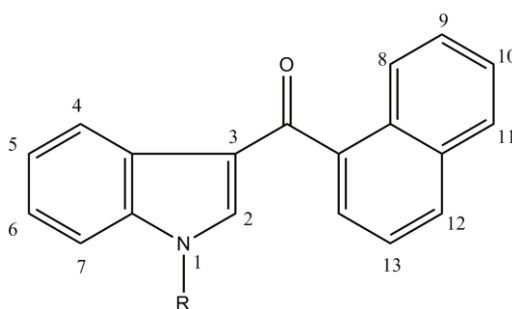


Figure 3.6 The general structure of a cannabimimetic aryl alkyl indole

The same group showed that the length of the alkyl chain is vital for affinity to both CB₁ and CB₂ receptors. Similarly to THC, reducing the length of the N-1 alkyl chain in these cannabimimetic indoles (which putatively overlaps the alkyl chain on position 3 in THC) completely abolishes affinity to both cannabinoid receptors. A 3-carbon long chain (propyl) is minimal for any binding to either CB₁ or CB₂. Increasing the chain length beyond that to Butyl, pentyl and hexyl carbon chains increases affinity to both cannabinoid receptors, while increasing the length beyond 6 carbons abolishes affinity to both receptors. The length of this chain seems to play a role in the selectivity of the cannabinoid to either of the two CB receptors; using a propyl chain, for instance, as in JWH-015 (*Figure 3.7, B*) seems to shift affinity to the CB₂ receptor (CB₂/CB₁ affinity = 6) in contrast to the pentyl chain in JWH007 (*Figure 3.7, A*) which has virtually identical affinity to both CB₁ and CB₂ receptors (CB₂/CB₁ affinity = 1.1).

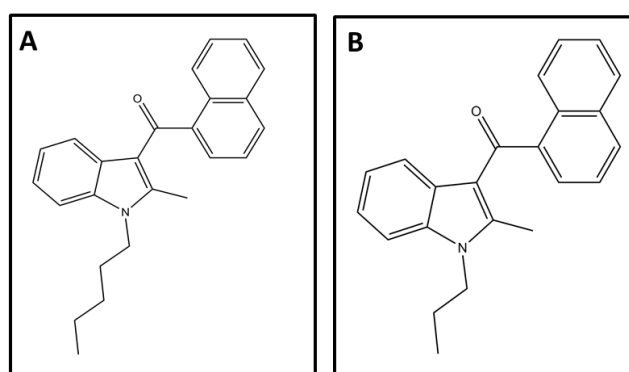


Figure 3.7 Two amino alkyl indole cannabinoids: (A) JWH007, a nonselective CB agonist with a pentyl chain at position 1. (B) JWH015, significantly CB₂ selective cannabinoid with a propyl chain at position 1.

The carbonyl group has also been shown to be vital for activity of these cannabimimetic indoles, where eliminating it using LiAlH_4 completely abolishes activity. It hasn't been shown however if replacing the carbonyl region with other oxygen containing groups (such as esters and ethers) would alter affinity as it has been shown that despite the vitality of the phenolic alcohol in THC (which putatively overlaps the carbonyl region in WIN 55,212-2), it can be substituted with an ester without any loss of activity.

The group also showed that attaching a methyl group at position 2 (as in the case with WIN 55,212-2), doesn't alter the affinity of the cannabinoid to its receptors.

The naphthoyl ring on the other hand is vital for activity. The addition of different groups to the ring significantly alters activity, and the addition of longer chains significantly attenuates CB_1 and CB_2 affinities.

The effect of adding different groups to the indolic benzene group (positions 4, 5, 6 and 7) has not been investigated so far.

3.1.4 Assessment of anti-inflammatory activity of Cannabinoid compounds

The first evidence of the involvement of cannabinoids in anti-inflammatory activity stems back to the mid-1980s when it was shown that THC can suppress the production of pro-inflammatory cytokines IFN- α and IFN- β in murine spleen cells following exposure to LPS stress *in-vitro* and *in-vivo* with mice infected with the herpes simplex virus [207, 208]. Additionally, other cannabinoids such as WIN 55,212-2 and the THC derivative, HU-210, have been shown to play a role in suppressing the release of cytokines TNF- α and interleukin-12 (IL-12) in mice injected with LPS [209]. Klein et al. [210] have additionally shown that cannabinoid agonists THC and 11-hydro-THC exhibit an immune-modulatory function through the suppression of the cytolytic activity of Natural Killer (NK) cells.

This effect of cannabinoid agonists is a property of the CB₂ receptor which is responsible for suppressing the release of cytokines and inflammatory mediators from immune cells. A few groups showed that CB₂ receptors are expressed in monocytes, macrophages and B and T immune cells [105, 106]. It has also been shown the CB₂ receptors are expressed in the murine macrophage cell line RAW 264.7 [211]. Additionally, Hunter et al. [212] showed that challenging RAW 246.7 cells with CB₂ antisense significantly decreased the THC induced release of arachidonic acid indicating the functionality of these receptors in this cell line. Furthermore, several groups demonstrated the

functionality of CB₂ receptors in RAW 264.7 with decreases in LPS-regulated release of nitric oxide from this cell line upon the use of THC as a cannabinoid agonist [213, 214]. Gallily et al. [215] also demonstrated that the CB₂ selective THC derivative HU-211 suppresses LPS-regulated production of TNF- α by the same murine macrophage cell line.

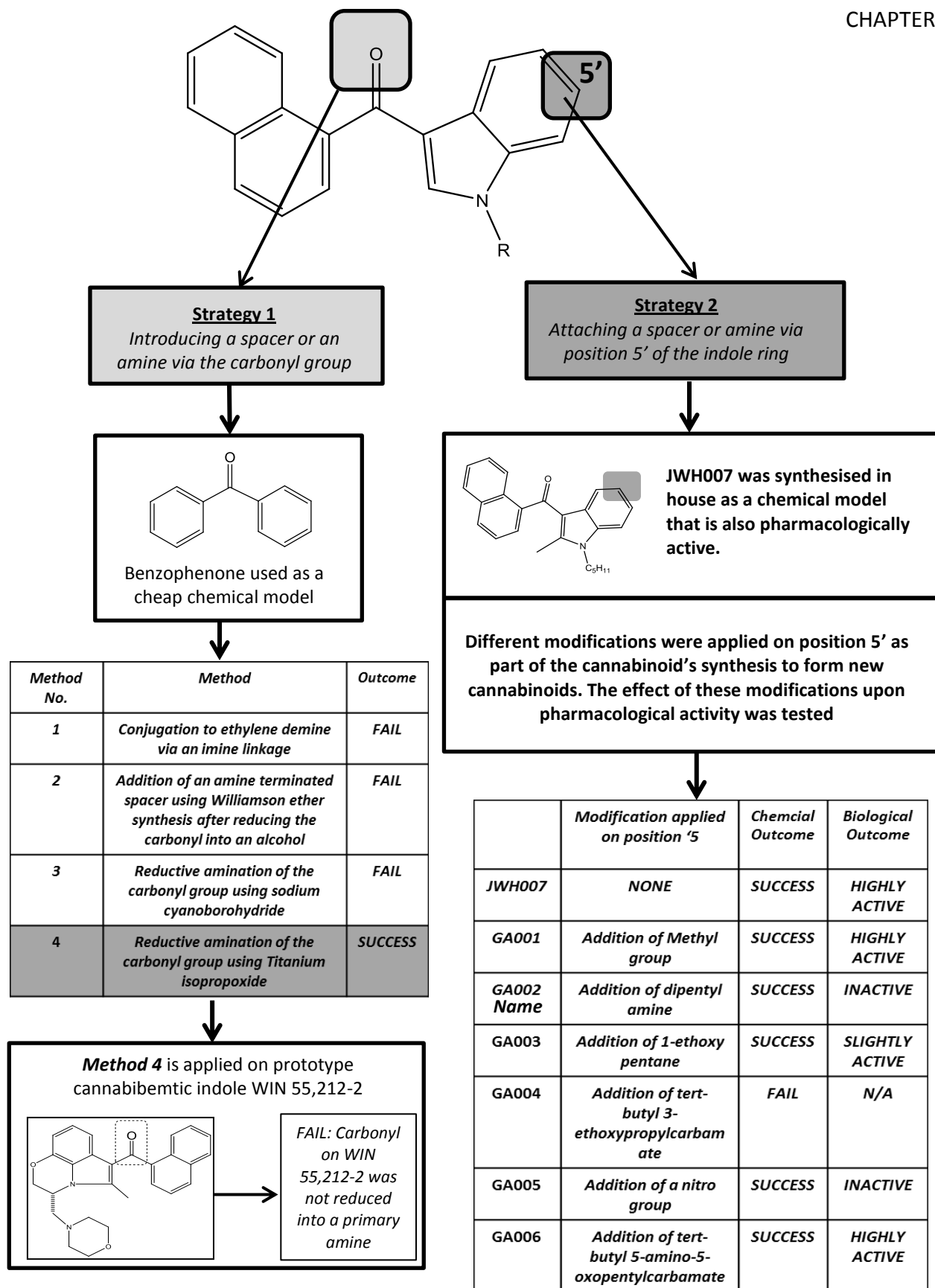
The ability of cannabinoids to suppress the release of different pro-inflammatory cytokines can be exploited as a tool for the rapid *in-vitro* screening of the anti-inflammatory activity of different cannabinoid compounds. This is further facilitated by the development of reliable and quick methods for high sensitivity Enzyme linked Immunosorbent assays (ELISA) in the quantification of a range of different cytokines.

3.1.5 Aims, Objectives and Overall Strategy

The aim of studies described in this chapter was to assess SAR of cannabimimetic indoles, as a potent class of cannabinoid compounds that has been extensively used in the literature, and to investigate possible sites at which chemical modifications can be implemented while maintaining the cannabinoid's pharmacological activity. This involves the identification of sites that are not vital for pharmacological activity and studying the effect of modifying them upon the overall pharmacological activity of the cannabinoid.

This is done in the ultimate goal of conjugating a cannabinoid to a PAMAM dendrimer in later studies (discussed in Chapter 4). An amine group has to be present in a compound to facilitate its conjugation to an anionic PAMAM dendrimer (containing amine-reactive carboxylic groups on its surface), and therefore one of the aims in this chapter was the synthesis of a pharmacologically active cannabinoid that bares a primary amine in its structure.

To investigate SAR of cannabimimetic indoles in this chapter, a number of chemical modifications on prototypical cannabinoids such as WIN 55,212-2 were attempted. Additionally, a number of novel cannabimimetic indoles were synthesised in-house and their pharmacological activity investigated to assess the importance of different sites of cannabimimetic indoles on their pharmacological activity. The overall strategy for all the modifications that were attempted and achieved is outlined in *Schematic 3.1*.



Schematic 3.1 Outlined Strategy for SAR studies in cannabinoid compounds

3.2 Material and Methods

3.2.1 Materials

Organic Solvents Dichloromethane, Ethanol, Methanol, Cyclohexane, Ethyl acetate, Toluene, Dimethyl formamide (DMF), Dimethyl sulfoxide (DMSO) were purchased from Fisher Scientific (UK). LPS (*Escherichia coli* 0111:B4), and all other used chemicals used in organic reactions were from Sigma-Aldrich *inc.*, unless otherwise stated.

Murine macrophage cell line RAW 264.7 was obtained from the European Tissue Culture Collection ECACC (London, UK). DMEM, Penicillin/streptomycin, and foetal bovine serum were obtained from Invitrogen (UK).

TNF- α analysis was performed using an ELISA kit from R&D systems, UK.

3.2.2 Methods

Chemical Reactions

Chemical reactions were generally performed in glass round bottom flasks (100mL size) and magnetic stirring. Primary analyses were performed using thin layer chromatography on silica plates using Cyclohexane-Ethylacetate solvent systems. Desired compounds were then purified using silica flash chromatography.

NMR analyses were performed using a 500Mhz NMR. ESI+ Mass spectrometry analyses were performed using a Quatro-ultima Mass spectrometer as a service supplied by the Chemistry Department, Cardiff University.

Cell Culture

RAW 264.7 cells were cultured using Dulbecco's Modified Eagle medium (DMEM) supplemented with 10% (v/v) heat inactivated FBS and 2% penicillin G/Streptomycin (100U/mL). Cell cultures were maintained at 37°C in 5% CO₂/95% atmospheric air and relative humidity. While cells were grown in T-25 and T-75 culture flasks, they were routinely cultured to 70-80% confluence. RAW 264.7 cells were seeded at a density of 50,000 cells/cm² on 24-well culture plates for 5-6 days prior to inducing TNF- α release using LPS.

LPS induced TNF- α production by RAW 264.7 cells

Cells were cultured on 24 well plates for 5-6 days in DMEM full media supplemented with antibiotics. Before executing LPS-induced TNF- α suppression experiments, cells were treated with different concentrations of various cannabinoid drugs (10 μ M-25 μ M in DMEM full media) and 0.1% DMSO as a control treatment as all the used cannabinoid drugs described in this chapter were prepared as 100x stock solutions in DMSO to be used in cell culture studies. After 1 hour of the treatment, cells were challenged with LPS, which was added as a 10 μ L saline solution to each well to create a final concentration of 200ng/mL in each of these wells. The cells were then incubated for 16 hours at 37°C. The media was collected and centrifuged for 10 minutes at 200g and the supernatants were collected for TNF- α analysis.

ELISA based TNF- α analysis

TNF- α levels in supernatants obtained from RAW 264.7 cells after LPS induced TNF- α production were analysed using a mouse TNF- α sandwich ELISA kit. Briefly, 96 well plates were coated overnight with TNF- α antibody at room temperature. Supernatants in all experiments were diluted 1:3 to achieve a TNF- α concentration that lies within the concentration capacity of the method for detection (30-2000pg/mL) and were then added along with supplied TNF- α standards to the antibody pre-coated plates. The conjugate antibody was added to all wells after thorough washing and this was followed by the addition

of Streptavidin HRP and the addition of substrate solution (1:1 mixture peroxide : chromogen solutions). 2.5M aqueous sulphuric acid solution was added to all wells to stop the experiment. The plate was then analysed using UV-visible spectroscopy at a wavelength of 450nm. TNF- α was quantified according to a 7-point calibration curve that ranges between 0-2000pg/mL that is generated in each ELISA experiment. Statistical analysis to assess the performance of a certain cannabinoid drug was performed by comparing the quantity of TNF- α released by RAW 264.7 cells when treated with this drug, and when they are subject to the control treatment (0.1% DMSO, or the final concentration of the solvent to use the drug).

Toxicity Studies

After collecting supernatant media in RAW 264.7 TNF- α studies, 0.5mL of fresh full DMEM media was added directly to the each of the wells in the 24-well culture plate. 50 μ L of a 5mg/mL PBS solution of Thiazolyl Blue Tetrazolium Bromide (MTT) were added to each well. The culture plate was then incubated for 4 hours at 37°C, 5% CO₂ and relative humidity. The media containing the MTT was then aspirated and discarded and 400 μ L of DMSO were added to every well to resuspend the MTT metabolic product (formazan) which indicates cell viability. 200 μ L of DMSO containing formazan were transferred from each well to a separate well in a 96 well plate. Optical density was then measured on a UV plate reader at a wavelength of 560nm.

3.3 Results and Discussion

WIN 55,212-2 is cannabimimetic indole that has been established as a prototype cannabinoid extensively used in the cannabinoid literature since its development two decades ago [216]. The understanding of its SAR has been well established with both CB₁ and CB₂ receptors. It is also commercially available albeit expensive. It was hence decided to further investigate its SAR to identify sites where modifications can be attempted without loss in pharmacological activity, and where amines can be introduced in the ultimate aim of conjugating the cannabinoid to a dendrimer.

WIN 55,212-2 like other cannabinoids doesn't comprise many reactive functional groups where it can be chemically manipulated or modified to study the effect of such modifications upon SAR. The carbonyl group that connects the naphthalene group to the indole part of the compound (shown in *Figure 3.8*) however, can be reactive, and it was hence chosen as an initial target for a chemical modification.

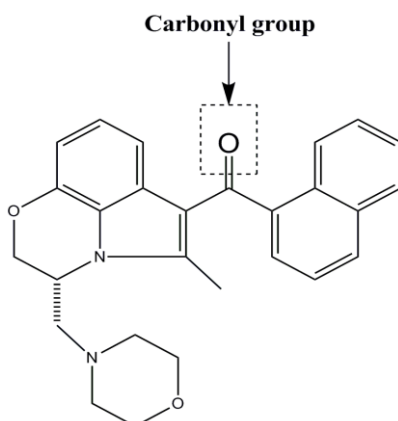


Figure 3.8 Structure of WIN 55,212-2 showing carbonyl group

Although it is speculated that this oxygen plays an important role in the interaction with CB receptors and contributes to hydrogen bonding at these sites [205], as it is correlated with the phenolic oxygen in THC which plays the same role, manipulating it doesn't necessarily abolish activity. As previously discussed, conversion of the phenolic alcohol in THC, for instance, into an ester doesn't affect the natural cannabinoid's pharmacological activity, and hence modifications that maintain a polar group that achieves hydrogen bonding to the receptor can result in pharmacologically active compounds. Additionally, conversion of this oxygen atom into an amine (through reductive amination for instance) shouldn't necessarily abolish pharmacological activity because nitrogen, like oxygen can also contribute to hydrogen bonding.

3.3.1 Choice of a model for WIN 55,212-2

WIN 55,212-2 is a commercially available drug. However, its extremely expensive price (like most other commercially available cannabinoid compounds) has necessitated the use of a model compound to perform chemical experiments which require high quantities of any compound. The use of such quantities of the expensive WIN 55,212-2 for chemical reactions is not financially feasible.

A useful chemical model compound should comprise the functional groups needed to be modified on the cannabinoid drug, contain similar structure to the drug and be relatively cheap in large quantities to allow multiple experimentations using different methods.

As the target in WIN 55,212-2 was to modify the carbonyl group present on the junction between the indolic and naphthoylic groups, a model that comprises the same group connected to similar conjugated structures was needed.

Figure 3.9 shows Benzophenone, a cheap compound comprising a carbonyl group between two conjugated systems (benzene rings). The carbonyl group on benzophenone is expected to have similar properties to that present in the WIN 55,212-2.

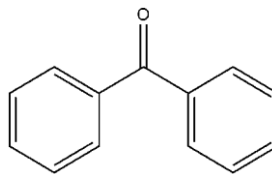
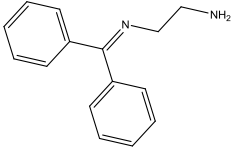
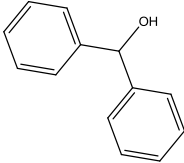
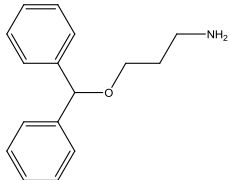
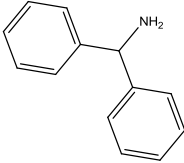
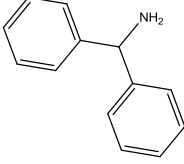


Figure 3.9 Benzophenone, chosen as model to manipulate carbonyl group on cannabinoid drug.

Different chemical strategies can be tested on the cheap benzophenone, and successful ones can be optimised and applied on WIN 55,212-2 to save on costs.

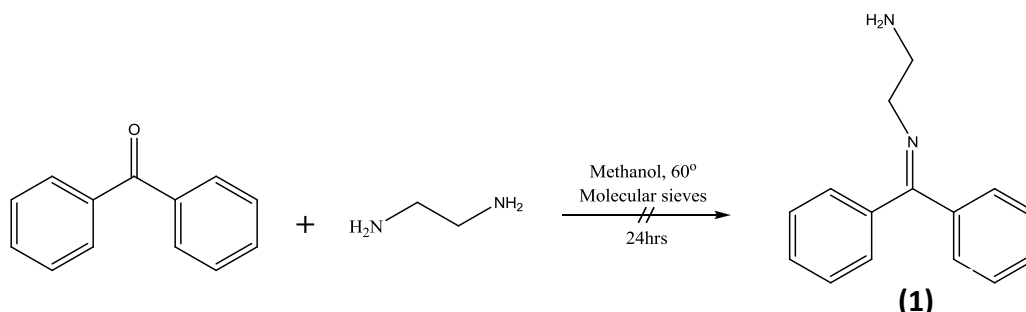
Table 3.1 shows different attempts the different attempts used to manipulate the carbonyl group on benzophenone either by attaching an amine-containing spacer or transforming the entire group into an amine by reductive amination.

Table 3.1 Strategies used to manipulate carbonyl group and introduce an amine in benzophenone

STRATEGY FOR ADDING THE SPACER OR ALTERING THE CARBONYL GROUP	OUTCOME	Structure of expected product
(1) Conjugation to ethylene diamine via an imine linkage	FAIL	
(2a) Simple reduction using Sodium borohydride	Success (>85% yield)	
(2b) Addition of tert-Butyl 5-bromopentylcarbamate to (2) via williamson synthesis	FAIL	
(3) Reductive amination using sodium cyanoborohydride	FAIL	
(4) Reductive amination using Titanium isopropoxide, ammonia and sodium borohydride .	Success (>60% yield)	

Strategy 1

A primary amine can be attached to a compound comprising a ketone via the formation of an imine bond where the nitrogen in the amine compound replaces the oxygen in the ketone [217].



Schematic 3.2 Failed reaction of benzophenone and ethylene diamine to produce (1)

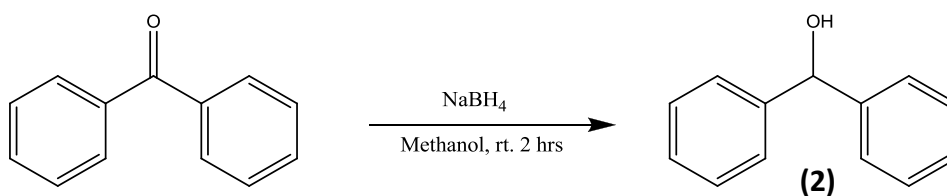
Ethylenediamine (EDA) was reacted with benzophenone in methanol in an attempt to produce an imine linkage between EDA and benzophenone as shown in *Schematic 3.2*. Activated molecular sieves were used to quench the generated water from the reaction, as imines are highly sensitive to water. If the reaction was successful, the imine bond can be later reduced to a stable amine using a previously described method of hydrogenation [218].

The reaction did not work as evidenced from TLC analysis using the amine reactive dye ninhydrin to visualise the spots. It is unknown why this reaction hasn't worked. One explanation can be the high stability of the ketone's electrons as the ketone attached to two strong electron withdrawing groups (benzene rings).

Note: All reactions are detailed in *Appendix A* at the end of this chapter.

Strategy 2a

In this strategy, the ketone was attempted to be reduced into the corresponding alcohol using a reducing agent, so a halide containing spacer can be later attached to the formed alcohol using williamson ether synthesis. A ketone group can be simply reduced into an alcohol by using the reducing agent sodium borohydride [219].



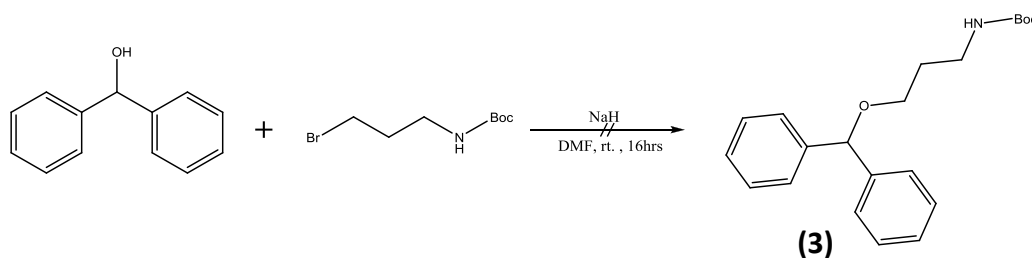
Schematic 3.3 reduction of the carbonyl group in benzophenone to the corresponding alcohol to produce (2)

Reduction of benzophenone to diphenyl methanol using sodium borohydride as shown in *Schematic 3.3* was successful as evident from TLC and NMR analyses.

The use of another stronger reducing agent, LiAlH₄, was also successful in reducing the carbonyl to achieving the same end product.

Strategy 2b

A compound bearing a halide can be attached via an ether linkage to an alcohol group using Williamson ether synthesis which has been extensively used in organic syntheses [219].

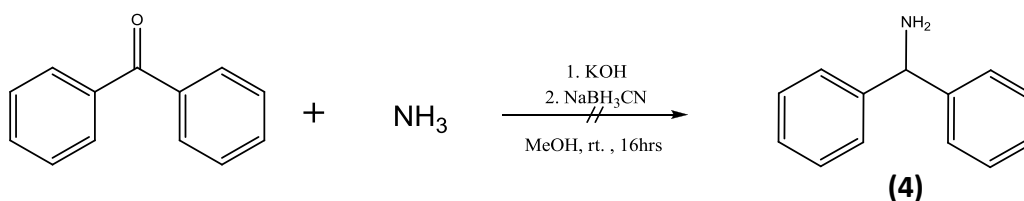


Schematic 3.4 Failed attempt to attach tert-Butyl 5-bromopropylcarbamate to diphenyl methanol via Williamson ether synthesis

Addition of a halide containing spacer bearing a BOC protected amine on its terminus to diphenyl methanol using Williamson ether synthesis as shown in *Schematic 3.4* was unsuccessful. The failure of this reaction might be due to the high electron withdrawing power of the conjugated rings making the electron on the nucleophilic alkoxide (formed by the addition of sodium hydride [NaH]) less prone to attack the electron deficient spacer.

Strategy 3

Sodium Cyanoborohydride (NaBH_3CN) has been used in the literature as an agent in the reductive amination of aldehydes and ketones in the presence of ammonia [220].



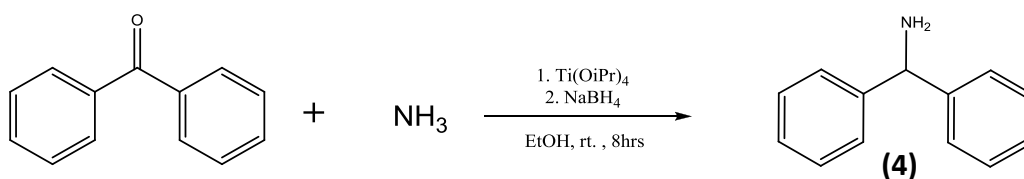
Schematic 3.5 Reductive amination of benzophenone using Sodium cyanoborohydride and ammonia

The reducing agent sodium cyanoborohydride was used to convert the carbonyl group present on benzophenone into a primary amine using ammonia as a source of nitrogen atoms as shown in *Schematic 3.5*.

The reaction however has failed as evidenced from TLC analysis. The reason of why this reaction hasn't worked is not known, although it might be due to the same reason suggested for the failure of previous reactions and that is the high electron stability on the oxygen atom that stems from the strong electron withdrawing effect exerted by the benzene rings.

Strategy 4

A method previously described by Sukanta et al. [221] which employs the use of titanium isopropoxide and sodium borohydride in the reductive amination of various compounds, including benzophenone itself, was used to achieve reductive amination in this strategy.



Schematic 3.6 Reductive amination of benzophenone with ammonia using titanium isopropoxide and sodium borohydride.

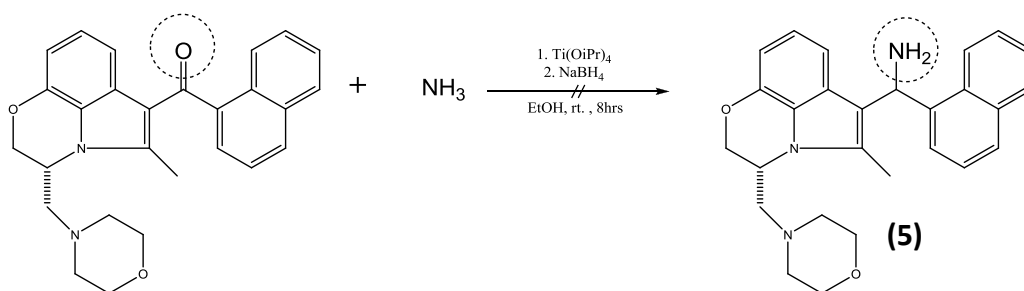
Unlike reductive amination using sodium cyanoborohydride, reductive amination using Titanium isopropoxide and sodium borohydride was successful in converting the carbonyl group into an amine as evident from TLC and ^1H NMR analysis.

The results from these 4 strategies with benzophenone show that the only applicable strategy to alter the carbonyl moiety and introduce an amine to it would be the reductive amination using Titanium isopropoxide and sodium borohydride. Other strategies to attach an amine through the use of an imine linkage or through reducing the carbonyl into an alcohol and then attaching a spacer via Williamson ether synthesis weren't successful, most possibly due to the strong electron withdrawing effect exerted by the two benzene rings; the

same electron withdrawing effect upon the carbonyl's electrons is also expected with WIN 55,212-2. It was hence decided to apply the successful reductive amination strategy of benzophenone to WIN 55,212,2 and convert its carbonyl group into a primary amine. This would allow investigating the effect of altering the carbonyl group in WIN 55,212-2 upon its pharmacological activity and to assess if it is feasible to attach a PAMAM dendrimer through this site.

3.3.2 Reductive Amination with WIN 55,212-2

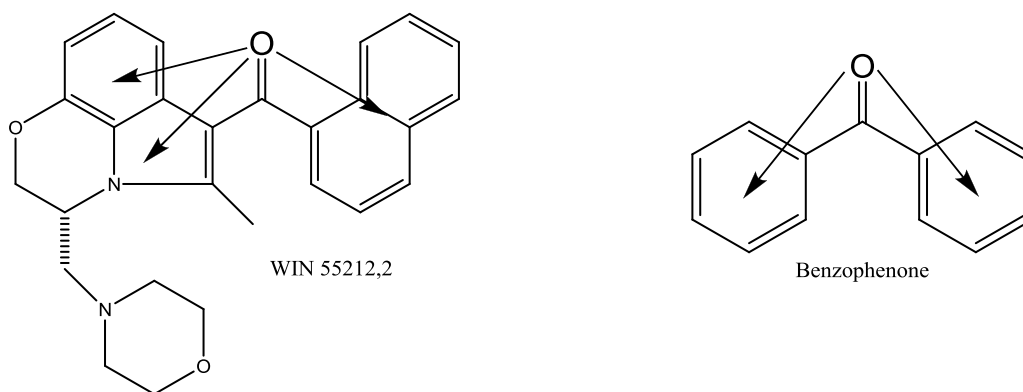
The successful reductive amination strategy with benzophenone was identically applied to WIN 55,212-2 to convert its carbonyl into an amine (both groups circled in *Schematic 3.6*) to generate a cannabinoid that can be attached to the anionic PAMAM dendrimer.



Schematic 3.7 Reductive amination of WIN 55,212-2 using Titanium isopropoxide and sodium borohydride.

The reductive amination with WIN 55,212-2 using the Titanium isopropoxide strategy, however, hasn't worked as obvious from TLC and ESI+ Mass Spectroscopic analysis.

The reason of why the reductive amination strategy has worked with benzophenone but not with WIN 55,212-2 can be attributed the high stability of the carbonyl group in WIN 55,212-2 when compared to the one on benzophenone. Although the chosen model (benzophenone) contained two strong withdrawing groups as in the cannabinoid, WIN 55,212-2 contains an amine on a distance that might play role in further stabilisation the carbonyl group via electron delocalisation as shown in *Schematic 3.8*. The conjugation with the indole amine means that the carbonyl acts as a vinylogous amide.



Schematic 3.8 The oxygen's electrons are more delocalised in WIN 55,212,2 than in benzophenone. This might be due to the conjugated indolic amine which further delocalises electrons.

To further prove this hypothesis, the reduction of the carbonyl group in WIN 55,212-2 with the reducing agent sodium borohydride was attempted as

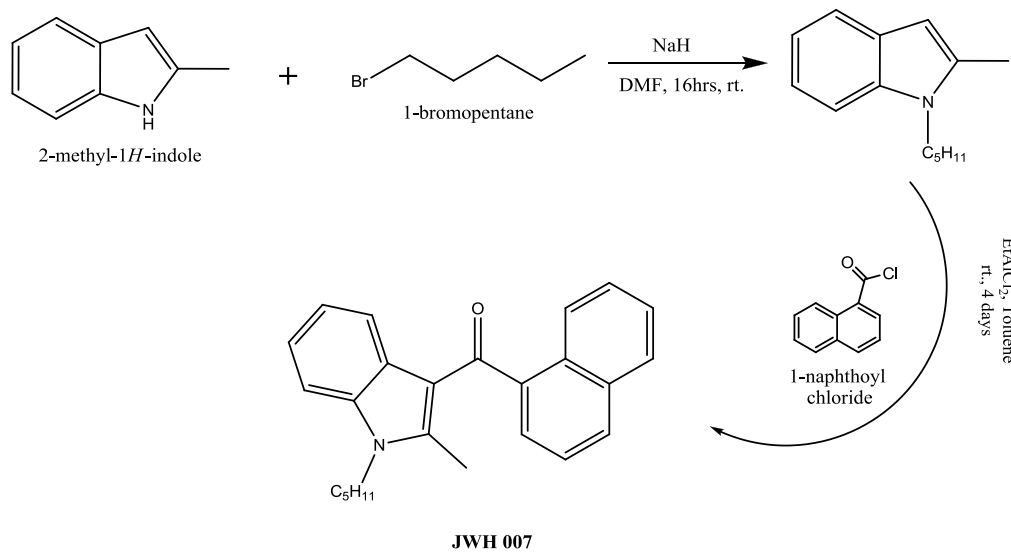
previously described with benzophenone. Sodium borohydride failed to reduce the carbonyl as evidenced from TLC and ESI+ mass spectroscopic analysis which both showed that the carbonyl hasn't been reduced to the corresponding alcohol.

The high stability of this oxygen makes it increasingly difficult to alter the structure of WIN 55,212-2 and to introduce the amine group which is vital for conjugation with a carboxylic PAMAM dendrimer. Additionally, the previous results have shown that the benzophenone model might fail in predicting the reactivity of the carbonyl group in WIN 55,212-2.

It has hence been decided that a more appropriate indole based model should be synthesised for further experimentation with conjugation strategies with cannabinoids.

3.3.3 Synthesis of a new cannabinoid model

The model of choice to be synthesised was a previously developed amino-alkyl indole by the group of Huffman et al. [205], JWH 007. This compound (seen as the end product in *Schematic 3.9*) is a biologically tested cannabinoid that has been shown to interact with both CB₁ and CB₂ receptors. The synthesis of this model cannabinoid can be performed through a cheap and efficient two-step process, previously described by Huffman et al. [205] as shown in *Schematic 3.9*. The final product was characterised using ¹H, ¹³C NMR and ESI+ Spectroscopy.



Schematic 3.9 Synthesis of JWH-007: an amino alkyl indole cannabinoid.

JWH-007 has been successfully synthesised starting from 2-methyl indole. All the components used in the reactions leading to its synthesis were relatively cheap and highly available in bulk quantities. This facilitates the synthesis of large quantities of such a model and consequently offers an avenue for further experimentations at a low cost.

3.3.4 Structural Similarities between JWH007 and WIN 55,212-2

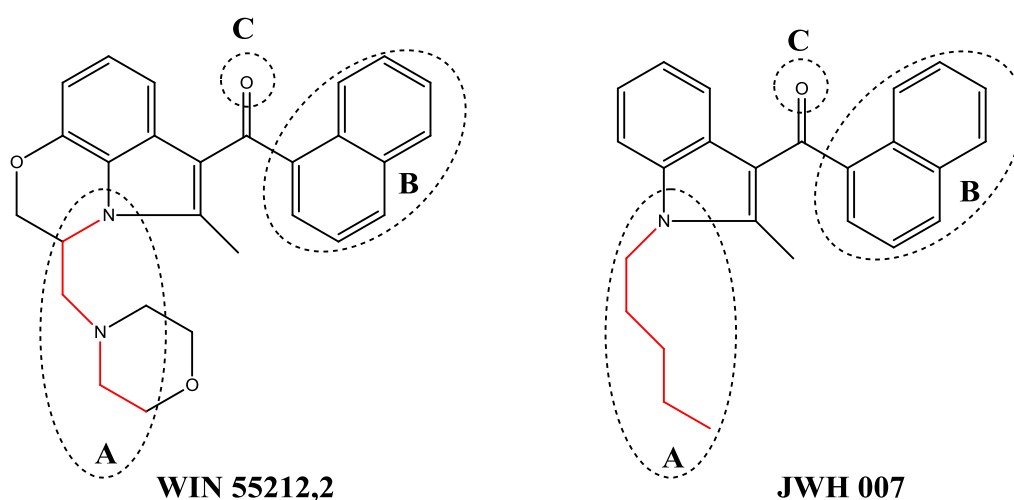


Figure 3.10 Structures of WIN 55,212-2 and JWH007. Moieties contributing to cannabinoid pharmacological activity marked in circles.

As seen in *Figure 3.10*, JWH007 shares the major moieties contributing to cannabinoid based pharmacological activity. Both compounds contain a naphthalene ring which, as discussed before in the introduction to this chapter, is vital for activity. Similarly, both compounds contain the carbonyl group which should have identical chemical properties.

The major difference between the two compounds is that the two morpholine rings in WIN 55,212-2 are replaced in JWH007 by a simpler alkyl chain (compare regions labelled (A) in *Figure 3.10*). The length of this alkyl chain in

JWH007 however, is equivalent to the length created by the two morpholine rings as shown in the figure above.

3.3.5 Biological Evaluation of JWH007 and WIN 55,212-2

JWH007 is an active cannabinoid itself, so it is possible to use it as a model cannabimimetic indole instead of WIN 55,212-2 if a comparable pharmacological activity was demonstrated.

To assess the pharmacological activity of JWH007, WIN 55,212-2, and indeed any other synthesised cannabinoid derivatives, an efficient biological model would be needed to achieve quick evaluation of these compounds' activity. The model of choice to assess cannabinoid activity of these compounds was the murine macrophage cell line RAW 264.7. These cells have been shown to express functional CB₂ receptors that regulate the production of nitric oxide and TNF- α under stress [211-215]. An efficient method to assess the pharmacological activity of different cannabinoids was to test their ability to suppress the release of the pro-inflammatory cytokine TNF- α from these cells when they're challenged with the endotoxin Lipopolysaccharides (LPS). This method provides a quick and cheap tool to predict the biological activities of these cannabinoid compounds.

To assess the activity of JWH007 and WIN 55,212-2, both compounds' activities were evaluated through their ability to suppress the LPS induced production of TNF- α .

Figure 3.11 shows the effect of these compounds upon the suppression of LPS (200ng/mL) induced TNF- α production from the murine macrophage cell line. At a concentration of 10 μ M, both compounds exhibited a significant suppression in TNF- α release when compared to the vehicle control (0.1% DMSO+200ng LPS).

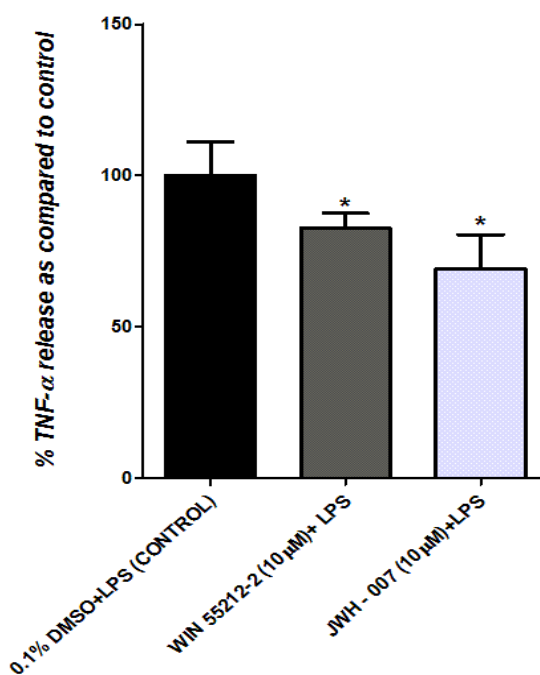
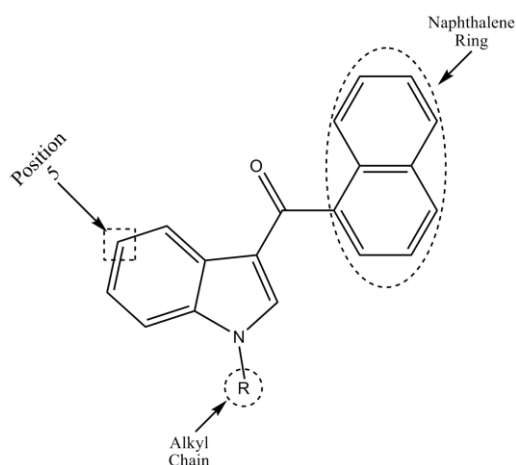


Figure 3.11 The effect of synthesised JWH007 and WIN 55212,2 (10 μ M) to suppress LPS induced (200ng/mL for 16 hours) production of TNF- α in the murine macrophage cell line, RAW 264.7. Results are mean \pm S.D, n=4. * indicates $P < 0.05$

JWH007 showed comparable biological activity to WIN 55,212-2 in suppressing the production of TNF- α . These results indicate that JWH007 can serve as a good prototype cannabinoid on which different chemical manipulation

strategies can be applied and then rapidly screened for biological activity using the macrophage model.

3.3.6 Synthesis of Novel Cannabimimetic indoles



Schematic 3.10 A classical aminoalkyl indole

The ability to synthesise a classical amino-alkyl indole (like JWH007 for instance) from basic chemical components gives more flexibility in tailoring the compound to specific needs as different building blocks or functional groups can be incorporated to the cannabinoid in different sites during the synthesis process.

The moieties marked in circles in *Schematic 3.10* are crucial for pharmacological activity of a classical amino-alkyl indole [216]. Manipulation of any of these moieties should be carefully considered before being applied. For

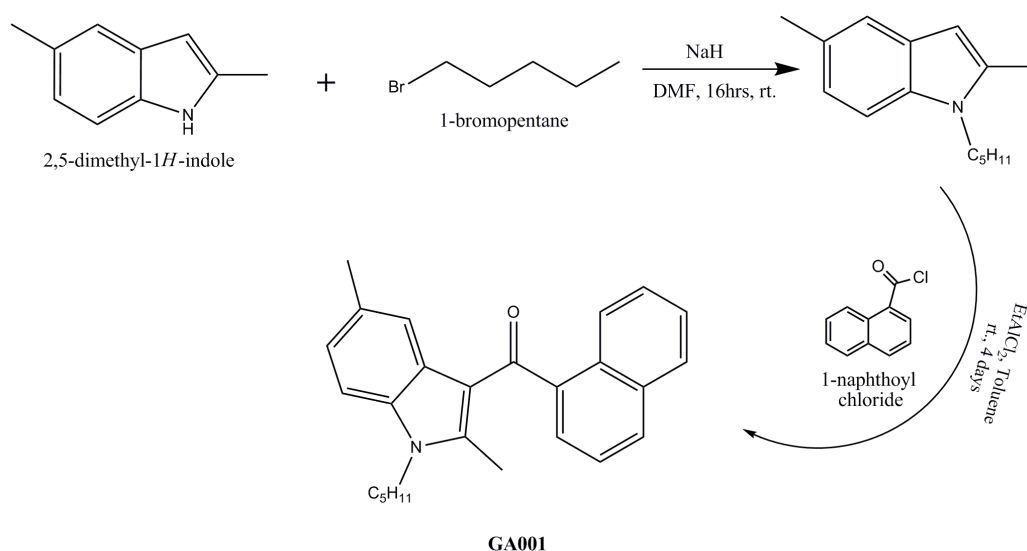
instance, previous data in the literature shows that adding different functional groups to the naphthalene ring can have significant effects on pharmacological activity and the addition of longer carbon chains leads to complete abolishment of activity [205]. Similarly, the length of the alkyl chain that protrudes from the indole amine (R in *Schematic 3.10*) is vital for activity, with shorter or longer chains leading to significant decrease in CB₁ and CB₂ interaction [206]. It was hence decided to avoid any manipulation with these groups and explore other avenues that haven't already been shown to be crucial for pharmacological activity. Exploiting the carbonyl group would still be a valid pathway to be explored. The high stability of this group in an indole system, however, has made it extremely difficult to manipulate as it was previously shown.

It has been decided to explore a new site on the cannabimimetic indole that hasn't been investigated before, and that is position 5' (shown in *Schematic 3.10*). It is clearly very difficult to modify this site in an intact cannabimimetic indole as it is not reactive. Various changes can be applied on this position however as a part of its synthesis of the cannabinoid.

The following sections show the various alterations that were applied to position 5' in a series novel cannabinoids that have been synthesised in-house.

3.3.6.1 Synthesis and Pharmacological Evaluation of GA001

To investigate the influence of position 5' in the classical amino-alkyl indole on cannabinoid activity, a simple methyl group was incorporated to this position during the synthesis of the new compound. This was simply achieved by replacing the indole which was used as the primary building block in the synthesis of JWH007 (2-methyl-1H-indole) with another indole containing a methyl group at position 5' (2,5-dimethyl-1H-indole). The synthesis of the new compound was then carried on using the previous strategy used to synthesise JWH007 as shown in *Schematic 3.11*.



Schematic 3.11 Synthesis of GA001

The synthesis was successful as confirmed by ^1H NMR analysis with similar yields to JWH007. The resulting new compound was labelled GA001.

The pharmacological activity of GA001 was tested using the RAW 264.7 macrophage cell model used previously to assess pharmacological activity of JWH007 and WIN 55,212-2. JWH007 was used as a positive control in the assessment of the activity of GA001. Both GA001 and JWH007 were used in a range of 6.25 μM and 25 μM .

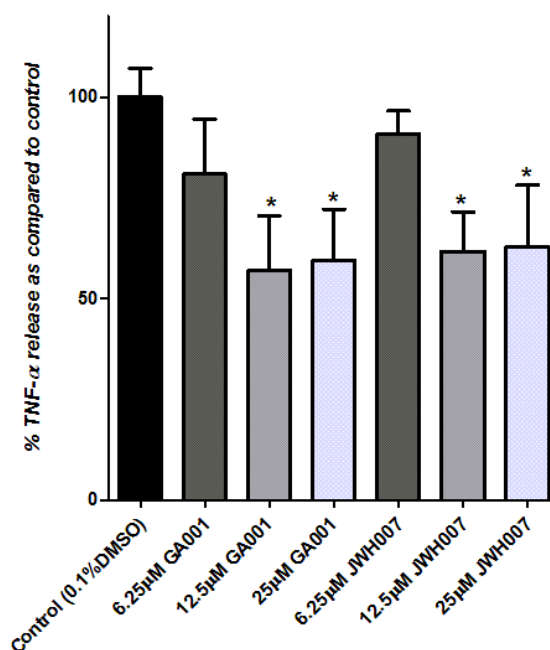


Figure 3.12 The effect of GA001 and JWH007 (6.25 μM - 25 μM) in suppressing LPS induced (200ng/mL for 16 hours) production of TNF- α in the murine macrophage cell line, RAW 264.7. Results are mean \pm S.D, n=4. * indicates $P < 0.05$

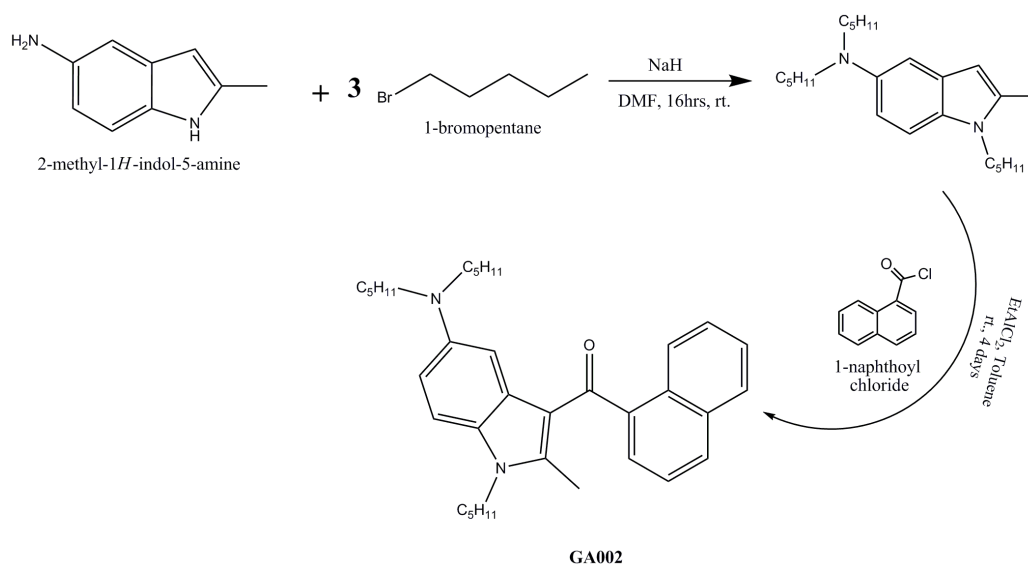
The results shown in *Figure 3.12* clearly demonstrate that GA001 has similar pharmacological activity in suppressing the LPS induced release of TNF- α in the murine cell line RAW 264.7.

This result suggests that altering position 5' in an amino-alkyl indole doesn't necessarily alter its activity or reduce it, as GA001 comprising the methyl group on position 5' exhibited similar dose-response relationship to the positive control used, JWH007.

3.3.6.2 Synthesis and Pharmacological Evaluation of GA002

After confirming that the addition of a functional group to position 5 in an amino-alkyl indole doesn't necessarily abolish or alter pharmacological activity, the effect of adding a bulky group at the same position was investigated. This was investigated to predict the effect of attaching the cannabinoid directly to a dendrimer which in itself is a chemically bulky entity. A simple method was exploited to attach such a bulky group as it is far more complicated to directly attach an anionic dendrimer to the cannabinoid.

Two pentyl alkyl chains were attached to position 5' through a nitrogen atom starting from (2-methyl-1*H*-indol-5-amine) as the initial indole bloc as shown in *Schematic 3.12*.



Schematic 3.12 Synthesis to GA002

GA002 was successfully synthesised as evidenced from NMR analysis. The final yields however were significantly lower than yields in the synthesis of JWH007 and GA001. Lower yields were noticed at both steps of the synthesis of the final product. This is probably due to the bulky nature of the compound where steric hindrance can play a role in restricting the reaction process.

The pharmacological activity of GA002 was assessed using the RAW 264.7 model and JWH007 used as a positive control.

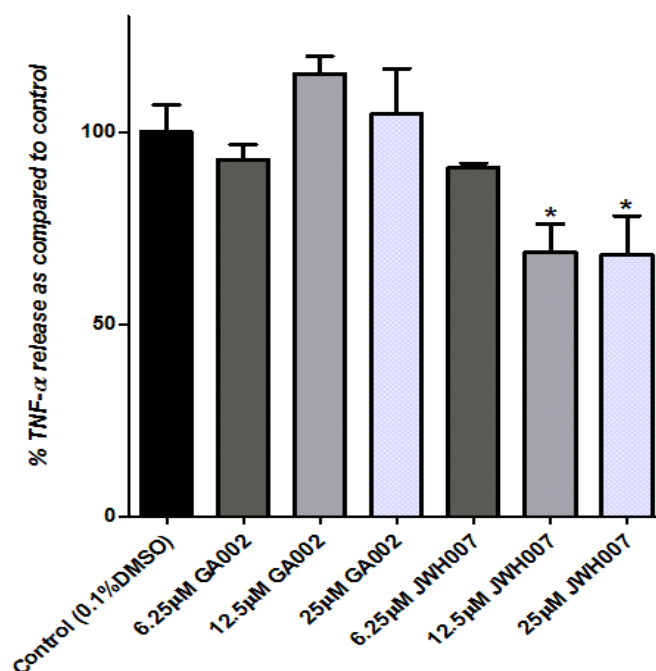


Figure 3.13 The effect of GA002 and JWH007 (6.25 μ M - 25 μ M) in suppressing LPS induced (200ng/mL for 16 hours) production of TNF- α in the murine macrophage cell line, RAW 264.7. Results are mean \pm S.D, n=4. * indicates $P < 0.05$ (ONE-WAY ANOVA, Dunnett's post-test).

As Figure 3.13 shows, GA002 was inactive and failed to suppress the release of LPS induced TNF- α release from RAW 264.7 even at the highest concentration used, 25 μ M, in contrast to JWH007 and GA001 which were both active at 12.5 μ M and 25 μ M.

The reason of why GA002 was inactive in contrast to GA001 can be attributed to the bulkiness of the group which is too close to the cannabinoid drug preventing it from moving freely and binding to the receptor. If this was the reason of the complete loss in activity with GA002, then this would strongly suggest that conjugating a dendrimer directly to an amino-alkyl indole without a spacer is likely to completely abolish the cannabinoid's activity. Attaching an

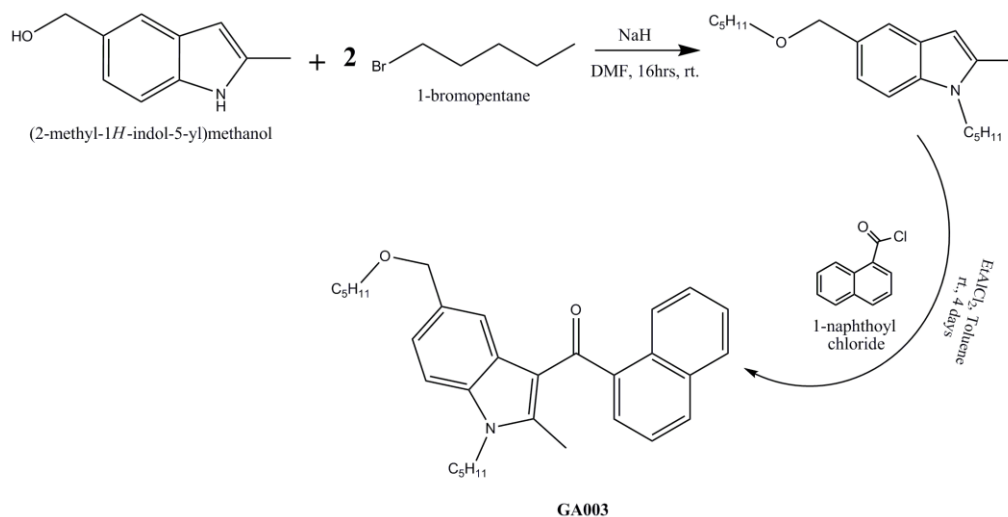
anionic PAMAM dendrimer to the cannabinoid through a long spacer however, might have a different effect as this gives the cannabinoid compound more flexibility in aligning itself for ideal binding to its receptors.

Another reason behind the complete loss in activity upon attaching two alkyl chains on position 5' would be the increase in the lipophilicity of the final compound that contains two additional hydrophobic chains.

3.3.6.3 *Synthesis and Pharmacological Evaluation of GA003*

An amino alkyl-indole with a linear alkyl spacer was to be synthesised in order to investigate the effect of a less bulky moiety such as a linear spacer upon pharmacological activity. This can further elucidate whether the bulkiness at position 5' was the reason behind the loss in activity in GA002.

A simple alkyl spacer was attached at position 5' through an ethereal linkage as part of the synthesis of the final compound starting from (2-methyl-1H-indol-5-yl)methanol as shown *Schematic 3.13*.



Schematic 3.13 Synthesis of GA003

The synthesis of GA003 was successful as evidenced from ¹H NMR analysis.

However, yields were significantly lower than those achieved during the synthesis of JWH007 and GA001.

The pharmacological activity of GA003 was assessed, and JWH007 was used as the positive control.

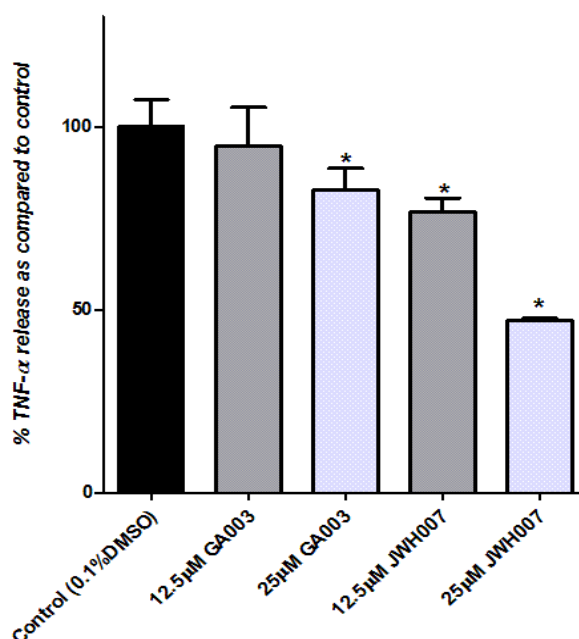


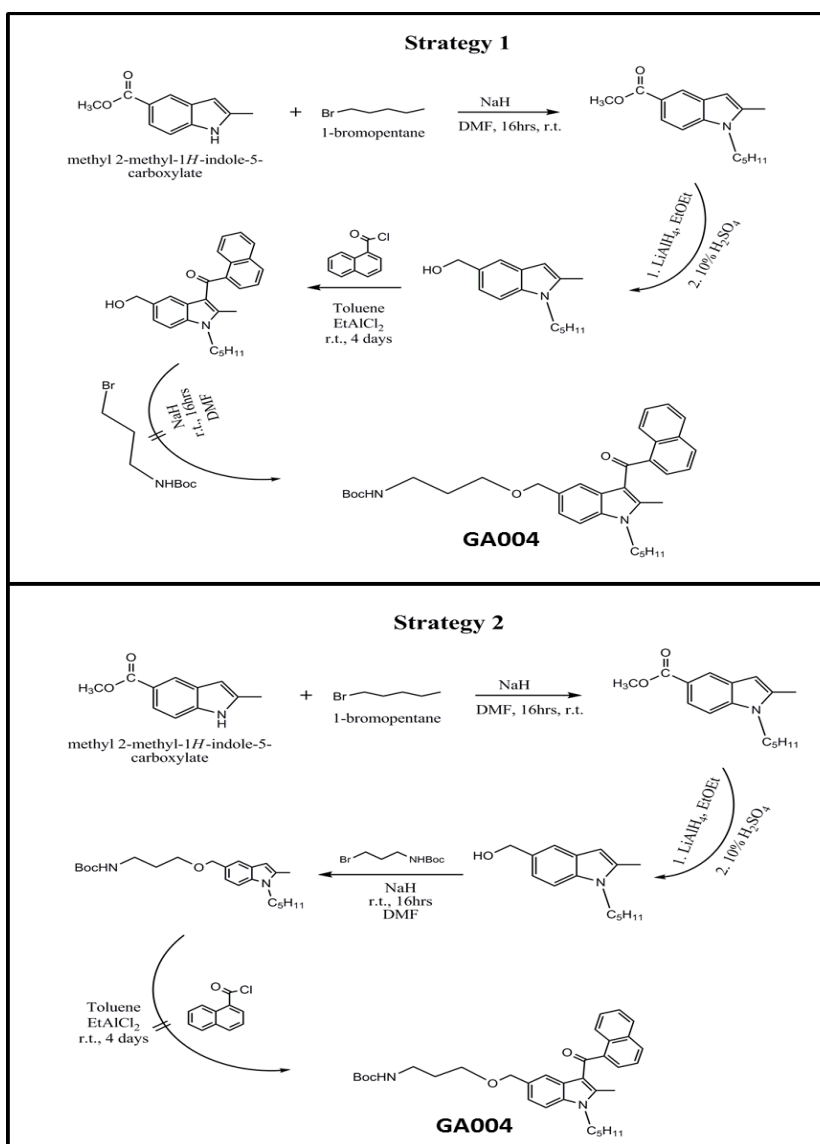
Figure 3.14 The effect of GA002 and JWH007 (6.25 μ M - 25 μ M) in suppressing LPS induced (200ng/mL for 16 hours) production of TNF- α in the murine macrophage cell line, RAW 264.7. Results are mean \pm S.D, n=4. * indicates $P < 0.05$ (ONE-WAY ANOVA, Dunnett's post-test).

Results in *Figure 3.14* show that GA003 which comprises an alkyl chain linked via an ethereal bond at position 5' of the amino-alkyl indole, is significantly less active than JWH007 which doesn't possess this chain. GA003, however, has shown significant LPS induced TNF- α suppression activity at the higher concentration of 25 μ M albeit less than that exhibited by JWH007.

GA003 with a single alkyl chain attached to position 5' is less bulky than GA002 which possesses two alkyl chains emanating from the same position. This can explain why GA003 was more active at higher concentrations than GA002. However, GA003 with a hydrophobic chain at position 5' is still significantly

more lipophilic than JWH007. This can be the reason behind the reduced pharmacological activity that was displayed by GA003.

3.3.6.4 Attempts in Synthesising GA004



Schematic 3.14 Attempts used to synthesise GA004

After showing that GA003 which comprises a linear spacer attached via an ethereal linkage at position 5', a spacer with a functional terminus that can be linked to an anionic PAMAM dendrimer was to be attached to the same position using a similar ethereal linkage. The chosen spacer was tert-Butyl 3-bromopropylcarbamate which is a propyl chain comprising a protected amine on its terminus which can be deprotected at a later stage and reacted with the carboxylic PAMAM dendrimer.

Two strategies were attempted to attach this spacer. As shown in *Schematic 3.14*, strategy 1 incorporates the naphthoyl ring to the indole prior to attaching the spacer, while in strategy 2, the spacer is incorporated before attaching the naphthoyl ring. Both strategies exploit the carboxylate group as a protecting group which allows attaching the alkyl chain to the indole nitrogen while avoiding side reactions. The carboxylate group can be later reduced using Lithium Aluminium Hydride (LiAlH_4).

In strategy 1, attaching the spacer through the alcohol group at position 5' using Williamson ether synthesis was not successful. This was obvious through TLC analysis where streaks appeared on the TLC plates indicating that the compound has been broken down upon attaching the spacer using Sodium Hydride (NaH). Attaching the spacer was successful in strategy 2 as obvious from NMR analysis. Attaching the naphthoyl ring at the last step, however, was not successful as evidenced from TLC analysis.

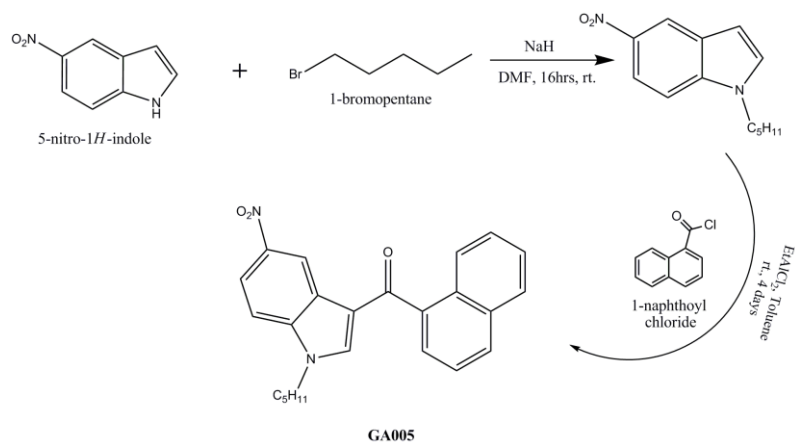
The reason behind the failure in attaching the spacer in strategy 1 might be due to the harsh conditions created by the strong base NaH. These conditions could have caused the breakdown of the reactant compound. Attaching the spacer using NaH, however, was successful in strategy 2 where it is added at an earlier stage (before attachment of the naphthoyl ring). Attaching the naphthoyl ring in strategy 2 using the Ethyl Aluminium Chloride catalysed Friedel-Craft acylation, however has failed, most likely due to the highly acidic nature of the catalyst used in this reaction which causes the breakdown of the Boc protection group, which in turn exposes the reactive amine and leads to various side reactions.

The synthesis of an amino-alkyl indole comprising a spacer attached via an ethereal linkage has hence failed using two different strategies and was temporarily abandoned.

3.3.6.5 *Synthesis and Pharmacological Evaluation of GA005 and GA006*

Another strategy was chosen to attach a spacer with a functional terminus that can be attached to an anionic PAMAM dendrimer.

GA005 was synthesised as a cannabimimetic indole that contains a nitro group on position 5'. This was achieved by beginning the synthesis of the amino alkyl indole from 5-nitro-1*H*-indole as shown in *Schematic 3.15*.



Schematic 3.15 Synthesis of GA005

The synthesis of an amino alkyl indole that comprises a nitro group at position 5' can be helpful as this nitro group can be reduced to the corresponding amine which in turn can be incorporated into a functional spacer. GA005 can hence serve as a stable cannabinoid template that can be flexibly altered at position 5' upon reducing the nitro group to the reactive amine.

The pharmacological activity of GA005 was studied using the RAW 264.7 macrophage cell line and JWH007 as a positive control.

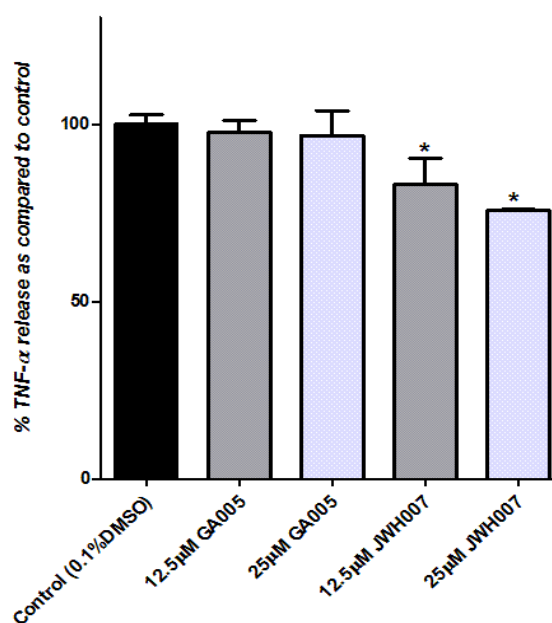


Figure 3.15 The effect of GA005 and JWH007 (12.5 μ M - 25 μ M) in suppressing LPS induced (200ng/mL for 16 hours) production of TNF- α in the murine macrophage cell line, RAW 264.7. Results are mean \pm S.D, n=4. * indicates $P < 0.05$ (ONE-WAY ANOVA, Dunnett's post-test).

Results presented in *Figure 3.15* clearly exhibit the complete loss in pharmacological activity of GA005 which comprises the nitro electron withdrawing group at position 5'. This comes in contrast with the electron donating groups that were attached to the same position such as the methyl group which didn't abolish the pharmacological activity.

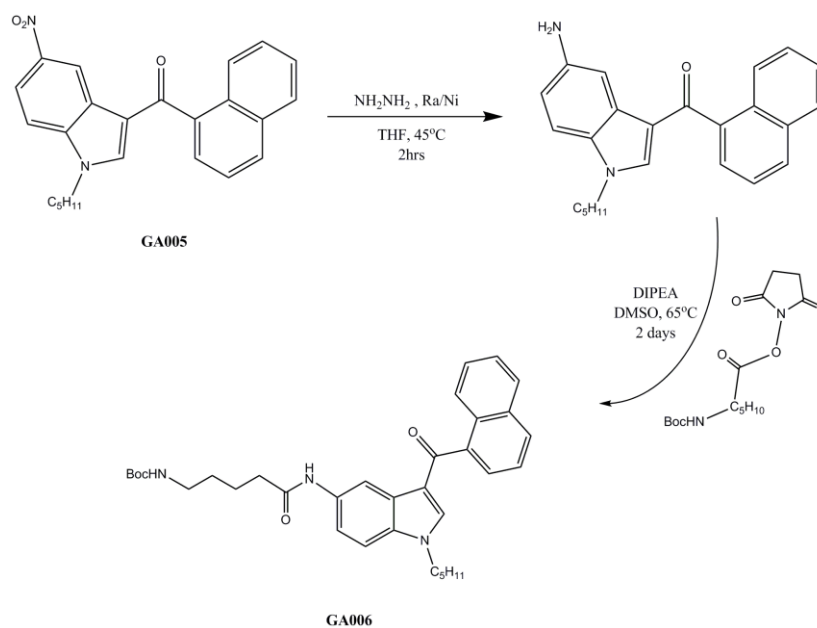
The next step was to reduce the nitro group to the corresponding amine group and attach a functional spacer comprising an amine at its terminus that can be attached to an anionic PAMAM dendrimer.

The first step in attaching a spacer at position 5' of GA005 was to reduce the nitro group to the corresponding amine group at the same position. An amine reactive spacer can then be attached to the amine.

Reducing the nitro group into a primary amine was achieved through employing Hydrazine hydrate and Raney Nickel as a catalyst as previously described by Balcom et al. [222].

This was followed by the addition a 6-carbon long spacer bearing a Boc-protected amine on one of its termini and a highly amine reactive succinimidyl ester group on the other. The succinimidyl ester would still react with the amine group at position 5' even though its attached to an indole ring (whose strong withdrawing group is expected to decrease the amine's reactivity); Pirrung et al. [223] reported 95% yield in a reaction between the same succinimidyl ester spacer used in this experiment and an indole compound comprising an amine at a similar position. This bocylated amine can be deprotected at a later stage and attached to an anionic dendrimer.

Schematic 3.16 shows the synthesis of GA006 starting from GA005 through the steps described steps.



Schematic 3.16 Synthesis of GA006

The synthesis of GA006 was successful as evident from NMR analysis and ESI+ mass spectrometry.

Pharmacological activity of GA006 was tested using the macrophage RAW 264.7 model.

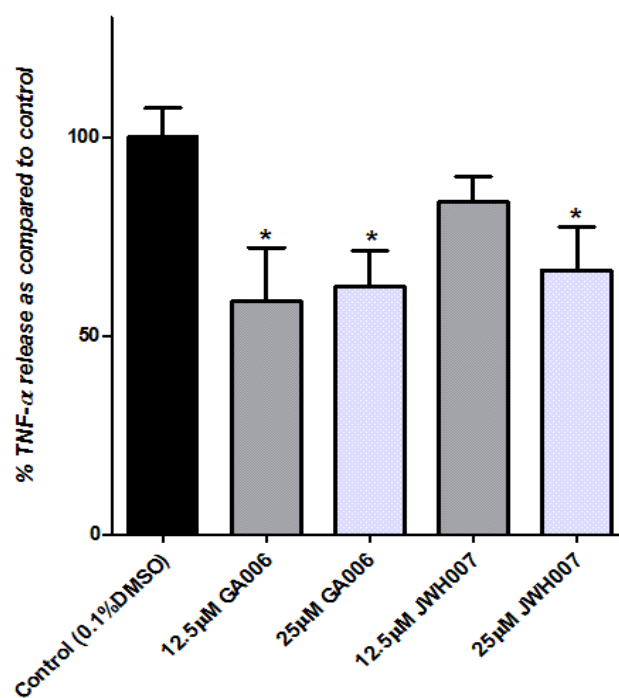


Figure 3.16 The effect of GA006 and JWH007 (12.5 μM – 25 μM) in suppressing LPS induced (200 ng/mL for 16 hours) production of TNF-α in the murine macrophage cell line, RAW 264.7. Results are mean ± S.D, n=4. * indicates P<0.05 (ONE-WAY ANOVA, Dunnett's post-test).

Results in *Figure 3.16* show that GA006 which comprises a 12 nm long spacer with a protected amine terminus is pharmacologically active. Moreover, attaching this spacer has not compromised the activity of the amino-alkyl indole.

3.3.7 Toxicity Studies

All synthesised compounds that displayed a significant inhibitory effect upon the release of TNF- α by LPS-challenged RAW 264.7 cells were subsequently tested for their biocompatibility with the macrophage cell line. These tests were performed to ensure that the observed decrements in TNF- α production are not associated with decreased cell viability, but rather through a pharmacological pathway that is mediated by the used cannabinoids.

The MTT+ assay was used as a tool to assess the viability of cells after the end of the experiment. Such a test offers a better assessment of cell viability than cell counting as it is more selective for viable cells. Additionally, it offers a faster method to determine the viability of the cells with every treatment.

The effect of LPS and the vehicle used for all treatments (0.1% DMSO) upon cell viability were first assessed as shown in *Figure 3.17*. This was performed to ensure that all other treatments apart from the cannabinoid drug have no impact upon cell viability when the experiments are performed. Results indicate that LPS at the concentrations used in these experiments to induce TNF- α release, i.e. 200ng/mL LPS, and the final concentrations of DMSO in the media systems containing the cannabinoid drug, i.e. 0.1%, have no impact upon cell viability over 16 hours (Time course of all reported experiments).

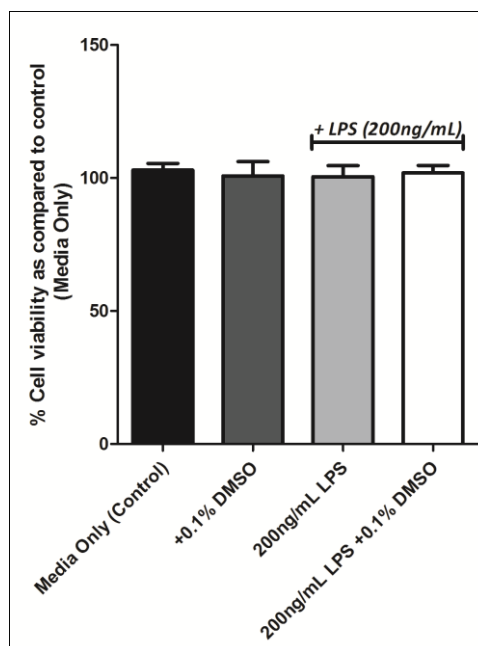


Figure 3.17 Effect of 0.1% DMSO (The solvent concentration used to prepare all cannabinoid treatments on cells) and 200ng/mL LPS over 16 hours (The treatment used to induce TNF- α release in all experiments) upon the viability of RAW 264.7 macrophage cell line as assessed using the MTT+ assay. Results are mean \pm S.D, n=4. All treatments resulted in no significant effect upon RAW 264.7 viability (ONE-WAY ANOVA, Dunnett's post-test).

Toxicity studies were performed to assess the viability of RAW 264.7 cells treated with JWH007, A cannabinoid drug that was synthesised in house as a cheap alternative for WIN 55,212-2 and which displayed anti-inflammatory properties in RAW 264.7 that are similar, if not superior, to those displayed by the prototype cannabinoid WIN 55,212-2. Results show that JWH007 does not compromise RAW 264.7 cell viability in concentrations as high as 25 μ M. WIN 55,212-2 on the other hand displayed significant toxic effects upon the macrophage cell line (52% decrease in cell viability) as shown in *Figure 2.20*.

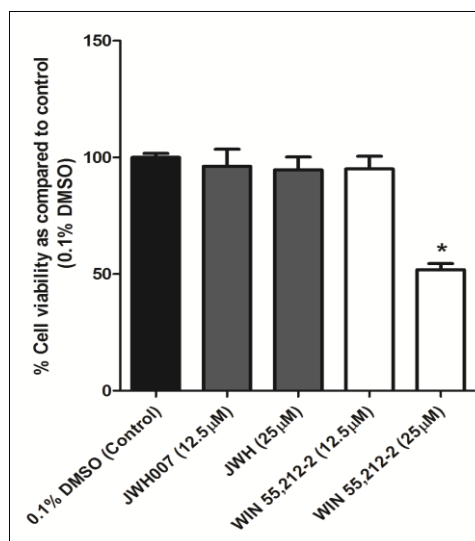


Figure 3.18 Effect of the in-house synthesised cannabinoid JWH007 and the prototype amino-indole alkyl cannabinoid WIN 55,212-2 upon the viability of RAW 264.7 macrophage cell line as assessed using the MTT+ assay. Results are mean \pm S.D, n=4. * indicates $P < 0.05$ (significant toxic effect), (ONE-WAY ANOVA, Dunnett's post-test).

These results show that the model cannabinoid that was synthesised, JWH007, is significantly more biocompatible than its expensive counterpart, WIN 55,212-2 which makes it a more appealing cannabinoid to be used in further studies and applications than WIN 55,212-2.

Similarly to JWH007, all the synthesised novel cannabinoids did not compromise the viability of the murine macrophage cell line RAW 264.7, at the used concentrations (12.5µM - 25µM). *Figure 3.19* shows the toxicity profiles of all the novel synthesised cannabinoids that displayed an anti-inflammatory effect in the in-vitro system.

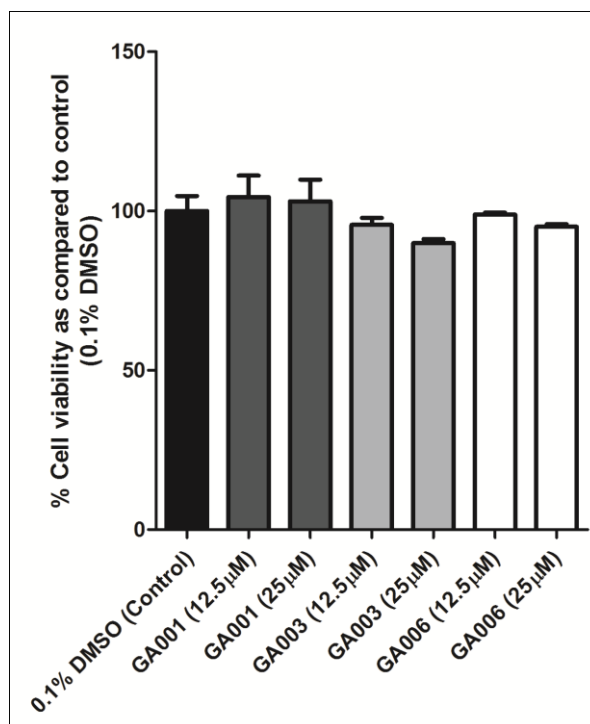


Figure 3.19 Effect of novel synthesised cannabinoids GA001, GA003 and GA006 upon the viability of RAW 264.7 macrophage cell line as assessed using the MTT+ assay. Results are mean \pm S.D, $n=4$. All these cannabinoids resulted in no significant effect upon RAW 264.7 viability (ONE-WAY ANOVA, Dunnett's post-test).

Appendix A : Chemical Syntheses

N1-(diphenylmethylene)ethane-1,2-diamine (1)

Benzophenone (1.05g, 5.8mmol) was dissolved in methanol (20mL). Ethylene diamine (1.15mL, 17.3mmol) was added as one portion to the mixture. The reaction was allowed to stir over night at 60°C. Upon checking the reaction progress on TLC, it was obvious that benzophenone hasn't reacted with ethylenediamine (no new spots formed on the plate).

diphenylmethanol (2)

Benzophenone (1.00g, 5.5mmol) was dissolved in methanol (20mL). Sodium borohydride (1.25g, 33.0 mmol) was added to the methanolic solution. The reaction was allowed to stir for 3 hours. Methanol was evaporated in vacuo and the product was extracted via solvent extraction with 3 portions of ethyl acetate against water. The product was then purified using flash chromatography (cyclohexane: ethyl acetate 8.5:1.5). The resulting oil, diphenyl methanol was obtained in a yield of 86%.

¹H NMR (500MHz, Methanol-d₄) δ 7.52 (3H, t), 7.33-7.27 (3H, m), 7.17-7.11 (2H, m), 5.89 (1H, d), 5.73 (1H, d)

tert-Butyl 3-(benzhydryloxy)propylcarbamate (3)

Diphenylmethanol (1.10g, 6.1mmol) was dissolved in DMF (10mL). NaH powder was added in small portions while stirring on ice until bubbling stopped. The mixture was allowed to stir for a further 30 minutes at room temperature. tert-Butyl 3-bromopropylcarbamate hydrochloride (3.3g, 12.2mmol) was added in

one portion to the mixture. The reaction was allowed to stir for 16 hours. TLC analysis showed that the reaction has failed as no new spots were formed on the plate as compared to spots taken before the initiation of the reaction.

Diphenylmethanamine (4)

Method (1)

Potassium hydroxide (1.12g, 20mmol) was added and left to dissolve in a solution of 2M ammonia in methanol (20mL). Benzophenone (1.05g, 5.8mmol) was added in one portion to the mixture after all the potassium hydroxide has dissolved. Sodium cyanoborohydride (0.25g, 0.16mmol) was added in one portion to the stirring solution. The stirring was continued for 30 minutes and Potassium hydroxide (4.48g, 80mmol) was added to the stirring solution. After 45 minutes the mixture was filtered, and methanol was evaporated in vacuo. Solvent extraction was performed. The reaction has failed as evident by TLC as no new spots appeared on the plate.

Method (2)

Benzophenone (1.05g, 5.8mmol) was dissolved in 2M ammonia solution in ethanol (20mL) in a nitrogen purged flask. Titanium isopropoxide (3.5mL, 11.4mmol) was added to the solution using a glass syringe. The mixture was allowed to stir under nitrogen for 6 hours. Sodium borohydride (1.25g, 33.0 mmol) dissolved in dry ethanol was added to the mixture via a glass syringe. The mixture was allowed to stir for 2 hours. 5mL of ammonium hydroxide was added to quench the solution. The solution was diluted with 20mL of water. Solvent extraction was performed against ethyl acetate. The aminated product was then extracted and purified using acid/base extraction.

^1H NMR (500MHz, Methanol-d₄) δ 7.51-7.42 (10H, m), 5.76 (1H, s), 5.62 (1H, s)

JWH007*Step (1)*

2-Methyl-1H-indole (1.1g, 8.4mmol) were dissolved in dry DMF (15mL) Sodium hydride (NaH) was added in small portions until the solution stopped bubbling. 1-bromopentane (2.5g, 16.8mmol) was added in one portion and the flask was immersed in ice for 30 minutes while the solution was stirring. After 16 hours, the reaction was quenched by the addition of 15 mL of distilled H₂O, and extracted with three portions of ethyl acetate. The organic phase was evaporated *in vacuo* and the residue was purified using flash chromatography; Cyclohexane : Ethylacetate (8 : 2) giving 91% yield of 2-methyl-1-pentyl-1H-indole.

¹H NMR (500MHz, DMSO-d₆) δ 7.43 (1H, d), 7.33 (1H, d), 7.06 (1H, t), 6.99 (1H, t), 6.22 (1H, s), 4.07-4.03 (2H, m), 2.44 (3H, s), 1.66-1.60 (2H, m), 1.46-1.41 (4H, m), 0.88-0.82 (3H, m)

Step (2)

2-Methyl-1-pentyl-1H-indole (0.85g, 4.2mmol) was dissolved in dry toluene (15mL). 1-naphtoyl chloride (0.96g, 5mmol) was added to the mixture. The mixture was stirred on ice. Ethylaluminium dichloride, supplied as a 25 wt. % solution in toluene, (2.8mL, 5mmol) was added to the solution. The reaction was allowed to proceed for 4 days. The reaction was then quenched with 20mL of distilled H₂O and the product was extracted with three portions of ethyl acetate. The organic phase was evaporated *in vacuo* and the product was purified using flash chromatography; Cyclohexane : Ethyl acetate (8:2) giving 36% yield of JWH007.

¹H NMR (500MHz, DMSO-d₆) δ 8.03 (1H, d), 7.86 (1H, d), 7.79 (1H, d), 7.40 (1H, d), 7.38 (2H, t), 7.36 (1H, t), 7.33 (1H, d), 7.20 (2H, t), 6.88 (1H, t), 3.97 (2H, t), 2.35 (3H, s), 1.65 (2H, s), 1.24-1.21 (4H, m), 0.91-0.78 (3H, m)

$m/z = 356.2000 [m+H]^+$

GA001

Step (1)

2,5-Dimethyl-1H-indole (1.2g, 8.3mmol) was dissolved in dry DMF (15mL). Sodium hydride (NaH) was added in small portions until the solution stopped bubbling. 1-Bromopentane (2.5g, 16.6mmol) was added in one portion and the flask was immersed in ice for 30 minutes while the solution was stirring. After 16 hours, the reaction was quenched by the addition of 15 mL of distilled H₂O, and extracted with three portions of ethyl acetate. The organic phase was evaporated *in vacuo* and the residue was purified using flash chromatography; Cyclohexane : Ethylacetate (8 : 2) giving 88% yield of 2,5-dimethyl-1-pentyl-1H-indole.

¹H NMR (500MHz, DMSO-d₆) δ 7.39 (1H, s), 7.27 (1H, d), 7.02 (1H, d), 6.23 (1H, s), 4.07 (2H, t), 2.51- 2.46 (5H, m), 1.87-1.82 (1H, m), 1.41 (4H, s), 1.00 (3H, t)

Step (2)

2,5-Dimethyl-1-pentyl-1H-indole (0.9g, 4.2mmol) was dissolved in dry toluene (15mL). 1-Naphtoyl chloride (0.96g, 5mmol) was added to the mixture. The mixture was stirred on ice. Ethylaluminium dichloride, supplied as a 25 wt. % solution in toluene, (2.8mL, 5mmol) was added to the solution. The reaction was allowed to proceed for 4 days. The reaction was then quenched with 20mL of distilled H₂O and the product was extracted with three portions of ethyl acetate. The organic phase was evaporated *in vacuo* and the product was purified using flash chromatography; Cyclohexane : Ethylacetate (7:3) giving 36% yield of GA001.

^1H NMR (500MHz, DMSO- d_6) δ 8.17 (1H, d), 8.03 (1H, d), 7.96 (1H, d), 7.61 (1H, d), 7.50 (2H, t), 7.46 (1H, t), 7.22 (2H, t), 7.10 (1H, d), 4.11 (3H, t), 2.39 (3H, s), 2.36 (3H, s), 1.75 (1H, s), 1.36 (4H, s), 0.98 (3H, t)

GA002

Step (1)

2-Methyl-1H-indol-5-amine (1.1g, 7.5mmol) were dissolved in dry DMF (15mL) Sodium hydride (NaH) was added in small portions until the solution stopped bubbling. 1-Bromopentane (4.6g, 30.1mmol) was added in one portion and the flask was immersed in ice for 30 minutes while the solution was stirring. After 16 hours, the reaction was quenched by the addition of 15 mL of distilled H_2O , and extracted with three portions of ethyl acetate. The organic phase was evaporated *in vacuo* and the residue was purified using flash chromatography; Cyclohexane : Ethylacetate (9 : 1) giving 36% yield of *2-methyl-N,N,1-tripentyl-1H-indol-5-amine*.

^1H NMR (500MHz, DMSO- d_6) δ 7.14 (1H, d), 6.91 (1H, s), 6.76 (1H, s) 6.12 (1H, s), 4.09-4.02 (4H, m), 3.25-3.20 (6H, m), 2.48 (2H, s), 2.2 (2H, s), 1.71- 1.62 (2H, m), 1.53- 1.68 (6H, m), 1.48 (3H, s), 1.41 – 1.39 (9H, m)0.99-0.81 (6H, m).

Step (2)

2-Methyl-N,N,1-tripentyl-1H-indol-5-amine (0.27g, 0.76mmol) was dissolved in dry Toluene (10mL). 1-Naphtoyl chloride (0.19g, 1mmol) was added to the mixture. The mixture was stirred on ice. Ethylaluminium dichloride, supplied as a 25 wt. % solution in toluene, (0.56mL, 1mmol) was added to the solution. The reaction was allowed to proceed for 4 days. The reaction was then quenched with 10mL of distilled H_2O and the product was extracted with three portions of ethyl acetate. The organic phase was evaporated *in vacuo* and the product

was purified using flash chromatography; Cyclohexane : Ethylacetate (8:2) giving 12% yield of GA002.

^1H NMR (500MHz, CDCl_3) δ 8.10 (1H, d), 7.96 (1H, d), 7.91 (1H, d), 7.57 (1H, d), 7.51 (2H, t), 7.49 (1H, t), 7.12 (2H, d), 6.61 (1H, d), 6.14 (1H, s), 4.1-4.01 (2H, m), 3.95-2.88 (4H, m), 2.61 (3H, s), 2.19 (6H, s), 1.85- 1.74 (2H, m), 1.47- 1.39 (3H, m), 1.29-1.20 (6H, s), 1.12 – 1.04 (3H, m), 0.99-0.91 (3H, m), 0.90-0.84 (3H, m).

^{13}C NMR (75.5MHz, CDCl_3) δ 12.7, 13.9, 22.9, 14.1, 22.4, 22.6, 26.9, 29.2, 29.32, 29.4, 29.7, 43.3, 51.8, 103.8, 109.8, 110.07, 114.0, 125.1, 125.2, 125.8, 126.1, 126.7, 128.1, 129.0, 129.3, 130.3, 133.8, 141.3, 144.7, 145.4

GA003

Step (1)

(2-Methyl-1H-indol-5-yl)methanol (1.4g, 8.7mmol) was dissolved in dry DMF (15mL). Sodium hydride (NaH) was added in small portions until the solution stopped bubbling. 1-bromopentane (4.5g, 30.1mmol) was added in one portion and the flask was immersed in ice for 30 minutes while the solution was stirring. After 16 hours, the reaction was quenched by the addition of 15 mL of distilled H_2O , and extracted with three portions of ethyl acetate. The organic phase was evaporated *in vacuo* and the residue was purified using flash chromatography; Cyclohexane : Ethylacetate (8 : 2) giving 32% yield of 2-methyl-1-pentyl-5-(pentyloxymethyl)-1H-indole

^1H NMR (500MHz, DMSO-d_6) δ 7.82 (1H, s), 7.33 (1H, d) 7.23 (1H, d), 6.48 (1H, s), 1.91-1.82H (6H, t), 1.45-1.28 (9H, m), 0.98-0.91 (6H, t)

Step (2)

2-Methyl-N,N,1-tripentyl-1H-indol-5-amine (0.3g, 1mmol) was dissolved in dry toluene (10mL). 1-Naphtoyl chloride (0.24g, 1.25mmol) was added to the mixture. The mixture was stirred on ice. Ethylaluminium dichloride, supplied as a 25 wt. % solution in toluene, (0.56mL, 1mmol) was added to the solution. The reaction was allowed to proceed for 4 days. The reaction was then quenched with 10mL of distilled H₂O and the product was extracted with three portions of ethyl acetate. The organic phase was evaporated *in vacuo* and the product was purified using flash chromatography; Cyclohexane : Ethylacetate (8:2) giving 16% yield of GA003.

¹H NMR (500MHz, DMSO-d₆) δ 8.23 (1H, d), 8.00 (1H, d), 7.94 (1H, d), 7.67 (1H, d), 7.55 (1H, t), 7.48 (1H, t), 7.32-7.28 (2H, m), 7.20 (1H, d), 7.12 (1H, t), 4.12 (1H, s), 4.08-4.02 (2H, m), 3.75 (2H, q), 2.32 (3H, s), 1.84-1.75 (2H, m), 1.38-1.22 (12H, m), 0.92-0.81 (3H, m).

GA004**Step (1)**

Methyl 2-methyl-1H-indole-5-carboxylate (2.0g, 10.6mmol) was dissolved in dry DMF (20mL). Sodium hydride (NaH) was added in small portions until the solution stopped bubbling. 1-Bromopentane (3.02g, 20.0mmol) was added in one portion and the flask was immersed in ice for 30 minutes while the solution was stirring. After 16 hours, the reaction was quenched by the addition of 20 mL of distilled H₂O, and extracted with three portions of ethyl acetate. The organic phase was evaporated *in vacuo* and the residue was purified using flash chromatography; Cyclohexane : Ethylacetate (7 : 3) giving 76% yield of *methyl-1-pentyl-1H-indole-5-carboxylate*.

^1H NMR (500MHz, DMSO- d_6) δ 7.37 (1H, s), 7.29 (1H, s), 7.21 (1H, d), 7.04 (1H, d), 6.21 (1H, s), 4.08-4.00 (2H, m), 2.51–2.40 (3H, m), 1.82-1.71 (2H, 2), 1.45-1.31 (4H, m), 0.99-0.90 (3H, m)

Step (2)

Methyl 1-pentyl-1H-indole-5-carboxylate (0.96g, 3.9mmol) was dissolved in 10 mL of anhydrous ether (Solution A). In a separate flask, LiAlH_4 (0.61g, 15.6mmol) was dissolved in 10mL of anhydrous ether (Solution B), the flask was immersed in ice. Solution A was added drop wise to Solution B using a drop funnel over 30 minutes. The ice was removed, and the reaction was allowed to proceed at room temperature for 2 hours. The reaction was quenched by the drop-wise addition of ice-cold water until effervescence has halted. 10% Aqueous sulphuric acid solution (20mL) was added to the mixture afterwards. The organic phase was collected and washed 3 times with water. The residue was purified using flash chromatography; Cyclohexane: Ethylacetate (6.5 : 3.5) giving 97% yield of *(1-pentyl-1H-indol-5-yl)methanol*.

^1H NMR (500MHz, DMSO- d_6) δ 8.47 (1H, s), 7.95 (1H, d), 7.35 (1H, d), 7.15 (1H, s), 6.62 (1H, s), 4.48 (1H, t), 4.19-4.10 (1H, m), 3.95 (1H, s), 1.89-1.78 (3H, m), 1.40-1.22 (4H, m), 0.92-0.82 (3H, m).

Step (3)

(1-Pentyl-1H-indol-5-yl)methanol (0.81g, 3.7mmol) was dissolved in dry toluene (10mL). 1-Naphtoyl chloride (1.1g, 5.6mmol) was added to the mixture. The mixture was stirred on ice. Ethylaluminium dichloride, supplied as a 25 wt. % solution in toluene, (3.1mL, 5.6mmol) was added to the solution. The reaction was allowed to proceed for 4 days. The reaction was then quenched with 10mL of distilled H_2O and the product was extracted with three portions

of ethyl acetate. The organic phase was evaporated *in vacuo* and the product was purified using flash chromatography; Cyclohexane : Ethylacetate (8:2) giving 37% yield of (5-(hydroxymethyl)-1-pentyl-1H-indol-3-yl)(naphthalen-1-yl)methanone.

¹H NMR (500MHz, DMSO-d₆) δ 8.21 (1H, d), 8.00 (1h, d), 7.93 (1H, d), 7.59 (1H, d), 7.50 (1H, t), 7.45 (1H, t), 7.22 (1H, t), 7.04 (1H, d), 4.07 (2H, t), 2.38 (3H, s), 2.30 (1H, s), 1.82-1.72 (2H, m), 1.42 (2H, s), 1.35 (3H, s), 0.96-0.82 (3H, m).

Step (4)

(5-(Hydroxymethyl)-1-pentyl-1H-indol-3-yl)(naphthalen-1-yl)methanone (0.31g, 0.84mmol), was dissolved in dry DMF (20mL). Sodium hydride (NaH) was added in small portions until the solution stopped bubbling. *tert*-Butyl 3-bromopropylcarbamate (0.40, 1.7mmol) was added as a 2mL solution in DMF in one portion and the flask was immersed in ice for 30 minutes while the solution was stirring. After 16 hours, the reaction was quenched by the addition of 20 mL of distilled H₂O, and extracted with three portions of ethyl acetate. The organic phase was evaporated *in vacuo*. The residue showed multiple streaks upon TLC analysis and no final product could be extracted.

GA005

Step (1)

5-Nitro-1H-indole (2g, 12.3mmol) was dissolved in dry DMF (15mL). Sodium Hydride (NaH) was added in small portions until the solution stopped bubbling. 1-Bromopentane (3.7g, 24.6mmol) was added in one portion and the flask was immersed in ice for 30 minutes while the solution was stirring. After 16 hours, the reaction was quenched by the addition of 15 mL of distilled H₂O, and extracted with three portions of ethyl acetate. The organic phase was

evaporated *in vacuo* and the residue was purified using flash chromatography; Cyclohexane : Ethylacetate (8 : 2) giving 71% yield of *5-nitro-1-pentyl-1H-indole*

^1H NMR (500MHz, DMSO-d6) δ 9.13 (1H, s), 8.72 (1H, d) 8.62 (1H, d), 6.14 (1H, s), 4.63 (2H, t), 2.45- 2.32 (5H, m), 1.88-1.82 (1H, m), 1.31 (3H, t)

Step (2)

5-Nitro-1-pentyl-1H-indole (0.3g, 1mmol) was dissolved in dry toluene (10mL). 1-Naphtoyl chloride (0.24g, 1.25mmol) was added to the mixture. The mixture was stirred on ice. Ethylaluminium dichloride, supplied as a 25 wt. % solution in toluene, (0.56mL, 1mmol) was added to the solution. The reaction was allowed to proceed for 4 days. The reaction was then quenched with 10mL of distilled H₂O and the product was extracted with three portions of ethyl acetate. The organic phase was evaporated *in vacuo* and the product was purified using flash chromatography; Cyclohexane : Ethylacetate (7.5:2.5) giving 67% yield of GA005.

^1H NMR (500MHz, DMSO-d6) δ 9.21 (1H, s), 8.22 (1H, d), 8.15 (1H, d), 8.10 (1H, d), 7.90 (2H, t), 7.77 (1H, t), 7.59 (2H, t), 7.55 (1H, d), 5.78 (1H, s) , 4.29 (2H, t), 2.48 (1H, s), 1.80-1.61 (2H, m), 1.39-1.12 (4H, m), 0.85-0.74 (2H, m).

^{13}C NMR (75.5MHz,DMSO-d6) δ 13.7, 21.55, 28.1, 29.11, 46.6, 111.9, 116.2, 117.3, 118.0, 124.9, 125.7, 126.9, 127.5, 128.3, 129.8, 130.3, 132.9, 133.4, 137.4, 139.8, 142.6, 190.9

GA006**Step (1)**

GA005 (0.1g, 0.26mmol), was dissolved in 5 mL of THF. Hydrazine hydrate (130 μ L, 2.5mmol) was added. Raney[®] Nickel suspension in H₂O (0.5mL) was added to the stirring solution. The reaction was allowed to stir for 2 hours. The contents were filtered to separate the nickel from the contents, and the solution was dried in vacuum. The product was purified using flash chromatography; Cyclohexane : Ethyl acetate (6 : 4) giving 89% yield of (5-amino-1-pentyl-1H-indol-3-yl)(naphthalen-1-yl)methanone (GA005a).

Step (2)

GA005a (0.07g, 0.20 mmol) was dissolved in 5 mL anhydrous DMSO. 100 μ L of dry N,N diisopropylethylamine (*DIPEA*) was added. *2,5-Dioxopyrrolidin-1-yl 6-(tert-butoxycarbonylamino)hexanoate* (0.13g, 0.39mmol) was added to the stirring solution. The solution was stirred at 65^o for 2 days. The reaction was quenched by the addition of 5 mL of water and extracted with three portions of ethyl acetate. The organic phase was evaporated *in vacuo* and the residue was purified using flash chromatography; Cyclohexane : Ethylacetate (7 : 3) giving 92% yield of tert-Butyl 5-(3-(1-naphthoyl)-1-pentyl-1H-indol-5-ylamino)-5-oxopentylcarbamate (GA006).

¹H NMR (500MHz, DMSO-d₆) δ 8.37 (1H, s), 8.24 (1H, s), 8.16 (1H, d), 8.02 (1H, s), 7.87 (1H, d), 7.51 (1H, s), 7.44 (1H, t), 7.34 (1H,t) 7.25 (1H, t), 7.12 (1H, t), 7.02 (1H, s), 4.26 (2H, t), 3.45 (9H, s) 3.11 (1H, s), 2.51 (1H, s), 2.09 (2H, m), 1.81 (3H, t), 1.57 (1H, t), 1.52 (3H, m), 1.51-1.43 (4H, m), 0.96 (3H, d).

m/z 556.43 [m + H]⁺

Chapter 4

Dendrimer Conjugates

4.1 Introduction

4.1.1 Dendrimers as Drug Carriers

It has been suggested that the compact structure of the dendrimer would make it a superior drug carrier to conventional linear polymers such as PEG, because its compact structure would not wrap around therapeutic molecules and mask their active sites [224].

Drugs can be associated with dendrimers in various ways:

- 1- They can be simply encapsulated in a dendrimer's cavity. As discussed previously in Chapter 1, this comes as a result of the dendrimer's architectures whereby drugs can be encapsulated within the dendrimer's interior through hydrophobic interactions [17] or hydrogen bonding with abundant nitrogen and oxygen atoms [225].
- 2- Drugs can be electrostatically attached to the surface of a dendrimer through the high density of surface functional groups on the polymer. Several laboratories have attached weakly acidic compounds such as anti-inflammatory and anti-bacterial drugs to cationic dendrimer surfaces [53, 226, 227].

Note: For the purpose of this thesis, the term dendrimer complexation will be used to describe non-covalent drug-dendrimer entities. For covalent linkages

formed between drug and dendrimer, the term dendrimer conjugate will be applied.

- 3- Formation of stable dendrimer-drug conjugates: In contrast to the previous two methods, chemical conjugation of drugs to dendrimers through covalent linkage can offer stable drug-dendrimer entities. The release of drugs covalently attached to dendrimers is dependent on the chemical and enzymatic activity of the environment. This offers more controlled, slower and targeted release of conjugated drugs. Many groups have reported the covalent attachment of different low molecular weight drugs to dendrimers where the conjugated drug can be released to its target through enzymatic or chemical cleavage [23, 162, 228].

Conjugation or complexation of (therapeutic) molecules to dendrimers can enhance their delivery through a multitude of pathways:

- 1- *Solubilisation*. The precise structure and multivalent surface functionality of dendrimers make them good excipients for enhancing the solubility of hydrophobic drugs. The previously described methods of encapsulation, electrostatic attraction or covalent bonding between a hydrophobic drug and a dendrimer can all lead to enhanced aqueous solubility of hydrophobic drugs.

- 2- *Enhanced Permeation and Retention (EPR) effect*. The discrepancy between 'leaky' tumour vasculature and more restrictive healthy tissue vasculature is one of the most important aspects that can be exploited in the specific targeting of tumours, and is often referred to as the EPR effect [170]. Dendrimers can offer the platform for a drug carrying device that has a molecular size that is too large to leak through healthy vasculature while being small enough to leak through the less restrictive tumour vasculature achieving specific tumour targeting [23, 229].
- 3- *Evasion of membrane efflux transporters*. Efflux transporters such as P-glycoprotein are amongst the most limiting factors in the oral absorption of small molecular weight drugs. Efflux transporters are also the primary reason behind multiple drug resistance properties displayed by cancerous cells. It has been reported that P-gp substrates such as propranolol [162], terfenadine[163] and doxorubicin[164] can evade the P-gp pump when conjugated to PAMAM dendrimers and hence had increased absorptive transport and decreased secretory transport across cells expressing P-gp *in-vitro*. It has also been argued that not only do dendrimers by-pass P-glycoprotein transporters but can also inhibit them. It has been reported that the concomitant presence of G3 PAMAM dendrimers with P-gp substrates doxorubicin and vinblastine significantly improves their accumulation in the gut-sac [230].

4.1.2 Active Dendrimer-drug conjugates

An intriguing area of research that is still under-developed is that of generating stable dendrimer-drug conjugates that are active in their own right. Although most reported dendrimer-drug conjugations in the literature rely on the release of the drug from the dendrimer to exert the pharmacological effect, some examples exist for stable and intact dendrimer-drug conjugates that exert pharmacological activity as the conjugate itself. Wang et al. [224] conjugated the thrombolytic agent streptokinase to a PAMAM G3.5 dendrimer without any loss in pharmacological activity based on *in-vitro* fibrinolytic assays. Because of their multivalent surface functionality, dendrimers can offer an interesting platform where various compounds and drugs can be attached to the same dendrimer to achieve combinatorial targeting and activity. Many groups [231-234] reported a cationic PAMAM Methotrexate-Folic Acid (FA) conjugates where methotrexate maintains its pharmacological (anti-tumour) activity *in-vitro* while FA increases the specific targeting of the whole conjugate. Some of these groups have additionally incorporated fluorescein into the conjugate to achieve visualisation of the drug inside the target cells.

4.1.3 Aims and Objectives

The overall aim of the thesis was to synthesise a dendrimer-cannabinoid conjugate that it is active in its own right as the conjugate. The experimental objectives specific to this chapter are:

1- The synthesis of radiolabel-dendrimer conjugate which serves two purposes:

(A) As a model for chemical conjugation to a dendrimer via an amide linkage that can serve to assess stability of linkage to biological media.

(B) As a labelled dendrimer that can be analysed in biological fluids for future absorption and biodistribution in-vivo studies

2- Conjugation of a novel cannabinoid (GA006) to an anionic PAMAM dendrimer using a stable amide linkage and the subsequent testing of pharmacological activity of the conjugate.

4.2 Materials and Methods

4.2.1 Materials

[³H] Acetic Anhydride (5mCi, specific activity 72mCi/mmol) was purchased from American Radiolabeled Chemicals (St. Louis, USA). PD-10 gel columns were purchased from GE Healthcare, (UK). Anionic PAMAM dendrimers were purchased from Sigma-Aldrich, (UK). DMEM media and foetal bovine serum were purchased from Invitrogen, UK. All other chemicals and solvents were purchased from Fisher (UK) unless otherwise stated.

4.2.2 Methods

Radiolabeling of Dendrimers

Two strategies were pursued in the radiolabeling of anionic PAMAM dendrimers using [³H] acetic anhydride as the radioactive source. [³H] Acetic anhydride was prepared as a 1mCi/mL solution in anhydrous acetonitrile and stored at 4°C.

Method 1

Anionic PAMAM dendrimers were labelled in a similar approach to that previously described by Kitchens et al. [235]. 200µL of anionic PAMAM dendrimer G3.5 methanolic solution (containing 20mg of dendrimer) was transferred to a round bottom flask and was dried *in-vacuo*. The flask was sealed and flushed with nitrogen, before re-dissolved the residue with anhydrous methanol (2mL to achieve a concentration of 10mg/mL) under a

stream of nitrogen. Using a dry Hamilton syringe, 60 μ L (60 μ Ci) of [3 H] acetic anhydride solution in acetonitrile were transferred to the flask (leading to a ratio of 3 μ Ci of radiolabel per 1mg of dendrimer). 10 μ L of Triethylamine were also added to the flask under a stream of nitrogen. The contents of the flask were then left stirring for 24 hours before terminating the reaction by the addition of 5mL of distilled water adjusted with HCL to pH 3. The contents were then dried under vacuum and the residue was re-dissolved in 2.5mL of distilled water. Under acidic aqueous conditions, it is expected that unreacted acetic anhydride would break down to acetic acid which will consequently evaporate under vacuum. To completely separate the dendrimer from unreacted acetic anhydride, the polymer was purified using PD-10 gel column. The eluted fraction at which the dendrimer is expected to appear was collected and dried under vacuum. The purity of the dendrimer was then analysed using a PD-10 column to ensure no free radio-label was present with the dendrimer.

Method 2

Step 1 : Amination of the Carboxylic terminus

200 μ L of anionic PAMAM dendrimer G3.5 methanolic solution (containing 20mg of dendrimer) was transferred to a round bottom flask and was dried *in vacuo*. The residue was then re-dissolved with phosphate buffer saline (PBS, pH 7.4, 2mL). 10 Molar equivalent of 1-ethyl-3- [3-dimethylaminopropyl] carbodiimide hydrochloride (EDC) and 10 molar equivalent of N-hydroxysulfosuccinimide (Sulfo-NHS) were added to the dendrimer solution. The solution

was left to stir for 30 minutes. 3 molar equivalent of ethylenediamine were added to the stirring solution. The reaction was allowed to stir for 16hrs. The solvent was dried *in vacuo*, and the contents were re-dissolved in 2.5mL of ddH₂O. To completely separate the dendrimer from unreacted acetic acid, the polymer was purified using PD-10 gel column. The eluted fraction at which the dendrimer is expected to appear (0-5 mL in a PD-10 as previously shown in chapter 2) was collected and dried under vacuum.

Step 2: Addition of Radiolabel

55 μ l (55 μ Ci) of [³H] Acetic anhydride acetonitrile solution was dissolved in 4mL of PBS. 10 molar equivalent of EDC and 10 molar equivalent of Sulfo-NHS were added to the stirring solution. After 30 minutes, 18.3 mg of aminated PAMAM G3.5 dendrimer (dissolved in 1mL of PBS) was added to the stirring solution (leading to a ratio of 3 μ Ci of radiolabel/1mg dendrimer) and the solution was allowed to stir for 16hrs. The reaction solvent was then dried *in vacuo*, and the radiolabelled dendrimer was triple purified using a PD-10 column as previously described in step 1.

Assessment of Limits of Quantitation

The limits of quantitation of the radiolabeled dendrimers were calculated through serially diluting a radiolabeled PAMAM dendrimer and assessing the lowest concentration of radiolabeled PAMAM dendrimer that can be

quantified. The limit of quantitation was calculated according to the following formula:

$$LOQ = BR + 10 \cdot SD_{BR}$$

LOQ stands for the lower limit of quantitation, BR for background reading and SD_{BR} for the standard deviation which is calculated from 10 different background readings.

Stability testing of Radiolabeled dendrimers

Radiolabeled dendrimers were incubated in either total Foetal bovine serum (FBS) or in dulbecco modified eagle medium (DMEM) supplemented with 10% FBS proteins (at a concentration of $1\mu\text{Ci}/\text{mL}$ media) at 37°C and relative humidity. Several samples were taken at different time intervals from 0-24 hours and stored at -20°C before analysis. Collected samples were then loaded into PD-10 columns and chromatograms were generated by analysing separate 1mL fractions that were eluted from the column to quantify radiolabel that is either associated with the dendrimer or is in a free form.

Cannabinoid – Dendrimer Conjugation

Step 1

The Boc group protecting the amine group in GA006 was broken by dissolving the cannabinoid in an aqueous solution of 1M HCl for 3 hours. The solution was then basified by the addition of concentrated sodium hydroxide (NaOH) until a pH of 12 was achieved as evident by pH paper. The basified solution was extracted with 3 portions of ethylacetate. All ethyl acetate portions were pooled and dried in-vacuo. The resulting compound was analysed using ^1H NMR and used with no further purification.

Anionic PAMAM dendrimer G3.5, 20 mg (1.61 mmol) was dissolved in in a 50:50 mixture of MeOH : H₂O. 10 molar equivalent of EDC and 10 molar equivalent of Sulfo-NHS were added to the stirring solution. After 30 minutes, 3.66mg (8.02mmol) of the cannabinoid N-(3-(1-naphthoyl)-1-pentyl-1H-indol-5-yl)-5-aminopentanamide (GA006a) was added to the stirring solution, and the solution was allowed to stir for 16hrs. The reaction solvent was then dried *in vacuo*, and the dendrimer-cannabinoid conjugate was triple purified using a PD-10 column as previously described in step 1.

Pharmacological testing of PAMAM-Cannabinoid Conjugate

Pharmacological testing of the PAMAM-Cannabinoid conjugate was performed with RAW 264.7 as described in the methods section in Chapter 3.

4.3 Results and Discussion

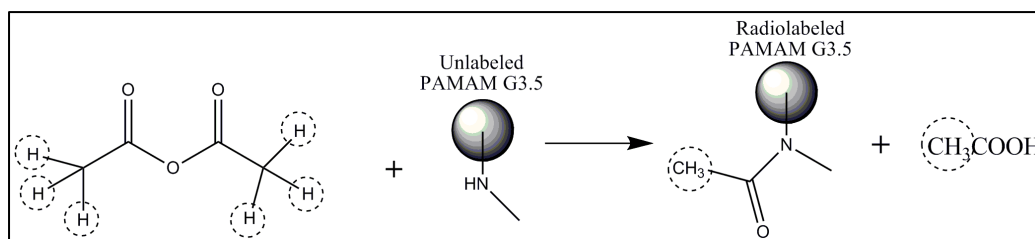
4.3.1 Radiolabeling of G3.5 PAMAM dendrimers

This was undertaken to :

- (A) Generate a dendrimer moiety that could be used in in-vivo biodistribution studies providing a sensitive analytical tool.
- (B) To mimic the chemistry of coupling via an amide linkage to the surface of a PAMAM G3.5 dendrimer and thus provide a ready model to initially explore the stability of this coupling linkage in biological fluids.

Previously described methods in radiolabelling anionic PAMAM dendrimers include Wiwattanpatapee's method [26] in aminating one of the surface carboxylic groups on a PAMAM dendrimer followed by attaching radioactive iodine (^{125}I) which readily reacts with primary amines. Although this method achieves high specific radioactivity, it also depends on the use of radioactive species (^{125}I) which imposes more serious health and environmental risks than [^3H] or [^{14}C] isotopes. Another group used tritiated acetic anhydride to radiolabel both cationic and anionic dendrimers [235]. This last strategy

exploits (for anionic PAMAM dendrimers) the reactivity of secondary amines that are present in the dendrimer's interior which are present in its interior because of inaccuracies in polymer synthesis. This method was repeated in the first of the chemical strategies described in results to link acetic anhydride to anionic dendrimers (*Schematic 4.1*)



Schematic 4.1 Strategy No.1 used in the radiolabeling of PAMAM dendrimers.

4.3.1.1 Purification and Characterisation of PAMAM-radiolabel conjugates

Purification of radiolabeled dendrimer was performed using GPC chromatography to separate the unreacted free radiolabel (in this case [³H] acetic acid as all the free [³H] acetic anhydride will hydrolyse in the aqueous conditions of the GPC). A PD-10 sephadex column with a molecular weight cut-off (MWCO) of 5,000Da . This can safely separate the 13,000Da PAMAM G3.5 from small molecular weight impurities including the free radiolabel. To demonstrate that the column can separate between the dendrimer and the free radiolabel, *Figure 4.1* shows the GPC chromatograms of Oregon-green labelled PAMAM G3.5 dendrimer, and the free radio label, [³H] acetic acid.

PAMAM G3.5-OG dendrimer completely elutes within the first 5 mL as shown in the figure while [^3H] acetic acid starts eluting at the 6th mL of the mobile phase. It is therefore possible to purify the radiolabeled PAMAM G3.5 using GPC chromatography.

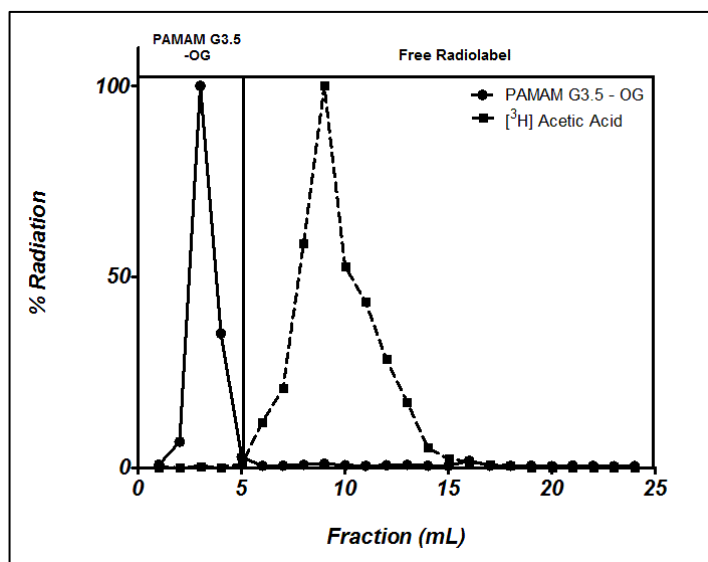


Figure 4.1 Over-layed GPC chromatograms generated by analysing eluted 1mL fractions from PD-10 columns (containing sephadex G25 gel.) Solid line represents chromatogram of pure Dendrimer-OG conjugate, dashed line represents free [^3H] acetic acid.

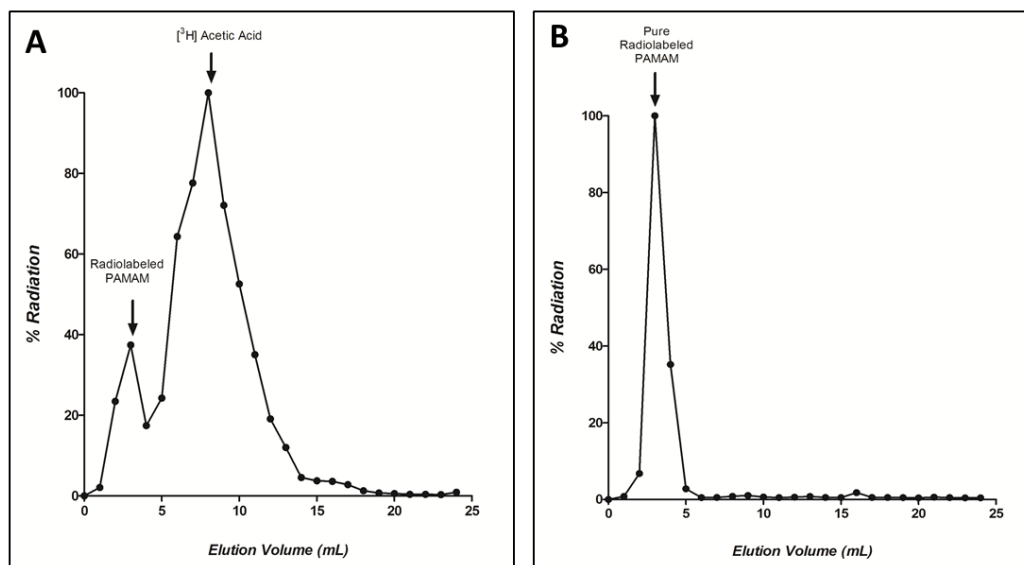


Figure 4.2 (A) GPC chromatogram of crude reaction mixture of PAMAM G3.5 and acetic anhydride displaying two peaks, first one for the radiolabeled G3.5 dendrimer, second for free [³H] acetic acid as acetic anhydride is expected to hydrolyse in an aqueous solution. (B) GPC chromatogram of radiolabeled anionic PAMAM G3.5

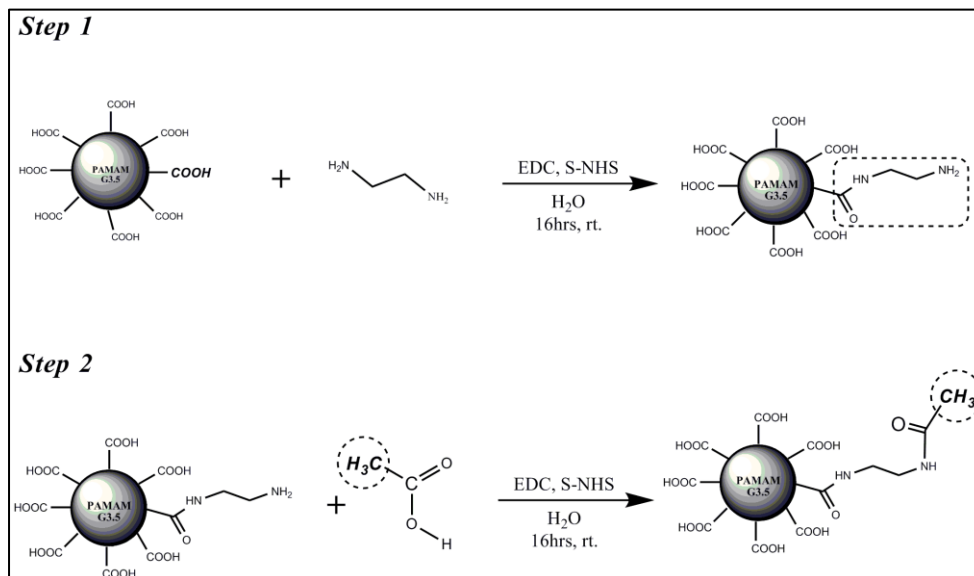
Figure 4.2 shows GPC chromatograms for (A) crude PAMAM G3.5-acetic anhydride reaction mixture (displaying two peaks corresponding respectively to the radio-labelled dendrimer and the free radiolabel) and (B) the pure PAMAM G3.5-radiolabel conjugate after purifying the dendrimer three times using GPC. These results show that the reaction was successful in coupling a radiolabel to the dendrimer. Having shown that the dendrimer-radiolabel is pure from free radiolabel, it is possible to quantify the specific radioactivity of the radio-labelled dendrimer.

The specific radioactivity of the labelled dendrimer was 0.3 μ Ci / mg of polymer. The limit of quantitation of the radiolabeled dendrimer was 2 μ g/mL as calculated from the minimum limit of quantitation (LOQ) as described in the

methods section of this chapter. This specific activity was significantly lower than that achieved by Sweet et al. who used the same method in radiolabeling, but generated labelled anionic PAMAM dendrimers with specific radioactivity of approximately $1\mu\text{Ci}/\text{mg}$ of polymer [236]. This might be due to the fact that this method exploits inaccuracies in the dendrimer structure which can be variable between different batches leading to different yields during radiolabeling. This method is hence not consistently reliable.

Another disadvantage that is associated with this method is the low stability of acetic anhydride which hydrolyses over time to produce acetic acid. This would demand very stringent storage conditions for the radiolabel, and even then this radiolabel would ultimately breakdown to acetic acid due to its reaction with atmospheric moisture overtime once the ampoule seal is broken. Additionally, the breakdown of [^3H] acetic anhydride during the synthesis due to reactivity with atmospheric humidity is inevitable due to the miniscule amounts of radioactive acetic anhydride that is used in such reactions which makes any presence of atmospheric humidity in the reaction apparatus a considerable issue that can limit the reaction specially when the other reactant (i.e. the PAMAM dendrimer) is not particularly reactive with the anhydride as described earlier.

The second method however, employs a novel and cheap way to radiolabel anionic PAMAM dendrimers. The anionic PAMAM dendrimer radiolabeling procedure was carried out in two steps as shown in *Schematic 4.2*.



Schematic 4.2 Strategy No.2 used in radiolabeling of anionic PAMAM dendrimers. Step 1 involves aminating one of the 64 surface groups using ethylene diamine . Step 2 involves using [^3H] acetic acid, generated by the hydrolysis of [^3H] acetic anhydride, in radiolabeling the aminated dendrimer.

The method by which anionic PAMAM dendrimers were labelled in these studies is novel and has not been reported before. The method depends on aminating one of the 64 carboxylic group so it becomes reactive to a carboxylic radioactive carboxylic compound. Acetic anhydride was chosen as a chemical source for the radioactive chemical because of its high availability and cheap price. As it would have been easier and more chemically efficient to use a radioactive amine that can directly react with the carboxylic groups on the PAMAM dendrimer's surface, radioactive compounds bearing amine termini are very expensive and are not readily available.

The specific radioactivity for the radiolabeled polymers was calculated to be $0.9\mu\text{Ci}/\text{mg}$ and a lower limit of quantitation of $0.71\mu\text{g}/\text{mL}$. This level of activity

was similar to that described previously by Wiwattanapattapee et al. [26] and Sweet et al. [236]. This method however is superior to that used by Wiwattanapattapee as it employs the use of a safer and cheaper isotope, tritium, and is superior to that of Sweet et al. as it is more consistent and reliable because it's not dependant on random secondary amines that can be present or absent to varying degrees in anionic PAMAM dendrimers. Additionally, stability of the acetic anhydride is not an issue with this method as it employs the use of its break-down product, acetic acid, which is generated from acetic anhydride once dissolved in an aqueous environment such as that used in the dendrimer reaction.

This method was hence adopted for all future radiolabeling of PAMAM dendrimers.

4.3.1.2 Stability of Radiolabeled Dendrimer

It is of vital importance to assess the stability of the Dendrimer-radiolabel conjugate to ensure that the radioactivity measured in any experiment would be only dendrimer associated and doesn't correspond to the free radio label, which can skew experimental results.

Additionally, because the radiolabel is attached using an amide bond, stability data generated from dendrimer-radiolabel conjugate would give an indication about the stability of the dendrimer-cannabinoid conjugate synthesised earlier.

Radiolabeled dendrimers were incubated in Cell culture medium (DMEM) supplemented with 10% FBS to assess the stability of these radiolabeled dendrimers when using them in *in-vitro* studies. Additionally, stability was tested in total foetal bovine serum to preliminarily assess stability of these dendrimers when used *in-vivo*.

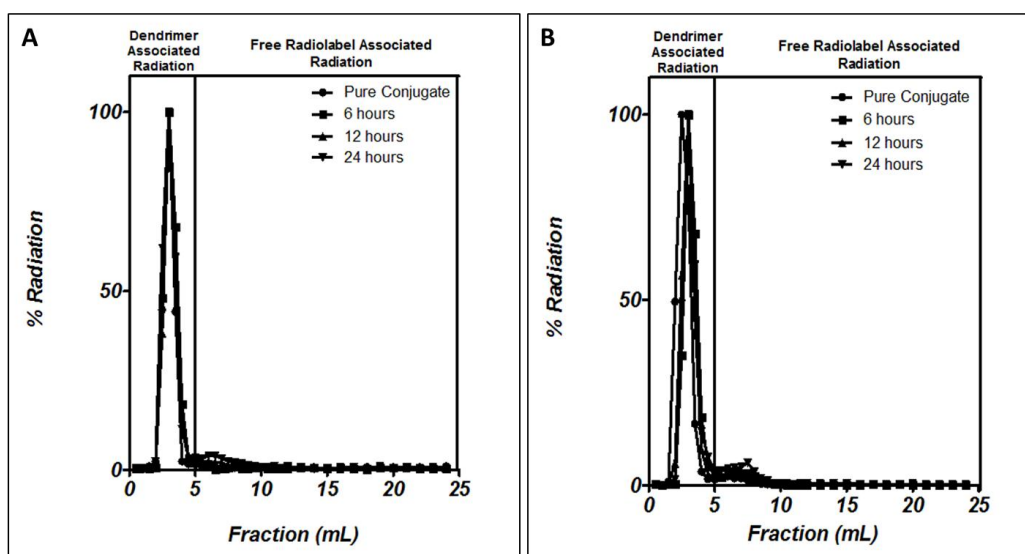


Figure 4.3 Stability of PAMAM-radiolabel conjugates. (A) GPC chromatograms of radiolabeled PAMAM incubated in cell culture media containing 10% FBS serum over 24 hours. GPC chromatograms of radiolabeled PAMAM incubated in (FBS) over 24 hours.

Table 4.1 Stability of radiolabeled PAMAM dendrimers. Purity calculated as the ratio between the area of the chromatogram representing free radiolabel associated radiation and area representing dendrimer associated radiation.

Time (hrs)	Incubation in full cell culture media			incubation in total FBS		
	Area of dendrimer associated radiation [%Radiation. Elution Volume]	Area of free radiolabel associated radiation [%Radiation. Elution Volume]	% Purity	Area of dendrimer associated radiation [%Radiation. Elution Volume]	Area of free radiolabel associated radiation [%Radiation. Elution Volume]	% Purity
0	111.8	1.22	98.9%	136.2	1.148	99.2%
6	133.1	3.88	97.2%	129.5	5.52	95.9%
12	117.8	6.76	94.6%	125.6	5.31	95.9%
24	142.9	12.51	92.0%	140.3	12.93	91.6%

Results presented in *Figure 4.3* and *Table 4.1* show that the Radiolabel displays <5% dissociation from the dendrimer over 6-12 hours when incubated in total FBS or in cell culture media while dissociation of the radiolabel does not exceed 9% over 24 hours. This suggests that the PAMAM-radiolabel conjugate is fairly stable in physiological conditions over 24 hours. To overcome the issue of the slight radiolabel dissociation over time in physiological conditions, experimental analyses can be performed on GPC purified samples to ensure that radioactive measurements correspond solely to the PAMAM dendrimer and not to the free radiolabel.

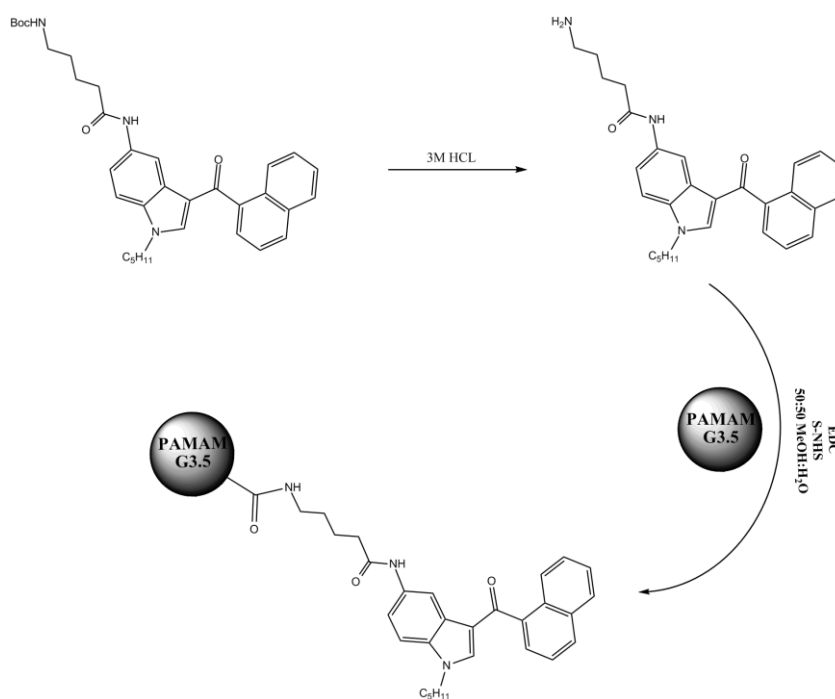
Results from these experiments additionally show that a compound conjugated to a dendrimer with an amide bond is stable in physiological conditions over 24 hours. The previously described Dendrimer-cannabinoid conjugate is hence

expected to be stable in physiological conditions as it is attached to the dendrimer via an amide bond too.

4.3.2 Cannabinoid-Dendrimer Conjugation

4.3.2.1 GA006 coupling to PAMAM G3.5 dendrimer

GA006 which comprises a protected amine separated by a spacer from the cannabinoid can be conjugated to an anionic PAMAM dendrimer as this amine, once unprotected can react with the carboxylic groups on the shell on the PAMAM dendrimer forming a stable amide bond.



Schematic 4.3 De-protection of the amine on GA006 and conjugation to a PAMAM G3.5 dendrimer.

Deprotection was swiftly achieved by hydrolysing the Boc group in a 3M HCl solution as shown in *Schematic 4.3*. The NMR spectrum provides evidence for the success in deprotecting the amine on GA006:

¹H NMR (500MHz, DMSO-d₆) δ 8.46 (1H, s), 8.34 (1H, s), 8.15 (1H, d), 8.10 (1H, d), 8.01 (1H, d), 7.66 (1H, d), 7.54 (1H, t), 7.48 (1H,t) 7.38 (1H, t), 7.28 (1H, s), 7.02 (1H, s), 4.61 (2H, s), 4.07 (1H, t) 3.11 (1H, s), 2.62 (2H, s), 2.13 (1H, t), 1.85-1.75 (2H, t), 1.61-1.55 (2H, t), 1.54-1.48 (6H, m), 1.38-1.22 (3H, m), 0.85 (2H, t).

The amine was hence exposed and ready to react with the carboxylic groups on the anionic G3.5 PAMAM dendrimer.

The conjugation was carried out in a 50:50 mixture of methanol : water to achieve complete dissolution of the hydrophobic cannabinoid while keeping the hydrophilic catalysts (EDC and S-NHS) in solution. The reaction proceeded for 16 hours.

4.3.2.2 Purification and Characterisation of PAMAM G3.5-GA006

Conjugate

The dendrimer-cannabinoid conjugate could not be purified using flash chromatography as the high hydrophilicity of the PAMAM dendrimer makes the affinity of the dendrimer to silica higher than any solvent system that can be used in flash chromatography including 100% methanol as evidenced from TLC analysis of PAMAM dendrimers with different solvent systems as shown in Figure 4.4.

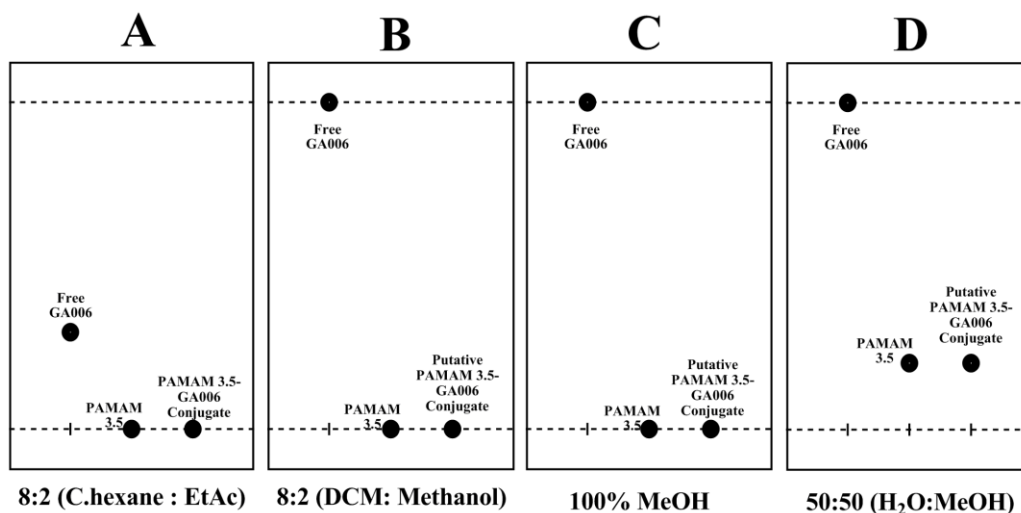


Figure 4.4 TLC analysis of PAMAM G3.5 dendrimers, cannabinoid GA006a and the putative PAMAM G3.5-cannabinoid conjugate. (A) silica plate developed using 8:2 Cyclohexane:Ethylacetate which results in an approximate R_f value of 0.3 for Free GA006, but PAMAM G3.5 and PAMAM G3.5-GA006 conjugate do not elute. (B) a significantly more polar system of Dichloromethane:Methanol (8:2) is used. This results in virtually no retention of GA006 but PAMAM G3.5 and the PAMAM-Cannabinoid conjugate still don't elute. (C) shows a TLC plate developed using 100% Methanol which similarly leads to very high elution of the free cannabinoid while no elution of PAMAM G3.5 or PAMAM G3.5-GA006 occurs. (D) 50:50 Methanol : Water is the only elution system that leads to the elution of PAMAM G3.5 and the Cannabinoid conjugate, however R_f values for both PAMAM G3.5 and the conjugate are not different.

As shown in *Figure 4.4*, the only solvent system that can lead to elution of PAMAM G3.5-GA006 involves the addition of water to the solvent system. Solvent systems containing more than 10% methanol however can result in dissolving the silica [237] that is used in flash chromatography leading to failure in extracting the desired pure components. Water naturally is not compatible with silica as it leads to dissolving it during flash chromatography because it is more polar than methanol.

Using reverse chromatography by HPLC on the other hand can overcome this problem. The large size of the dendrimer however, was not compatible with ordinary HPLC columns that were available.

The conjugate was hence purified using size exclusion chromatography/Gel permeation chromatography (GPC), where a sephadex G-25 gel matrix is used to separate the large polymer from smaller free molecules as previously described in the chapter. Pre-packed PD-10 columns (G-25 Sephadex gel) were used for this separation, as their molecular cut off of 5,000Da is ideal for separating between the 14,000Da conjugate and the 455Da free cannabinoid.

It was expected that the dendrimer conjugate would elute at the first 5mL fraction. This was confirmed using ^1H NMR analyses as shown in *Figure 4.5*.

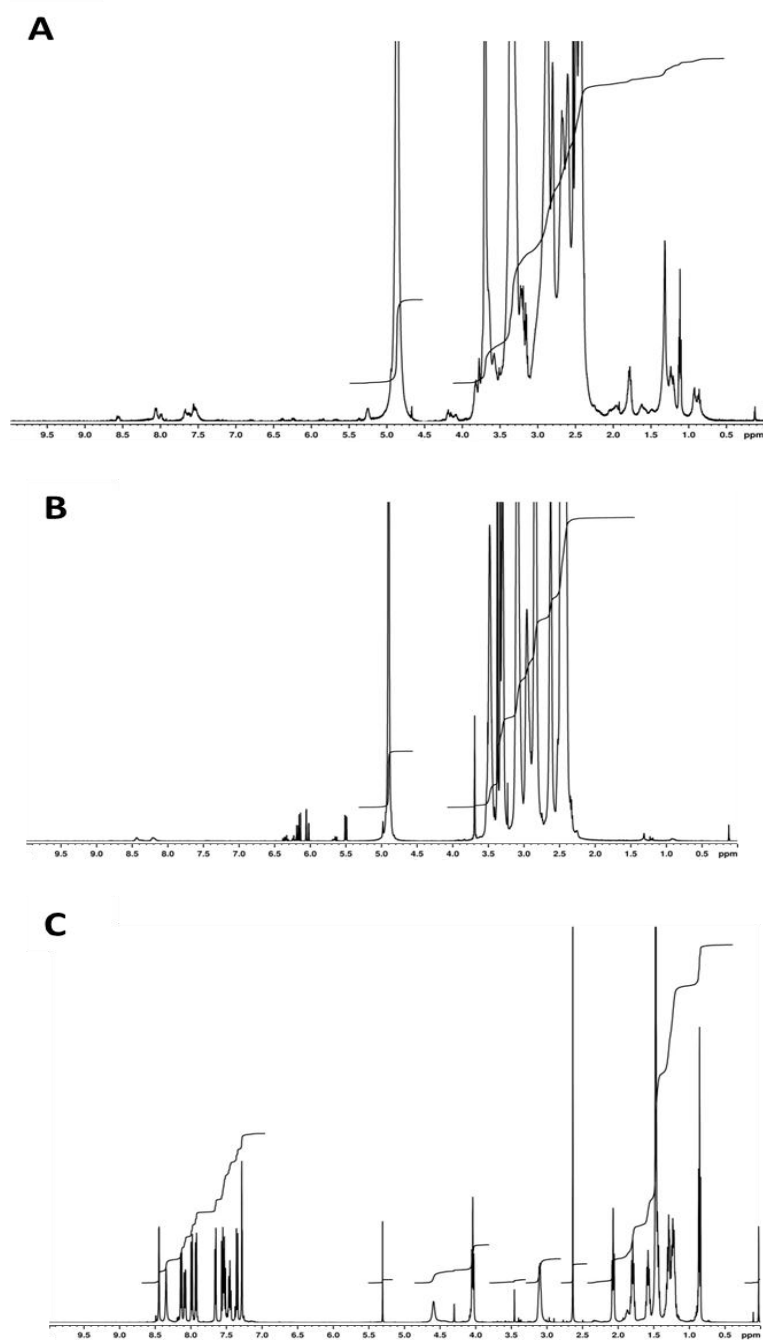


Figure 4.5: NMR spectra for:

(A) ^1H NMR spectrum of PAMAM G3.5-GA00a6 Conjugate as eluted within the first 5mL fraction from a PD-10 GPC column. The spectrum shows signals corresponding to both PAMAM G3.5 and GA006a.

(B) ^1H NMR spectrum of the first 5mL eluted from a PD-10 column when loading a mixture of PAMAM G3.5 and free GA00s6 which essentially represents a typical PAMAM G3.5 spectrum with no signals corresponding to GA006a

(C) ^1H NMR spectrum of GA006a

NMR analyses of different GPC fractions of PAMAM G3.5-GA006a conjugate and mixtures of PAMAM G3.5 and free GA006a show that an intact PAMAM G3.5-GA006a has been achieved. Both GA006a and PAMAM G3.5 signals are visible when analysing the first 5 mL fraction that elutes when loading the putative conjugate. When loading a mixture of free dendrimer and free cannabinoid however, the first 5mL fraction only shows signals that are associated with the PAMAM dendrimer and not the cannabinoid which proves that the purification process pursued can efficiently separate between the free cannabinoid and the dendrimer conjugate.

Upon analysing the NMR spectrum of the PAMAM G3.5-GA006 conjugate, a ratio of 1.5 : 1 of cannabinoid to PAMAM G3.5 can be estimated. This was calculated as the ratio between protons corresponding to total PAMAM dendrimer (δ 5.5-2.0 ppm as shown in *Figure 4.5, B*) and signals corresponding to the aromatic protons (visible at δ 8.5-7.5 ppm as shown in the NMR spectrum of free GA006a in *Figure 4.5, A*) PAMAM protons, and aromatic protons correspondent to aromatic protons in GA006 are completely separate and can hence be used to quantify the ratio between the cannabinoid and the dendrimer.

Previous stability studies in biological fluids with PAMAM G3.5-radiolabel show that the amide bond used to couple the radiolabel to the dendrimer is stable over 24 hours. The linkage between the cannabinoid and the dendrimer being an amide one as well, it is expected that the dendrimer-cannabinoid conjugate

will be similarly stable over the course of 24 hours. The conjugate is hence expected to be intact when administered with minimal dissociation of the cannabinoid and therefore decreasing the possibility the cannabinoid dissociating and accessing the CNS and causing CNS adverse effects. Clearly further *in-vivo* studies are needed for the complete assessment of the dendrimer-cannabinoid conjugate in the future.

4.3.2.3 Pharmacological activity of PAMAM G3.5 – GA006 Conjugate

The pharmacological activity of PAMAM G3.5-GA006 was assessed using the RAW 264.7 model with PAMAM G3.5 being used as negative control, and JWH007 used as a positive control. Results of TNF- α suppression of each of the used compounds are displayed in *Figure 4.6*.

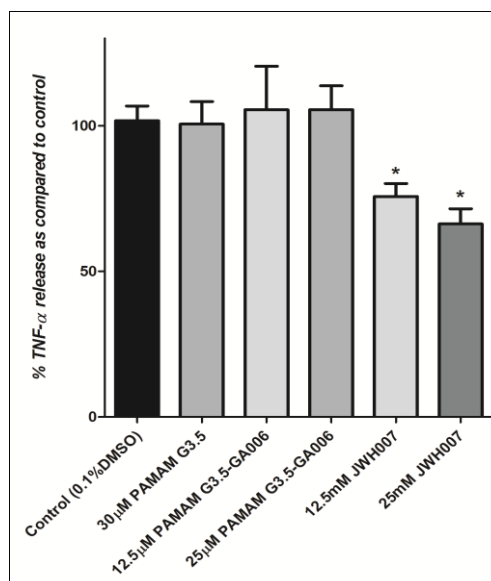


Figure 4.6 The effect of PAMAM G3.5, PAMAM G3.5-GA006 conjugate and JWH007 (12.5µM – 25µM) in suppressing LPS induced (200ng/mL for 16 hours) production of TNF- α in the murine macrophage cell line, RAW 264.7. Results are mean \pm S.D, n=4. * indicates $P < 0.05$ (ONE-WAY ANOVA, Dunnett's post-test).

Results show that the PAMAM G3.5 dendrimer does not have any inherent effects in suppressing TNF- α production by RAW 264.7 cells when used at equivalent molar concentrations to the highest concentrations used with Cannabinoids in these experiments. When treating LPS challenged RAW 264.7 cells with the previously synthesised and characterised PAMAM G3.5-GA006 conjugate, no TNF- α suppression effect is displayed indicating that the cannabinoid has lost its previous pharmacological activity when it was conjugated to a PAMAM G3.5 dendrimer. JWH007, used as a positive control, displayed an anti-inflammatory effect as before, which indicates that the assay is valid.

It is unknown why conjugating the cannabinoid to a dendrimer has resulted in a complete loss in activity. It is speculated however that the large size of the

dendrimer has made the conjugate too bulky to gain access to its receptors in the macrophage cell line. Additionally, the loss in activity may be due to the high hydrophilicity of the conjugate, this is because cannabinoids generally need to be highly hydrophobic to interact with the lipophilic regions of the receptor [205].

Chapter 5

General Discussion and Conclusions

5.1 *General Discussion*

The ultimate aim of the work described in this thesis was to utilise PAMAM dendrimers as a tool to achieve differential transport across the intestinal mucosa and the blood brain barrier, where these dendrimers can be used to achieve oral bioavailability but avoid BBB penetration and CNS access.

It was hypothesised that the large molecular size of the dendrimers combined with their compact, multivalent structure may achieve this aim. More precisely, dendrimer-drug conjugates would be created that are active in their own right but whose penetration to brain is prevented but whose intestinal activity is afforded. CNS adverse effects of cannabinoids currently limit their use as a therapeutic in IBD [67]. To produce their pharmacological activity in treating IBD, cannabinoids must be absorbed across the GI tract [111], and their CNS adverse effects clearly must be avoided.

Work to underpin the value of dendrimers to achieve selective barrier transport while creating a stable and pharmacologically active dendrimer-cannabinoid conjugate would represent a significant contribution.

In Chapter 2, a series of *in-vitro* epithelial permeability studies were undertaken examining the passive transport of cationic and anionic PAMAM dendrimers of varying molecular size. These studies aimed at showing a discriminative capacity of epithelial barriers of differing paracellular

restrictiveness toward the passive transport of dendrimers. In doing so, biological support would be provided for the hypothesis that dendrimers of an appropriate size are able to cross the intestinal mucosa but be restricted from crossing the BBB.

In-vitro investigations to mimic the intestinal permeability to different dendrimers were conducted using the CaCo-2 and MDCK II models. Both models have been used by other investigators to predict intestinal absorption to a wide variety of therapeutic molecules, although the predictive capacity of such *in-vitro* permeation studies to *in-vivo* absorption for high molecular polymers such as dendrimers has not been examined. For small molecular sized molecules the P_{app} data *in-vitro* in these two cell lines has been shown to provide good correlation to extents of oral absorption in humans [151, 156].

This thesis has shown that anionic PAMAM dendrimers at a size range of G1.5 – G5.5 display quantifiable transport across CaCo-2 and MDCK II “intestinal barrier” models in a size dependant manner, where smaller-sized dendrimers show the highest rate of transport. These anionic PAMAM dendrimers are biocompatible and did not compromise the integrity of the *in-vitro* epithelial monolayers as evidenced from maintenance of TEER measurements and of P_{app} data of co-instilled hydrophilic paracellular probes such as [^{14}C] mannitol. Indeed, anionic PAMAM dendrimers have been previously shown to be biocompatible when administered to rodents *in-vivo* [23]. The results support

the view that anionic PAMAM dendrimers can achieve oral bioavailability *in-vivo* to the level that could provide concentrations in intestinal sub mucosal tissue sufficient to elicit beneficial therapeutic responses.

In contrast to anionic PAMAM dendrimers, the cationic (G3 and G4) PAMAM dendrimers examined showed significantly higher transport rates and displayed P_{app} values that increased with increasing dendrimer size. These cationic dendrimers showed clear signs of epithelial barrier disruption as evidenced by significant decreases in TEER values and increases in co-instilled [^{14}C] mannitol. A number of groups have reported high P_{app} values for cationic dendrimers and suggested that they would be superior to other polymers in terms of barrier transport. However, the toxic effects of these multi-cationic entities are often overlooked. The data generated in this current thesis, as well as reports in the literature, for cationic PAMAM dendrimers were sufficient to exclude them from further consideration as the polymeric component in the development of a novel dendrimer-cannabinoid drug. The anionic PAMAM dendrimers were the lead polymer type for later cannabinoid conjugation experiments.

The other element of the hypothesis underpinning the thesis was that dendrimers would be effectively excluded from accessing the brain. The use of *in-vitro* BBB models to predict *in-vivo* penetration of drugs to the CNS is less clear than that for the intestine. In part this reflects the difficulty in quantifying brain penetration even in experimental animal models. However, beyond this

in-vitro BBB models simply do not establish the same levels of paracellular restrictiveness as the fully intact *in-vivo* BBB. For example, TEER measurements across the outer cerebral microvessels (pial vessels) of the brain can reach 8000 $\Omega\cdot\text{cm}^2$. Even the most restrictive *in-vitro* models reported, i.e. Porcine Brain primary microvascular cultures, reach only 1000 $\Omega\cdot\text{cm}^2$. More significantly paracellular permeability of such a model is at least x-10 fold greater than the *in-vivo* barrier. Other *in-vitro* BBB models are significantly worse at up to 1000-10000-fold greater paracellular permeability.

With the aim of using a restrictive but simple model for the BBB (but nevertheless one that still cannot mimic in quantitative terms the limiting nature of the *in-vivo* barrier) experiments in this thesis utilised the MDCK I cell line. This model has been used in both commercial and academic sectors as a surrogate BBB model. Further, MDCK I represents an equivalent cell line to MDCK II, except for higher TEER values reflective of differences in tight-junctional regulation. Nevertheless, MDCK I and II possess the same morphology and one anticipates very similar biochemistry.

None of the tested anionic PAMAM dendrimers showed any transport across the MDCK I model which contrasted to the findings for the MDCK II model in which all the tested anionic PAMAM dendrimers displayed permeation. Nevertheless, the permeability of the MDCK I cell monolayer to the small hydrophilic probe F-Na was evident, although to a much lesser extent than

across MDCK II. This confirmed that while the MDCKI cell monolayer is restrictive it should still be deemed as “leakier” to the passive transport of hydrophilic species than the *in-vivo* BBB barrier. The data therefore strongly support the conclusion that the anionic PAMAM dendrimers under study are very unlikely to penetrate the *in-vivo* BBB having failed to pass across a simpler barrier such as the MDCK I.

Therefore data is provided to strongly support the hypothesis that anionic PAMAM dendrimers can serve as a tool that affords transport across the intestinal mucosa while eliciting exclusion from the CNS. Naturally, *in-vivo* studies investigating both the intestinal transport and the CNS access of PAMAM dendrimers are needed in the future to further support the *in-vitro* data that has been generated so far.

In Chapter 3 the structure activity relationships (SAR) of cannabinoid compounds were explored as part of a strategy to identify suitable sites within the cannabinoid structure that may be used for conjugation to a dendrimer. Amongst the different classes of cannabinoid compounds it was decided to focus on the amino-alkyl indoles given their high potency and extensive use in the literature. After identifying sites within the cannabinoid that had previously been shown in the literature to be categorically vital for activity, the remaining sites were explored (i.e. carbonyl group and position 5' as shown in *Figure 5.1*) whose contribution to activity had not been previously examined.

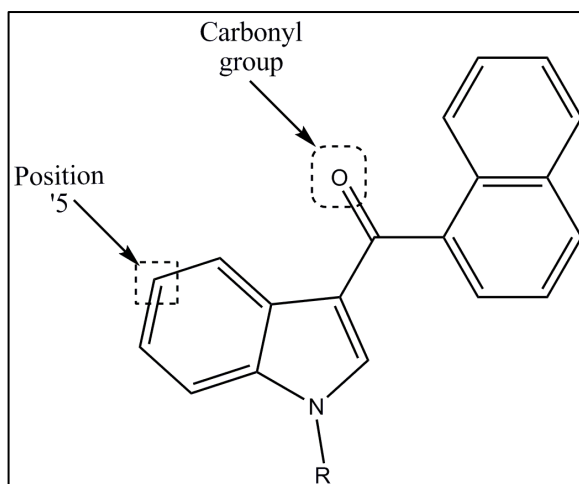


Figure 5.1 an amino alkyl indole showing sites that were manipulated in SAR studies.

Altering the carbonyl group proved to be technically challenging due to the high stability of the group. A variety of reducing agents failed to reduce this site to an alcohol or an amine. After this, position 5' was explored with various modifications applied. Many of the alterations at this site led to the maintenance of pharmacological activity indicating that this position is a suitable site to test dendrimer conjugation to allow retention of cannabinoid activity.

This finding was novel and significant to the studies within the cannabinoid field as it revealed a position that can be manipulated without any loss in activity. It will contribute to understanding of the SAR of this class of cannabinoids and opens new avenues in synthesising active cannabinoids with improved physicochemical properties; for example, functional groups could be attached to improve the aqueous solubility of these lipophilic compounds.

Given these findings, it seemed that position 5' would be the ideal site to investigate the conjugation of dendrimer. However, prior to this a reactive functional group needed to be introduced at position 5' in order to provide chemistry for the dendrimer linkage. The synthesis of a stable cannabimimetic compound, GA005, is described in chapter 3. This compound contains a nitro group at position 5' that can be reduced to a primary amine. The primary amine is reactive to a wide variety of chemical building blocks making it easier to manipulate the cannabinoid compound and tailor it as appropriate at this position. Using GA005 as a template, a 12Å long spacer bearing an amine on its terminus was successfully introduced at position 5'. The resulting cannabinoid, GA006, was pharmacologically active as predicted and was suitable to be conjugated to a dendrimer.

5.2 Conclusions

Overall the thesis has made the following scientific contributions to the respective field(s):

1. Promoted a strategy whereby an active polymer (dendrimer)-drug conjugates could be formed that is active in its own right and where the polymer can serve to provide differential biological barrier transport which with regard to cannabinoid pharmacology obviates adverse CNS effects.
2. Probed the SAR of cannabinoids based upon amino-alkyl indole chemistry and revealed a site, position 5', that can be functionally altered without loss of pharmacological activity.
3. Designed and synthesised novel and active cannabinoid structures that should have commercial interest
4. Developed a novel radiolabelling strategy for anionic polymers that offers a number of distinct advantages over other approaches
5. Successfully synthesised a novel Dendrimer-cannabinoid conjugate but biological testing revealed it to be inactive.

Clearly future studies will need to address reasons for failure of the dendrimer-cannabinoid conjugate to display biological activity. Approaches that could be considered include conjugation to a smaller dendrimer, molecular modelling of the conjugate interacting with the cannabinoid receptor. In addition thorough

in-vivo biodistribution studies with radiolabel dendrimer should be conducted with particular attention to the systemic bioavailability following oral dosing and the extent of CNS penetration.

References

1. Newkome, G.R., et al., *Dendritic Molecules: Concepts, Syntheses, Perspectives* 1996: WILEY-VCH. 262.
2. Patri, A.K., I.J. Majoros, and J.R. Baker, *Dendritic polymer macromolecular carriers for drug delivery*. *Curr Opin Chem Biol*, 2002. **6**(4): p. 466-71.
3. Dykes, G.M., *Dendrimers: a review of their appeal and applications*. *Journal of Chemical Technology & Biotechnology*, 2001. **76**(9): p. 903-918.
4. Buhleier, E., W. Wehner, and F. Vögtle, '*Cascade*'- and '*Non skid-Chain-like*' syntheses of molecular cavity topologies. *Synthesis*, 1978: p. 155-158.
5. Tomalia, D.A., et al., *A New Class of Polymers: Starburst-Dendritic Macromolecules*. *Polym. J.*, 1985. **17**: p. 117.
6. Kim, Y. and S.C. Zimmerman, *Applications of dendrimers in bio-organic chemistry*. *Curr Opin Chem Biol*, 1998. **2**(6): p. 733-42.
7. Frechet, J., *Functional polymers and dendrimers: reactivity, molecular architecture, and interfacial energy*. *Science*, 1994. **263**(5154): p. 1710-1715.
8. Boas, U. and P.M. Heegaard, *Dendrimers in drug research*. *Chem Soc Rev*, 2004. **33**(1): p. 43-63.
9. Tomalia, D.A., A.M. Naylor, and W.A. Goddard, *Starburst Dendrimers: Molecular-Level Control of Size, Shape, Surface Chemistry, Topology, and Flexibility from Atoms to Macroscopic Matter*. *Angewandte Chemie International Edition in English*, 1990. **29**(2): p. 138-175.
10. Hodge, P., *Polymer science branches out*. *Nature*, 1993. **362**(6415): p. 18-19.
11. Hawker, C.J. and J.M.J. Frechet, *Preparation of polymers with controlled molecular architecture. A new convergent approach to dendritic macromolecules*. *Journal of the American Chemical Society*, 1990. **112**(21): p. 7638-7647.
12. Esfand, R. and D.A. Tomalia, *Poly(amidoamine) (PAMAM) dendrimers: from biomimicry to drug delivery and biomedical applications*. *Drug Discov Today*, 2001. **6**(8): p. 427-436.
13. Caminati, G., N.J. Turro, and D.A. Tomalia, *Photophysical investigation of starburst dendrimers and their interactions with anionic and cationic surfactants*. *Journal of the American Chemical Society*, 1990. **112**(23): p. 8515-8522.

14. Farin, D. and D. Avnir, *Surface Fractality of Dendrimers*. *Angewandte Chemie International Edition in English*, 1991. **30**(10): p. 1379-1380.
15. Lee, I., et al., *Structural Molecular Dynamics Studies on Polyamidoamine Dendrimers for a Therapeutic Application: Effects of pH and Generation*. *Macromolecules*, 2002. **35**(11): p. 4510-4520.
16. Chen, W., D.A. Tomalia, and J.L. Thomas, *Unusual pH-Dependent Polarity Changes in PAMAM Dendrimers: Evidence for pH-Responsive Conformational Changes*. *Macromolecules*, 2000. **33**(25): p. 9169-9172.
17. Jansen, J.F.G.A., E.M.M. de Brabander-van den Berg, and E.W. Meijer, *Encapsulation of Guest Molecules into a Dendritic Box*. *Science*, 1994. **266**(5188): p. 1226-1229.
18. Duncan, R. and L. Izzo, *Dendrimer biocompatibility and toxicity*. *Advanced Drug Delivery Reviews*, 2005. **57**(15): p. 2215-2237.
19. Rittner, K., et al., *New basic membrane-destabilizing peptides for plasmid-based gene delivery in vitro and in vivo*. *Mol Ther*, 2002. **5**(2): p. 104-114.
20. Roberts, J.C., M.K. Bhalgat, and R.T. Zera, *Preliminary biological evaluation of polyamidoamine (PAMAM) Starburst™ dendrimers*. *Journal of Biomedical Materials Research*, 1996. **30**(1): p. 53-65.
21. Malik, N., et al., *Dendrimers: Relationship between structure and biocompatibility in vitro, and preliminary studies on the biodistribution of 125I-labelled polyamidoamine dendrimers in vivo*. *Journal of Controlled Release*, 2000. **65**(1-2): p. 133-148.
22. Chen, H.-T., et al., *Cytotoxicity, Hemolysis, and Acute in Vivo Toxicity of Dendrimers Based on Melamine, Candidate Vehicles for Drug Delivery*. *Journal of the American Chemical Society*, 2004. **126**(32): p. 10044-10048.
23. Malik, N., E.G. Evagorou, and R. Duncan, *Dendrimer-platinate: a novel approach to cancer chemotherapy*. *Anti-Cancer Drugs*, 1999. **10**(8): p. 767-776.
24. Jevprasesphant, R., et al., *The influence of surface modification on the cytotoxicity of PAMAM dendrimers*. *International Journal of Pharmaceutics*, 2003. **252**(1-2): p. 263-266.
25. Pantzar, N., et al., *Bidirectional Small-Intestinal Permeability in the Rat to Some Common Marker Molecules in vitro*. *Scandinavian Journal of Gastroenterology*, 1994. **29**(8): p. 703-709.
26. Wiwattanapatapee, R., et al., *Anionic PAMAM Dendrimers Rapidly Cross Adult Rat Intestine In Vitro: A Potential Oral Delivery System?* *Pharmaceutical Research*, 2000. **17**(8): p. 991-998.
27. Barth, R. and A. Soloway, *Boron neutron capture therapy of primary and metastatic brain tumors*. *Molecular and Chemical Neuropathology*, 1994. **21**(2): p. 139-154.
28. Klajnert, B. and M. Bryszewska, *Dendrimers: properties and applications*. *Acta Biochim Pol*, 2001. **48**(1): p. 199-208.

29. Haensler, J. and F.C. Szoka, Jr., *Polyamidoamine cascade polymers mediate efficient transfection of cells in culture*. *Bioconj Chem*, 1993. **4**(5): p. 372-9.
30. Wiener, E.C., et al., *Dendrimer-based metal chelates: a new class of magnetic resonance imaging contrast agents*. *Magn Reson Med*, 1994. **31**(1): p. 1-8.
31. Kobayashi, H., et al., *Polyamine dendrimer-based MRI contrast agents for functional kidney imaging to diagnose acute renal failure*. *Journal of Magnetic Resonance Imaging*, 2004. **20**(3): p. 512-518.
32. Kobayashi, H., et al., *Application of a macromolecular contrast agent for detection of alterations of tumor vessel permeability induced by radiation*. *Clin Cancer Res*, 2004. **10**(22): p. 7712-20.
33. Liu, M., K. Kono, and J.M.J. Fréchet, *Water-soluble dendritic unimolecular micelles: Their potential as drug delivery agents*. *Journal of Controlled Release*, 2000. **65**(1-2): p. 121-131.
34. Newkome, G.R., et al., *Micelles. Part 1. Cascade molecules: a new approach to micelles. A [27]-arborol*. *The Journal of Organic Chemistry*, 1985. **50**(11): p. 2003-2004.
35. Witvrouw, M., et al., *Polyanionic (i.e., Polysulfonate) Dendrimers Can Inhibit the Replication of Human Immunodeficiency Virus by Interfering with Both Virus Adsorption and Later Steps (Reverse Transcriptase/Integrase) in the Virus Replicative Cycle*. *Molecular Pharmacology*, 2000. **58**(5): p. 1100-1108.
36. Bourne, N., et al., *Dendrimers, a new class of candidate topical microbicides with activity against herpes simplex virus infection*. *Antimicrob Agents Chemother*, 2000. **44**(9): p. 2471-4.
37. Rupp, R., L. Rosenthal, and L.R. Stanberry, *VivaGel™ (SPL7013 Gel): A candidate dendrimer – microbicide for the prevention of HIV and HSV infection*. *International Journal of Nanomedicine*, 2007. **2**(4): p. 561-566.
38. O'Loughlin, J., et al., *Safety, tolerability, and pharmacokinetics of SPL7013 gel (VivaGel): a dose ranging, phase I study*. *Sex Transm Dis*, 2010. **37**(2): p. 100-4.
39. Supattapone, S., et al., *Branched polyamines cure prion-infected neuroblastoma cells*. *J Virol*, 2001. **75**(7): p. 3453-61.
40. Klajnert, B., et al., *Influence of heparin and dendrimers on the aggregation of two amyloid peptides related to Alzheimer's and prion diseases*. *Biochemical and Biophysical Research Communications*, 2006. **339**(2): p. 577-582.
41. Chen, C.Z., et al., *Quaternary Ammonium Functionalized Poly(propylene imine) Dendrimers as Effective Antimicrobials: Structure–Activity Studies*. *Biomacromolecules*, 2000. **1**(3): p. 473-480.
42. Pospisil, M., et al., *Glycodendrimeric ligands of c-type lectin receptors as therapeutic agents in experimental cancer*. *Adv Exp Med Biol*, 2001. **495**: p. 343-7.

43. Chauhan, A.S., et al., *Compositions and complexes containing a macromolecular compound as potential anti-inflammatory agents*. 2007, COUNCIL OF SCIENTIFIC AND INDUSTRIAL RESEARCH: UNITED STATES.
44. Chauhan, A.S., et al., *Solubility enhancement of indomethacin with poly(amidoamine) dendrimers and targeting to inflammatory regions of arthritic rats*. *J Drug Target*, 2004. **12**(9-10): p. 575-83.
45. Qi, R., et al., *PEG-conjugated PAMAM dendrimers mediate efficient intramuscular gene expression*. *AAPS J*, 2009. **11**(3): p. 395-405.
46. Strickley, R.G. and B.D. Anderson, *Solubilization and stabilization of an anti-HIV thiocarbamate, NSC 629243, for parenteral delivery, using extemporaneous emulsions*. *Pharm Res*, 1993. **10**(7): p. 1076-82.
47. Tuttle, C.B., *Intramuscular injections and bioavailability*. *Am J Hosp Pharm*, 1977. **34**(9): p. 965-8.
48. Vincent, L., et al., *Efficacy of dendrimer-mediated angiostatin and TIMP-2 gene delivery on inhibition of tumor growth and angiogenesis: In vitro and in vivo studies*. *International Journal of Cancer*, 2003. **105**(3): p. 419-429.
49. Vannucci, L., et al., *Effects of N-acetyl-glucosamine-coated glycodendrimers as biological modulators in the B16F10 melanoma model in vivo*. *International Journal of Oncology*, 2003. **23**: p. 285-296.
50. Bai, S., C. Thomas, and F. Ahsan, *Dendrimers as a carrier for pulmonary delivery of enoxaparin, a low-molecular weight heparin*. *Journal of Pharmaceutical Sciences*, 2007. **96**(8): p. 2090-2106.
51. Morris, C.J., et al., *Enhanced pulmonary absorption of a macromolecule through coupling to a sequence-specific phage display-derived peptide*. *Journal of Controlled Release*, 2010. **In Press, Corrected Proof**.
52. Chien, Y.W. and J.C. Liu, *Transdermal drug delivery systems*. *J Biomater Appl*, 1986. **1**(2): p. 183-206.
53. Yiyun, C., X. Tongwen, and F. Rongqiang, *Polyamidoamine dendrimers used as solubility enhancers of ketoprofen*. *European Journal of Medicinal Chemistry*, 2005. **40**(12): p. 1390-1393.
54. Lambkin, I. and C. Pinilla, *Targeting approaches to oral drug delivery*. *Expert Opinion on Biological Therapy*, 2002. **2**(1): p. 67-73.
55. El-Sayed, M., et al., *Trans epithelial transport of poly(amidoamine) dendrimers across Caco-2 cell monolayers*. *Journal of Controlled Release*, 2002. **81**(3): p. 355-365.
56. Tajarobi, F., et al., *Transport of poly amidoamine dendrimers across Madin-Darby canine kidney cells*. *International Journal of Pharmaceutics*, 2001. **215**(1-2): p. 263-267.
57. Florence, A.T., T. Sakthivel, and I. Toth, *Oral uptake and translocation of a polylysine dendrimer with a lipid surface*. *Journal of Controlled Release*, 2000. **65**(1-2): p. 253-259.

58. Vandamme, T.F. and L. Brobeck, *Poly(amidoamine) dendrimers as ophthalmic vehicles for ocular delivery of pilocarpine nitrate and tropicamide*. *Journal of Controlled Release*, 2005. **102**(1): p. 23-38.
59. Masteikova, R., Z. Chalupova, and A. Savickas, *[Biological availability of ophthalmic preparations. 2. Ophthalmic therapeutic systems]*. *Ceska Slov Farm*, 2004. **53**(5): p. 211-8.
60. Shaunak, S., et al., *Polyvalent dendrimer glucosamine conjugates prevent scar tissue formation*. *Nat Biotech*, 2004. **22**(8): p. 977-984.
61. Gaoni, Y. and R. Mechoulam, *Isolation, Structure, and Partial Synthesis of an Active Constituent of Hashish*. *Journal of the American Chemical Society*, 1964. **86**(8): p. 1646-1647.
62. Pacher, P., S. Batkai, and G. Kunos, *The Endocannabinoid System as an Emerging Target of Pharmacotherapy*. *Pharmacological Reviews*, 2006. **58**(3): p. 389-462.
63. Mechoulam, R., *The pharmacohistory of Cannabis Sativa*, in *Cannabinoids as Therapeutics*, R. Mechoulam, Editor. 1986, CRC Press, Inc., : Boca Raton, Florida. p. 1-19.
64. Devane, W.A., et al., *Determination and characterization of a cannabinoid receptor in rat brain*. *Molecular Pharmacology*, 1988. **34**(5): p. 605-613.
65. Melvin, L.S., et al., *Structure-activity relationships for cannabinoid receptor-binding and analgesic activity: studies of bicyclic cannabinoid analogs*. *Molecular Pharmacology*, 1993. **44**(5): p. 1008-1015.
66. Griffin, G., et al., *Evidence for the presence of CB2-like cannabinoid receptors on peripheral nerve terminals*. *Eur J Pharmacol*, 1997. **339**(1): p. 53-61.
67. Hanuř, L., et al., *HU-308: A specific agonist for CB2, a peripheral cannabinoid receptor*. *Proceedings of the National Academy of Sciences*, 1999. **96**(25): p. 14228-14233.
68. Beltramo, M., et al., *CB2 receptor-mediated antihyperalgesia: possible direct involvement of neural mechanisms*. *European Journal of Neuroscience*, 2006. **23**(6): p. 1530-1538.
69. Graham, E.S., et al., *Detailed characterisation of CB2 receptor protein expression in peripheral blood immune cells from healthy human volunteers using flow cytometry*. *Int J Immunopathol Pharmacol*, 2010. **23**(1): p. 25-34.
70. Calignano, A., et al., *Control of pain initiation by endogenous cannabinoids*. *Nature*, 1998. **394**(6690): p. 277-281.
71. Bouchard, J.F., P. Lepicier, and D. Lamontagne, *Contribution of endocannabinoids in the endothelial protection afforded by ischemic preconditioning in the isolated rat heart*. *Life Sci*, 2003. **72**(16): p. 1859-70.
72. Di Filippo, C., et al., *Cannabinoid CB2 receptor activation reduces mouse myocardial ischemia-reperfusion injury: involvement of*

- cytokine/chemokines and PMN*. Journal of Leukocyte Biology, 2004. **75**(3): p. 453-459.
73. Krylatov, A.V., et al., *Endogenous cannabinoids improve myocardial resistance to arrhythmogenic effects of coronary occlusion and reperfusion: a possible mechanism*. Bull Exp Biol Med, 2002. **133**(2): p. 122-4.
74. Krylatov, A.V., et al., *[Anandamide and R-(+)-methanandamide prevent development of ischemic and reperfusion arrhythmia in rats by stimulation of CB2-receptors]*. Eksp Klin Farmakol, 2002. **65**(3): p. 6-9.
75. Wagner, J.A., et al., *Endogenous cannabinoids mediate hypotension after experimental myocardial infarction*. J Am Coll Cardiol, 2001. **38**(7): p. 2048-2054.
76. Wagner, J.A., et al., *CB(1) cannabinoid receptor antagonism promotes remodeling and cannabinoid treatment prevents endothelial dysfunction and hypotension in rats with myocardial infarction*. Br J Pharmacol, 2003. **138**(7): p. 1251-8.
77. Munson, A.E., et al., *Antineoplastic activity of cannabinoids*. J Natl Cancer Inst, 1975. **55**(3): p. 597-602.
78. White, A.C., et al., *Effects of delta9-tetrahydrocannabinol in Lewis lung adenocarcinoma cells in tissue culture*. J Natl Cancer Inst, 1976. **56**(3): p. 655-8.
79. Tucker, A.N. and M.A. Friedman, *Effects of cannabinoids on L1210 murine leukemia. 1. Inhibition of DNA synthesis*. Res Commun Chem Pathol Pharmacol, 1977. **17**(4): p. 703-14.
80. Dvilansky, A., et al., *Effects of ethanol, CBD and delta 'THC on proliferation of K-562 cells*. Int J Tissue React, 1984. **6**(5): p. 409-12.
81. Sarfaraz, S., et al., *Cannabinoids for Cancer Treatment: Progress and Promise*. Cancer Research, 2008. **68**(2): p. 339-342.
82. Carracedo, A., et al., *The stress-regulated protein p8 mediates cannabinoid-induced apoptosis of tumor cells*. Cancer Cell, 2006. **9**(4): p. 301-12.
83. Massi, P., et al., *The non-psychoactive cannabidiol triggers caspase activation and oxidative stress in human glioma cells*. Cell Mol Life Sci, 2006. **63**(17): p. 2057-66.
84. Nelson, K., et al., *A phase II study of delta-9-tetrahydrocannabinol for appetite stimulation in cancer-associated anorexia*. J Palliat Care, 1994. **10**(1): p. 14-8.
85. Beal, J.E., et al., *Dronabinol as a treatment for anorexia associated with weight loss in patients with AIDS*. J Pain Symptom Manage, 1995. **10**(2): p. 89-97.
86. McLaughlin, P.J., et al., *The cannabinoid CB1 antagonists SR 141716A and AM 251 suppress food intake and food-reinforced behavior in a variety of tasks in rats*. Behav Pharmacol, 2003. **14**(8): p. 583-8.
87. FDA-Advisory-Committee, *FDA Briefing Document, NDA 21-888: Zimulti (rimonabant) Tablets, 20 mg, Sanofi Aventis*. 2007.

88. Xavier, R.J. and D.K. Podolsky, *Unravelling the pathogenesis of inflammatory bowel disease*. *Nature*, 2007. **448**(7152): p. 427-434.
89. Sartor, R.B., *Current concepts of the etiology and pathogenesis of ulcerative colitis and Crohn's disease*. *Gastroenterol Clin North Am*, 1995. **24**(3): p. 475-507.
90. Kunos, G. and P. Pacher, *Cannabinoids cool the intestine*. *Nat Med*, 2004. **10**(7): p. 678-9.
91. Summers, R.W., et al., *National Cooperative Crohn's Disease Study: results of drug treatment*. *Gastroenterology*, 1979. **77**(4 Pt 2): p. 847-69.
92. Sandberg-Gertzen, H., G. Jarnerot, and W. Kraaz, *Azodisal sodium in the treatment of ulcerative colitis. A study of tolerance and relapse-prevention properties*. *Gastroenterology*, 1986. **90**(4): p. 1024-30.
93. Baron, J.H., et al., *Sulphasalazine and salicylazosulphadimidine in ulcerative colitis*. *Lancet*, 1962. **1**(7239): p. 1094-6.
94. Truelove, S.C. and M.H. Hambling, *Treatment of ulcerative colitis with local hydrocortisone hemisuccinate sodium; a report on a controlled therapeutic trial*. *Br Med J*, 1958. **2**(5104): p. 1072-7.
95. Hanauer, S.B., et al., *Budesonide enema for the treatment of active, distal ulcerative colitis and proctitis: a dose-ranging study. U.S. Budesonide enema study group*. *Gastroenterology*, 1998. **115**(3): p. 525-32.
96. Greenberg, G.R., et al., *Oral budesonide for active Crohn's disease. Canadian Inflammatory Bowel Disease Study Group*. *N Engl J Med*, 1994. **331**(13): p. 836-41.
97. Truelove, S.C. and L.J. Witts, *Cortisone in ulcerative colitis; final report on a therapeutic trial*. *Br Med J*, 1955. **2**(4947): p. 1041-8.
98. Jewell, D.P. and S.C. Truelove, *Azathioprine in ulcerative colitis: final report on controlled therapeutic trial*. *Br Med J*, 1974. **4**(5945): p. 627-30.
99. Pearson, D.C., et al., *Azathioprine and 6-mercaptopurine in Crohn disease. A meta-analysis*. *Ann Intern Med*, 1995. **123**(2): p. 132-42.
100. Ogata, H., et al., *A randomised dose finding study of oral tacrolimus (FK506) therapy in refractory ulcerative colitis*. *Gut*, 2006. **55**(9): p. 1255-62.
101. Feagan, B.G., et al., *Methotrexate for the treatment of Crohn's disease. The North American Crohn's Study Group Investigators*. *N Engl J Med*, 1995. **332**(5): p. 292-7.
102. Massa, F., et al., *The endogenous cannabinoid system protects against colonic inflammation*. *J Clin Invest*, 2004. **113**(8): p. 1202-9.
103. Shire, D., et al., *An amino-terminal variant of the central cannabinoid receptor resulting from alternative splicing*. *J Biol Chem*, 1995. **270**(8): p. 3726-31.
104. Kulkarni-Narla, A. and D.R. Brown, *Localization of CB1-cannabinoid receptor immunoreactivity in the porcine enteric nervous system*. *Cell Tissue Res*, 2000. **302**(1): p. 73-80.

105. Galiegue, S., et al., *Expression of central and peripheral cannabinoid receptors in human immune tissues and leukocyte subpopulations*. Eur J Biochem, 1995. **232**(1): p. 54-61.
106. Bouaboula, M., et al., *Gi protein modulation induced by a selective inverse agonist for the peripheral cannabinoid receptor CB2: implication for intracellular signalization cross-regulation*. Mol Pharmacol, 1999. **55**(3): p. 473-80.
107. Germano, M.P., et al., *Cannabinoid CB1-mediated inhibition of stress-induced gastric ulcers in rats*. Naunyn Schmiedebergs Arch Pharmacol, 2001. **363**(2): p. 241-4.
108. Coruzzi, G., et al., *Inhibitory effect of the cannabinoid receptor agonist WIN 55,212-2 on pentagastrin-induced gastric acid secretion in the anaesthetized rat*. Naunyn Schmiedebergs Arch Pharmacol, 1999. **360**(6): p. 715-8.
109. Izzo, A.A., et al., *Inhibitory effect of cannabinoid agonists on gastric emptying in the rat*. Naunyn Schmiedebergs Arch Pharmacol, 1999. **360**(2): p. 221-3.
110. Krowicki, Z.K., et al., *Delta9-tetrahydrocannabinol inhibits gastric motility in the rat through cannabinoid CB1 receptors*. Eur J Pharmacol, 1999. **371**(2-3): p. 187-96.
111. Izzo, A.A., et al., *Cannabinoid CB1-receptor mediated regulation of gastrointestinal motility in mice in a model of intestinal inflammation*. Br J Pharmacol, 2001. **134**(3): p. 563-70.
112. Mathison, R., et al., *Effects of cannabinoid receptor-2 activation on accelerated gastrointestinal transit in lipopolysaccharide-treated rats*. Br J Pharmacol, 2004. **142**(8): p. 1247-54.
113. Marshall, C.R., *THE ACTIVE PRINCIPLE OF INDIAN HEMP: A PRELIMINARY COMMUNICATION.1*. The Lancet, 1897. **149**(3830): p. 235-238.
114. Chopra, G.S. and J.W. Smith, *Psychotic Reactions Following Cannabis Use in East Indians*. Arch Gen Psychiatry, 1974. **30**(1): p. 24-27.
115. Grossman, W., *Adverse reactions associated with Cannabis products in India*. Ann Intern Med, 1969. **70**(3): p. 529-33.
116. Keeler, M.H. and E. Moore, *Paranoid reactions while using marijuana*. Dis Nerv Syst, 1974. **35**(11): p. 535-6.
117. Green, B., D. Kavanagh, and R. Young, *Being stoned: a review of self-reported cannabis effects*. Drug Alcohol Rev, 2003. **22**(4): p. 453-60.
118. *The LaGuardia Committee Report: The Marijuana Problem in the City of New York*, in *The New York Academy of Medicine*. 1944: New York.
119. Ames, F., *A clinical and metabolic study of acute intoxication with Cannabis sativa and its role in the model psychoses*. J Ment Sci, 1958. **104**(437): p. 972-99.
120. D'Souza, D.C., et al., *The psychotomimetic effects of intravenous delta-9-tetrahydrocannabinol in healthy individuals: implications for psychosis*. Neuropsychopharmacology, 2004. **29**(8): p. 1558-72.

121. Sewell, R.A., et al., *[Behavioral, cognitive and psychophysiological effects of cannabinoids: relevance to psychosis and schizophrenia]*. Rev Bras Psiquiatr, 2010. **32 Suppl 1**: p. S15-30.
122. Morrison, P.D., et al., *The acute effects of synthetic intravenous Delta9-tetrahydrocannabinol on psychosis, mood and cognitive functioning*. Psychol Med, 2009. **39**(10): p. 1607-16.
123. Ranganathan, M. and D.C. D'Souza, *The acute effects of cannabinoids on memory in humans: a review*. Psychopharmacology (Berl), 2006. **188**(4): p. 425-44.
124. Heinrichs, R.W. and K.K. Zakzanis, *Neurocognitive deficit in schizophrenia: a quantitative review of the evidence*. Neuropsychology, 1998. **12**(3): p. 426-45.
125. Zachariou, M., et al., *Sensory gating and its modulation by cannabinoids: electrophysiological, computational and mathematical analysis*. Cogn Neurodyn, 2008. **2**(2): p. 159-70.
126. Dissanayake, D.W., et al., *Auditory gating in rat hippocampus and medial prefrontal cortex: effect of the cannabinoid agonist WIN55,212-2*. Neuropharmacology, 2008. **55**(8): p. 1397-404.
127. Patrick, G. and F.A. Struve, *Reduction of auditory P50 gating response in marijuana users: further supporting data*. Clin Electroencephalogr, 2000. **31**(2): p. 88-93.
128. Edwards, C.R., et al., *Sensory gating impairments in heavy cannabis users are associated with altered neural oscillations*. Behav Neurosci, 2009. **123**(4): p. 894-904.
129. Ilan, A.B., et al., *Neurophysiological and subjective profile of marijuana with varying concentrations of cannabinoids*. Behav Pharmacol, 2005. **16**(5-6): p. 487-96.
130. Nutt, D., et al., *Development of a rational scale to assess the harm of drugs of potential misuse*. The Lancet, 2007. **369**(9566): p. 1047-1053.
131. Moore, T.H., et al., *Cannabis use and risk of psychotic or affective mental health outcomes: a systematic review*. Lancet, 2007. **370**(9584): p. 319-28.
132. Cluny, N.L., et al., *Naphthalen-1-yl-(4-pentyloxynaphthalen-1-yl)methanone (SAB378), a peripherally restricted cannabinoid CB1/CB2 receptor agonist, inhibits gastrointestinal motility but has no effect on experimental colitis in mice*. J Pharmacol Exp Ther, 2010. **334**(3): p. 973-80.
133. Mitchell, V.A., et al., *Effect of the cannabinoid ajulemic acid on rat models of neuropathic and inflammatory pain*. Neurosci Lett, 2005. **382**(3): p. 231-5.
134. Farhadi, A., et al., *Intestinal barrier: An interface between health and disease*. Journal of Gastroenterology and Hepatology, 2003. **18**(5): p. 479-497.

135. Anderson, B.W., et al., *Physiological measurement of luminal stirring in perfused rat jejunum*. American Journal of Physiology - Gastrointestinal and Liver Physiology, 1988. **254**(6): p. G843-G848.
136. Ghandehari, H., et al., *Size-Dependent Permeability of Hydrophilic Probes Across Rabbit Colonic Epithelium*. Journal of Pharmacology and Experimental Therapeutics, 1997. **280**(2): p. 747-753.
137. Polentarutti, B.I., et al., *Evaluation of Viability of Excised Rat Intestinal Segments in the Ussing Chamber: Investigation of Morphology, Electrical Parameters, and Permeability Characteristics*. Pharmaceutical Research, 1999. **16**(3): p. 446-454.
138. Epple, H.-J., et al., *Impairment of the intestinal barrier is evident in untreated but absent in suppressively treated HIV-infected patients*. Gut, 2009. **58**(2): p. 220-227.
139. Smith, M.W. and M. Gumbleton., *Endocytosis at the blood-brain barrier: from basic understanding to drug delivery strategies*. J Drug Target, 2006. **14**(4): p. 191-214.
140. Kacem, K., et al., *Structural organization of the perivascular astrocyte endfeet and their relationship with the endothelial glucose transporter: A confocal microscopy study*. Glia, 1998. **23**(1): p. 1-10.
141. Meyer, J., J. Rauh, and H.-J. Galla, *The Susceptibility of Cerebral Endothelial Cells to Astroglial Induction of Blood-Brain Barrier Enzymes Depends on Their Proliferative State*. Journal of Neurochemistry, 1991. **57**(6): p. 1971-1977.
142. Tontsch, U. and H.-C. Bauer, *Glial cells and neurons induce blood-brain barrier related enzymes in cultured cerebral endothelial cells*. Brain Research, 1991. **539**(2): p. 247-253.
143. El Hafny, B., et al., *Modulation of P-glycoprotein activity by glial factors and retinoic acid in an immortalized rat brain microvessel endothelial cell line*. Neuroscience Letters, 1997. **236**(2): p. 107-111.
144. Dore-Duffy, P., et al., *Pericyte migration from the vascular wall in response to traumatic brain injury*. Microvasc Res, 2000. **60**(1): p. 55-69.
145. Alliot, F., et al., *Pericytes and periendothelial cells of brain parenchyma vessels co-express aminopeptidase N, aminopeptidase A, and nestin*. J Neurosci Res, 1999. **58**(3): p. 367-78.
146. Hardebo, J.E., B. Falck, and C. Owman, *A comparative study on the uptake and subsequent decarboxylation of monoamine precursors in cerebral microvessels*. Acta Physiol Scand, 1979. **107**(2): p. 161-7.
147. Thomas, W.E., *Brain macrophages: on the role of pericytes and perivascular cells*. Brain Res Brain Res Rev, 1999. **31**(1): p. 42-57.
148. Crone, C. and S.P. Olesen, *Electrical resistance of brain microvascular endothelium*. Brain Research, 1982. **241**(1): p. 49-55.
149. Butt, A.M., H.C. Jones, and N.J. Abbott, *Electrical resistance across the blood-brain barrier in anaesthetized rats: a developmental study*. The Journal of Physiology, 1990. **429**(1): p. 47-62.

150. Ohno, K., K.D. Pettigrew, and S.I. Rapoport, *Lower limits of cerebrovascular permeability to nonelectrolytes in the conscious rat*. American Journal of Physiology - Heart and Circulatory Physiology, 1978. **235**(3): p. H299-H307.
151. Artursson, P. and J. Karlsson, *Correlation between oral drug absorption in humans and apparent drug permeability coefficients in human intestinal epithelial (Caco-2) cells*. Biochemical and Biophysical Research Communications, 1991. **175**(3): p. 880-885.
152. Yamashita, S., et al., *Analysis of Drug Permeation Across Caco-2 Monolayer: Implication for Predicting In Vivo Drug Absorption*. Pharmaceutical Research, 1997. **14**(4): p. 486-491.
153. Lennernäs, H., *Human intestinal permeability*. Journal of Pharmaceutical Sciences, 1998. **87**(4): p. 403-410.
154. Misfeldt, D.S., S.T. Hamamoto, and D.R. Pitelka, *Transepithelial transport in cell culture*. Proc Natl Acad Sci U S A, 1976. **73**(4): p. 1212-6.
155. Cho, M.J., et al., *The Madin Darby canine kidney (MDCK) epithelial cell monolayer as a model cellular transport barrier*. Pharm Res, 1989. **6**(1): p. 71-7.
156. Irvine, J.D., et al., *MDCK (Madin-Darby canine kidney) cells: A tool for membrane permeability screening*. J Pharm Sci, 1999. **88**(1): p. 28-33.
157. Gumbleton, M. and K.L. Audus, *Progress and limitations in the use of in vitro cell cultures to serve as a permeability screen for the blood-brain barrier*. J Pharm Sci, 2001. **90**(11): p. 1681-98.
158. Cummins, C.L., et al., *In vivo modulation of intestinal CYP3A metabolism by P-glycoprotein: studies using the rat single-pass intestinal perfusion model*. J Pharmacol Exp Ther, 2003. **305**(1): p. 306-14.
159. Bjarnason, I., A. MacPherson, and D. Hollander, *Intestinal permeability: an overview*. Gastroenterology, 1995. **108**(5): p. 1566-81.
160. Kitchens, K., et al., *Transport of Poly(Amidoamine) Dendrimers across Caco-2 Cell Monolayers: Influence of Size, Charge and Fluorescent Labeling*. Pharmaceutical Research, 2006. **23**(12): p. 2818-2826.
161. Jevprasesphant, R., et al., *Engineering of Dendrimer Surfaces to Enhance Transepithelial Transport and Reduce Cytotoxicity*. Pharmaceutical Research, 2003. **20**(10): p. 1543-1550.
162. D'Emanuele, A., et al., *The use of a dendrimer-propranolol prodrug to bypass efflux transporters and enhance oral bioavailability*. Journal of Controlled Release, 2004. **95**(3): p. 447-453.
163. Najlah, M., et al., *Synthesis and Assessment of First-Generation Polyamidoamine Dendrimer Prodrugs to Enhance the Cellular Permeability of P-gp Substrates*. Bioconjugate Chemistry, 2007. **18**(3): p. 937-946.
164. Ke, W., et al., *Enhanced oral bioavailability of doxorubicin in a dendrimer drug delivery system*. Journal of Pharmaceutical Sciences, 2008. **97**(6): p. 2208-2216.

165. Lüllmann, H. and M. Wehling, *The binding of drugs to different polar lipids in vitro*. Biochemical Pharmacology, 1979. **28**(23): p. 3409-3415.
166. Gaush, C.R., W.L. Hard, and T.F. Smith, *Characterization of an Established Line of Canine Kidney Cells (MDCK)*. Proceedings of the Society for Experimental Biology and Medicine, 1966. **122**(3): p. 931-935.
167. Richardson, J.C. and N.L. Simmons, *Demonstration of protein asymmetries in the plasma membrane of cultured renal (MDCK) epithelial cells by lactoperoxidase-mediated iodination*. FEBS Lett, 1979. **105**(2): p. 201-4.
168. Lipschutz, J.H., et al., *Extracellular signal-regulated kinases 1/2 control claudin-2 expression in Madin-Darby canine kidney strain I and II cells*. J Biol Chem, 2005. **280**(5): p. 3780-8.
169. Bohets, H., et al., *Strategies for absorption screening in drug discovery and development*. Current Topics in Medicinal Chemistry, 2001. **17**: p. 367-383.
170. Iyer, A.K., et al., *Exploiting the enhanced permeability and retention effect for tumor targeting*. Drug Discovery Today, 2006. **11**(17-18): p. 812-818.
171. Nusrat, A., J.R. Turner, and J.L. Madara, IV. *Regulation of tight junctions by extracellular stimuli: nutrients, cytokines, and immune cells*. American Journal of Physiology - Gastrointestinal and Liver Physiology, 2000. **279**(5): p. G851-G857.
172. Bruewer, M., S. Samarin, and A. Nusrat, *Inflammatory bowel disease and the apical junctional complex*. Ann N Y Acad Sci, 2006. **1072**: p. 242-52.
173. Shen, L. and J.R. Turner, *Role of epithelial cells in initiation and propagation of intestinal inflammation. Eliminating the static: tight junction dynamics exposed*. Am J Physiol Gastrointest Liver Physiol, 2006. **290**(4): p. G577-82.
174. Komatsu, M., et al., *Tumor Necrosis Factor- in Serum of Patients with Inflammatory Bowel Disease as Measured by a Highly Sensitive Immuno-PCR*. Clin Chem, 2001. **47**(7): p. 1297-1301.
175. Patrick, D.M., et al., *Proinflammatory cytokines tumor necrosis factor-alpha and interferon-gamma modulate epithelial barrier function in Madin-Darby canine kidney cells through mitogen activated protein kinase signaling*. BMC Physiol, 2006. **6**: p. 2.
176. Foerg, C., et al., *Differentiation restricted endocytosis of cell penetrating peptides in MDCK cells corresponds with activities of Rho-GTPases*. Pharm Res, 2007. **24**(4): p. 628-42.
177. Blanchard, J., L.M. Tang, and M.E. Earle, *Reevaluation of the absorption of carbenoxolone using an in situ rat intestinal technique*. J Pharm Sci, 1990. **79**(5): p. 411-4.
178. Windmueller, H.G. and A.E. Spaeth, *Vascular autoperfusion of rat small intestine in situ*. Methods Enzymol, 1981. **77**: p. 120-9.

179. Hillard, C.J., R.A. Harris, and A.S. Bloom, *Effects of the cannabinoids on physical properties of brain membranes and phospholipid vesicles: fluorescence studies*. Journal of Pharmacology and Experimental Therapeutics, 1985. **232**(3): p. 579-88.
180. Martin, B.R., *Cellular effects of cannabinoids*. Pharmacol Rev, 1986. **38**(1): p. 45-74.
181. Howlett, A.C., J.M. Qualy, and L.L. Khachatrian, *Involvement of Gi in the inhibition of adenylate cyclase by cannabimimetic drugs*. Molecular Pharmacology, 1986. **29**(3): p. 307-313.
182. Herkenham, M., et al., *Neuronal localization of cannabinoid receptors in the basal ganglia of the rat*. Brain Research, 1991. **547**(2): p. 267-274.
183. Thomas, B.F., X. Wei, and B.R. Martin, *Characterization and autoradiographic localization of the cannabinoid binding site in rat brain using [3H]11-OH-delta 9-THC-DMH*. J Pharmacol Exp Ther, 1992. **263**(3): p. 1383-90.
184. Baker, D., et al., *In silico patent searching reveals a new cannabinoid receptor*. Trends in Pharmacological Sciences, 2006. **27**(1): p. 1-4.
185. Matsuda, L.A., et al., *Structure of a cannabinoid receptor and functional expression of the cloned cDNA*. Nature, 1990. **346**(6284): p. 561-564.
186. Munro, S., K.L. Thomas, and M. Abu-Shaar, *Molecular characterization of a peripheral receptor for cannabinoids*. Nature, 1993. **365**(6441): p. 61-65.
187. Matsuda, L.A., *Molecular aspects of cannabinoid receptors*. Crit Rev Neurobiol, 1997. **11**(2-3): p. 143-66.
188. Felder, C.C., et al., *Comparison of the pharmacology and signal transduction of the human cannabinoid CB1 and CB2 receptors*. Mol Pharmacol, 1995. **48**(3): p. 443-50.
189. Caulfield, M.P. and D.A. Brown, *Cannabinoid receptor agonists inhibit Ca current in NG108-15 neuroblastoma cells via a pertussis toxin-sensitive mechanism*. Br J Pharmacol, 1992. **106**(2): p. 231-2.
190. Mackie, K. and B. Hille, *Cannabinoids inhibit N-type calcium channels in neuroblastoma-glioma cells*. Proc Natl Acad Sci U S A, 1992. **89**(9): p. 3825-9.
191. Mackie, K., et al., *Cannabinoids activate an inwardly rectifying potassium conductance and inhibit Q-type calcium currents in AtT20 cells transfected with rat brain cannabinoid receptor*. J Neurosci, 1995. **15**(10): p. 6552-61.
192. Pan, X., S.R. Ikeda, and D.L. Lewis, *Rat brain cannabinoid receptor modulates N-type Ca²⁺ channels in a neuronal expression system*. Molecular Pharmacology, 1996. **49**(4): p. 707-714.
193. Herkenham, M., *Localization of cannabinoid receptors in brain and periphery*. Cannabinoid Receptors, ed. R.G. Pertwee. 1995, London: Academic Press. 145-166.

194. Pertwee, R.G., et al., *Further evidence for the presence of cannabinoid CB1 receptors in guinea-pig small intestine*. Br J Pharmacol, 1996. **118**(8): p. 2199-205.
195. Pertwee, R.G., G. Joe-Adigwe, and G.M. Hawksworth, *Further evidence for the presence of cannabinoid CB1 receptors in mouse vas deferens*. Eur J Pharmacol, 1996. **296**(2): p. 169-72.
196. Pertwee, R.G. and S.R. Fernando, *Evidence for the presence of cannabinoid CB1 receptors in mouse urinary bladder*. Br J Pharmacol, 1996. **118**(8): p. 2053-8.
197. Julien, B., et al., *Antifibrogenic role of the cannabinoid receptor CB2 in the liver*. Gastroenterology, 2005. **128**(3): p. 742-755.
198. Henry, D.J. and C. Chavkin, *Activation of inwardly rectifying potassium channels (GIRK1) by co-expressed rat brain cannabinoid receptors in Xenopus oocytes*. Neurosci Lett, 1995. **186**(2-3): p. 91-4.
199. Hanus, L., et al., *HU-308: a specific agonist for CB(2), a peripheral cannabinoid receptor*. Proc Natl Acad Sci U S A, 1999. **96**(25): p. 14228-33.
200. Piomelli, D., et al., *The endocannabinoid system as a target for therapeutic drugs*. Trends in Pharmacological Sciences, 2000. **21**(6): p. 218-224.
201. Adams, R., *Marihuana: Harvey Lecture, February 19, 1942*. Bull N Y Acad Med, 1942. **18**(11): p. 705-30.
202. Martin, B.R., et al., *Pharmacological evaluation of agonistic and antagonistic activity of cannabinoids*. NIDA Res Monogr, 1987. **79**: p. 108-22.
203. Razdan, R.K., *Structure-activity relationships in cannabinoids*. Pharmacol Rev, 1986. **38**(2): p. 75-149.
204. Mechoulam, R., et al., *Stereochemical requirements for cannabimimetic activity*. NIDA Res Monogr, 1987. **79**: p. 15-30.
205. Huffman, J.W., et al., *Structure-activity relationships for 1-alkyl-3-(1-naphthoyl)indoles at the cannabinoid CB1 and CB2 receptors: steric and electronic effects of naphthoyl substituents. New highly selective CB2 receptor agonists*. Bioorganic & Medicinal Chemistry, 2005. **13**(1): p. 89-112.
206. Aung, M.M., et al., *Influence of the N-1 alkyl chain length of cannabimimetic indoles upon CB1 and CB2 receptor binding*. Drug and Alcohol Dependence, 2000. **60**(2): p. 133-140.
207. Blanchard, D.K., et al., *In vitro and in vivo suppressive effects of delta-9-tetrahydrocannabinol on interferon production by murine spleen cells*. Int J Immunopharmacol, 1986. **8**(7): p. 819-24.
208. Cabral, G.A., J.C. Lockmuller, and E.M. Mishkin, *Delta 9-tetrahydrocannabinol decreases alpha/beta interferon response to herpes simplex virus type 2 in the B6C3F1 mouse*. Proc Soc Exp Biol Med, 1986. **181**(2): p. 305-11.

209. Smith, S.R., C. Terminelli, and G. Denhardt, *Effects of cannabinoid receptor agonist and antagonist ligands on production of inflammatory cytokines and anti-inflammatory interleukin-10 in endotoxemic mice*. *J Pharmacol Exp Ther*, 2000. **293**(1): p. 136-50.
210. Klein, T.W., et al., *Marijuana components suppress induction and cytolytic function of murine cytotoxic T cells in vitro and in vivo*. *J Toxicol Environ Health*, 1991. **32**(4): p. 465-77.
211. Ofek, O., et al., *Peripheral cannabinoid receptor, CB2, regulates bone mass*. *Proc Natl Acad Sci U S A*, 2006. **103**(3): p. 696-701.
212. Hunter, S.A. and S.H. Burstein, *Receptor mediation in cannabinoid stimulated arachidonic acid mobilization and anandamide synthesis*. *Life Sci*, 1997. **60**(18): p. 1563-73.
213. Jeon, Y.J., et al., *Attenuation of inducible nitric oxide synthase gene expression by delta 9-tetrahydrocannabinol is mediated through the inhibition of nuclear factor- kappa B/Rel activation*. *Mol Pharmacol*, 1996. **50**(2): p. 334-41.
214. Ross, R.A., H.C. Brockie, and R.G. Pertwee, *Inhibition of nitric oxide production in RAW264.7 macrophages by cannabinoids and palmitoylethanolamide*. *Eur J Pharmacol*, 2000. **401**(2): p. 121-30.
215. Gallily, R., et al., *Protection against septic shock and suppression of tumor necrosis factor alpha and nitric oxide production by dexanabinol (HU-211), a nonpsychotropic cannabinoid*. *J Pharmacol Exp Ther*, 1997. **283**(2): p. 918-24.
216. Huffman, J.W. and L.W. Padgett, *Recent developments in the medicinal chemistry of cannabimimetic indoles, pyrroles and indenenes*. *Curr Med Chem*, 2005. **12**(12): p. 1395-411.
217. Middleton, W.J. and H.D. Carlson, *HEXAFLUOROACETONE IMINE*. *Organic Syntheses*, 1988. **6**: p. 664.
218. Allen, C.H. and J. VanAllan, *m-Tolylbenzylamine*. *Organic Syntheses*, 1955. **3**: p. 827.
219. March, J., *Advanced Organic Chemistry: Reactions, Mechanisms, and Structure 93rd ed.*. 1985, New York: Wiley.
220. Dangerfield, E.M., et al., *Protecting-Group-Free Synthesis of Amines: Synthesis of Primary Amines from Aldehydes via Reductive Amination*. *Journal of Organic Chemistry*, 2010. **75**(16): p. 5470-5477.
221. Sukanta, B., *Titanium(IV) isopropoxide and sodium borohydride : A reagent of choice for reductive amination*. *Tetrahedron Letters*, 1994. **35**(15): p. 2401-2404.
222. Balcom, D. and A. Furst, *Reductions with Hydrazine Hydrate Catalyzed by Raney Nickel. I. Aromatic Nitro Compounds to Amines*^{1,2}. *Journal of the American Chemical Society*, 1953. **75**(17): p. 4334-4334.
223. Pirrung, M.C., et al., *Methyl Scanning: Total Synthesis of Demethylasterriquinone B1 and Derivatives for Identification of Sites of Interaction with and Isolation of Its Receptor(s)*. *Journal of the American Chemical Society*, 2005. **127**(13): p. 4609-4624.

224. Wang, X., et al., *Synthesis, Characterization, and in Vitro Activity of Dendrimer–Streptokinase Conjugates*. *Bioconjugate Chemistry*, 2007. **18**(3): p. 791-799.
225. Devarakonda, B., R.A. Hill, and M.M. de Villiers, *The effect of PAMAM dendrimer generation size and surface functional group on the aqueous solubility of nifedipine*. *International Journal of Pharmaceutics*, 2004. **284**(1-2): p. 133-140.
226. Chauhan, A.S., et al., *Dendrimer-mediated transdermal delivery: enhanced bioavailability of indomethacin*. *Journal of Controlled Release*, 2003. **90**(3): p. 335-343.
227. Ma, M., et al., *Evaluation of polyamidoamine (PAMAM) dendrimers as drug carriers of anti-bacterial drugs using sulfamethoxazole (SMZ) as a model drug*. *European Journal of Medicinal Chemistry*, 2007. **42**(1): p. 93-98.
228. Ihre, H.R., et al., *Polyester Dendritic Systems for Drug Delivery Applications: Design, Synthesis, and Characterization*. *Bioconjugate Chemistry*, 2002. **13**(3): p. 443-452.
229. Kaminskas, L.M., et al., *Pharmacokinetics and Tumor Disposition of PEGylated, Methotrexate Conjugated Poly-L-lysine Dendrimers*. *Molecular Pharmaceutics*, 2009. **6**(4): p. 1190-1204.
230. Carreno-gomez, B. and R. Duncan, *Compositions with enhanced oral bioavailability*. 2003, 20030211072: UNITED STATES.
231. Kurmi, B.D., et al., *Lactoferrin-conjugated dendritic nanoconstructs for lung targeting of methotrexate*. *Journal of Pharmaceutical Sciences*, 2011: p. n/a-n/a.
232. He, H., et al., *PEGylated Poly(amidoamine) dendrimer-based dual-targeting carrier for treating brain tumors*. *Biomaterials*, 2011. **32**(2): p. 478-487.
233. Tekade, R.K., et al., *Surface-engineered dendrimers for dual drug delivery: A receptor up-regulation and enhanced cancer targeting strategy*. *Journal of Drug Targeting*, 2008. **16**(10): p. 758-772.
234. Quintana, A., et al., *Design and function of a dendrimer-based therapeutic nanodevice targeted to tumor cells through the folate receptor*. *Pharm Res*, 2002. **19**(9): p. 1310-6.
235. Kitchens, K.M., et al., *Endocytosis Inhibitors Prevent Poly(amidoamine) Dendrimer Internalization and Permeability across Caco-2 Cells*. *Molecular Pharmaceutics*, 2008. **5**(2): p. 364-369.
236. Sweet, D.M., et al., *Transepithelial transport of PEGylated anionic poly(amidoamine) dendrimers: implications for oral drug delivery*. *J Control Release*, 2009. **138**(1): p. 78-85.
237. Iler, R.K., *The Chemistry of Silica: Solubility, Polymerization, Colloid and Surface Properties and Biochemistry*. 1979: Wiley-Blackwell.